Universidad Nacional Autonoma de México

Programa de Posgrado en Astrofísica

Instituto de Astronomía

Pruebas Astrofísicas de Modelos de Gravedad Modificada

TESIS

que para optar por el grado de:

doctora en ciencias (Astrofísica)

presenta

María Alejandra Jiménez Zúñiga

Tutor

Dr. Xavier Hernández Doring

Instituto de Astronomía-UNAM

México, D.F. junio 2014

A los zapatistas de Chiapas, por ser un ejemplo de otro mundo posible. Un mundo donde el conocimiento es placer de todos.
A Celia que es zapatista...

Agradecimientos

Durante el tiempo en que realice mi doctorado tuve la fortuna de estar rodeada de personas excepcionales que hicieron posible este trabajo y les que quiero expresar mi agradecimiento.

Sin duda el principal artífice de este trabajo fue mi director de tesis Xavier Hernández Doring; le agradezco haberme aceptado como su estudiante y de inmediato contagiarme con su pasión por esta área de estudio, por compartirme su forma de hacer ciencia valiente y honesta, nunca le falto emoción al trabajo y se lo agradezco. Los que hemos trabajado con Xavier sabemos que es de esos bichos raros en la ciencia que se dan de a poco y yo tuve la fortuna de trabajar con él.

A Javier Sanchéz y Margarita Rosado les agradezco haber sido parte de mi comité tutor durante el doctorado.

Agradezco también a Tonatiuh Matos, Roberto Susman, Christine Allen y Margarita Rosado por aceptar ser parte del sínodo para esta tesis.

A la UNAM por ser mi casa durante toda mi formación académica y al Instituto de Astronomía por brindarme la infraestructura necesaria para realizar mi trabajo.

A la gente trabajadora de mi querido país, que con sus impuestos por medio del CONACyT pagaron la beca para mis estudios de doctorado.

Por último quiero agradecer a las personas que me han acompañado en muchos caminos y su cercanía siempre fue un impulso para el llevar a buen termino el trabajo en mi doctorado.

A Alan por hacer siempre más ricas las ideas de esta tesis y por ser mi amigo de siempre.

A Benjamín, por ser mi compañero en todas las formas de disfrutar la vida, por su cariño y complicidad.

A Ivonne, por ser mi hermana de años.

A Juan Aldebaran, por sus comentarios siempre críticos a este trabajo y por su cariño.

A Gerardo y Mara por darme el hermoso regalo de hacerme tía de la bella Carmina.

A Ximena, por ser mi familia y el apoyo que siempre quiero.

A Celia mi madre, por ser mi ejemplo de lucha, amor y generosidad.

Resumen

La evidencia astronómica de que en ciertas circunstancias, la dinámica de los objetos en el universo no corresponde a la esperada dadas las leyes de la física que conocemos y la masa luminosa en estrellas y gas que observamos es conocida desde hace varias decadas. En las observaciones hechas por Zwicky (1933) y Oort (1932) ya se hace evidente esta discrepancia en el Cúmulo de Coma en el primer caso y en la vecindad solar en el segundo.

Esta discrepancia resulto ser irrefutable con la medición de las curvas de rotación galacticas hechas por Bosma (1981) y Rubin et al. (1982), donde para un gran número de glaxias espirales la velocidad de rotación no decae con la raíz cuadrada de la separación al centro gálactico r cómo se espera según la tercera ley de Kepler sino que, en la periferia de las galaxias se mantiene constante conforme r aumenta.

A una escala mucho más grande, mediciones de la masa de cúmulos de galaxias hechas usando la emisión en rayos X del gas caliente del cúmulo y por lentes gravitacionales muestran que su masa debe ser alrededor de siete veces más que la observada asumiendo equilibrio hidrostático y Relatividad General (RG) (Hoekstra et al. 1998).

En escalas cosmológicas surge también el problema de reconciliar las observaciones con la teoría; el rastro que dejó el contraste de densidad de las fluctuaciones de materia en la radiación cósmica de fondo en el momento de la recombinación muestra que estas debían tener una amplitud de $\sim 10^{-5}$, según la RG estas fluctuaciones crecen proporcionales al factor de escala del universo, y dado que la recombinación ocurrio en $z \sim 1000$, las fluctuaciones primordiales al día de hoy solo habrían crecido en tres ordenes de magnitud y la estructura que observamos en el universo no se habría formado aún.

Estos hechos son evidencia de que calculamos un potencial gravitacional menor al que observamos y esto puede ocurrir en principio por dos razones; la primera, que hay mas materia que contribuye a este potencial de la que observamos y las leyes de la física que usamos para calcular dicho potencial son las correctas o la cantidad de materia que vemos es la que existe y nuestras leyes de la física son incompletas.

Explorar la primer posibilidad ha llevado a la comunidad científica a construir el modelo cosmológico ΛCDM (Lambda Cold Dark Matter) o ΛWDM (Lambda Warm Dark Matter) según se trate de materia oscura fría o tibia. En este escenario

se asume que la RG y su límite de campo débil la dinámica newtoniana son validas a todas las escalas, y los ingredientes que dominan la densidad de energía en el universo son la materia y energía oscura. Este modelo, también llamado de concordancia, está definido por varios parámetros, los más importantes son los que definen un espacio-tiempo plano, donde la densidad de energía del universo se constituye por alrededor de 4 % materia bariónica, 23 % materia oscura y 73 % energía oscura. Este escenario, exitoso en la descripción de la estructura a gran escala del universo, a escalas más pequeñas presenta varios problemas que para una parte de la comunidad científica son consecuencia de la complicada física de los bariones involucrada en cada caso y para otros son evidencia de que el modelo está en crisis y debemos de cuestionarnos si la hipótesis de la materia oscura es la adecuada para describir nuestro universo (Kroupa 2012).

La segunda posibilidad es que estemos observando un régimen donde las leyes de la física son distintas a las que conocemos. Sabemos que la ley de gravedad newtoniana funciona muy bien a escalas del Sistema Solar y que la RG es adecuada para describir sistemas que involucran campos gravitacionales intensos, pero para aceleraciones del orden de la que experimenta una estrella en la periferia de una galaxia no hemos probado su validez y existe la posibilidad de tengan que ser modificadas a estas escalas.

La primera propuesta de introducir una modificación a la dinámica newtoniana para explicar las curvas de rotación galácticas fue hecha por Milgrom en 1983 (Milgrom 1983c,a,b) y es conocida como MOND (MOdified Newtonian Dynamics), en su propuesta Milgrom supone que la ley de inercia o la ley de gravedad sufren un cambio en escalas donde la aceleración es menor que $a_0 = 1.2 \times 10^{-8} cm/s^2$ y en escalas donde $a > a_0$ la física newtoniana queda intacta. Una consecuencia de esta modificación es que para una partícula de prueba orbitando una masa M, la velocidad de equilibrio de la partícula es constante con la distancia y escala con la masa total como $v^4 = Ga_0M$.

El esquema de Milgrom tiene la peculiaridad de lograr reproducir la curva de rotación de un gran número de galaxias sin la necesidad de suponer materia oscura (Sanders & McGaugh 2002, McGaugh 2011). Numerosos intentos por obtener una teoría relativista tal que su límite de campo débil sea tipo MOND han sido llevados a cabo sin que a la fecha exista una que logre describir en su totalidad las observaciones tanto a escalas galácticas como cosmológicas (Bekenstein 2004, Bernal et al. 2011, Moffat & Toth 2010). Las teorías de gravedad modificada cuyo límite a aceleraciones menores que a_0 son tipo MOND tienen en común que en los sistemas donde se cumpla la condición $a < a_0$ se puede esperar una transición del régimen newtoniano a un régimen de gravedad modificada, el cual se caracteriza por velocidades de equilibrio que no dependen de la separación al centro de masa y se cumple una relación del tipo Tully-Fisher entre la masa y la velocidad, esta predicción puede ser comprobada en sistemas astrofísicos.

En esta tesis estudiamos sistemas astrofísicos que se encuentran en el régimen donde la aceleración es del orden de a_0 y donde según el modelo estandar la materia oscura no juega un papel importante en la dinámica del sistema y esta queda determinada por la masa visible según las leyes de la dinámica newtoniana.

En el capítulo uno exponemos los aspectos más relevantes de los esquema de gravedad modificada para está tesis. En el capítulo dos nos ocupamos de las estrellas binarias abiertas ya que para un sistema de dos estrellas ligadas gravitacionalmente con masas alrededor de $1M_{\odot}$ la aceleración es menor que a_0 para separaciones mayores a $7000AU$, siendo este un sistema donde podemos poner a prueba las predicciones de los esquemas de gravedad modificada. Para ello usamos dos muestras de estrellas binarias tomadas de manera independiente. La primera, de la base de datos del SDSS (Sloan Digital Sky Survey) como se presentan en (Dhital et al. 2010), que consiste en miles de sistemas binarios con una baja señal a ruido en la velocidad relativa. La segunda muestra es tomada del satelite Hipparcos, (Shaya & Olling 2011) es una muestra más pequeña pero con una mejor señal a ruido ~ 2 en las velocidades relativas y separaciones más grandes que 10^4AU. Nuestros resultados muestran un límite superior constante de las velocidades relativas de las estrellas binarias para las dos muestras, el cúal es independiente de la separación en analogía con las curvas de rotación galácticas en el mismo regimen $a < a_0$. Este resultado es cuantitavamente inconsistente con la predicción hecha por la dinámica newtoniana para estos sistemas evolucionando en un ambiente galáctico (Jiang & Tremaine 2010). En este estudio hemos verificado la predicción de los esquemas de gravedad modificada de que en sistemas donde se cumpla que la aceleración es menor que a_0 tenemos una velocidad de equilibrio constante que no decae con la separación al centro de masa del sistema (Hernandez, Jiménez, & Allen 2012).

En el capítulo tres usamos la propuesta de gravedad modificada hecha por Mendoza et al. (2011) para construir modelos de equilibrio dinámico para dieciséis cúmulos globulares (CGs) donde en años recientes se ha medido la dispersión de velocidades como función de la separación al centro del cúmulo encontrado que la dispersión de velocidades no decae como se espera bajo la dinámica newtoniana sino que se mantiene constante (Scarpa et al. 2007, Scarpa & Falomo 2010, Scarpa et al. 2011). La ley de fuerza que usamos tiene la característica de que en el límite $a < a_0$ coincide con MOND y para $a > a_0$ recobramos la ley del inverso al cuadrado de la distancia de Newton. Con nuestros modelos encontramos que el aplanamiento del perfil de dispersión de velocidades proyectado ocurre en el lugar donde $a < a_0$ y logramos reproducir tanto el perfil de brillo superficial y el perfil de dispersión de velocidades proyectado sobre la línea de visión asi como todas las restricciones observacionales del CG que se trate (Hernandez & Jiménez 2012).

Además como una prueba de consistencia de los modelos de equilibrio desa-

rrollados en (Hernandez & Jiménez 2012) para CGs, los aplicamos ahora a la galaxia elíptica gigante NGC 4649, un sistema varios ordenes de magnitud en masa y tamaño mayor que un CG y nuevamente logramos construir modelos de equilibrio para esta galaxia que satisfacen todas las restricciones observacionales incluyendo la parte plana de su perfil de dispersión de velocidades proyectado sin la necesidad de incluir materia oscura, mientras que los modelos newtonianos requieren un halo de materia oscura con una masa de casi la mitad de la masa total de la galaxia a tres radios efectivos (Jiménez et al. 2013).

En el capítulo tres discutimos como es que dentro del modelo de concordancia los CGs son sistemas newtonianos y un perfil de dispersión de velocidades que se aplana en la periferia de un CG tiende a explicarse por la acción de la fuerza de marea que actua sobre las estrellas en la parte externa del CG. Sin embargo, dentro de un esquema de gravedad modificada este comportamiento es el esperado en escalas donde la aceleración de las estrellas en el CG sea $\sim a_0$. Para contrastar las dos explicaciones hemos calculado el radio de marea newtoniano para cada CG usando masas calculadas a través de modelos de síntesis de poblaciones estelares independientes de cualquierer suposición dinámica del CG. Encontramos que en el punto donde la órbita del cúmulo es más cercana al centro galáctico, el radio de marea es mucho más grande, diez veces más grande en algunos casos, que el radio en el cual el perfil se aplana. Es decir, en el lugar donde el perfil se aplana las fuerzas de marea no afectan la dinámica del CG. Por otro lado el radio donde el perfil se aplana correlaciona en promedio con el radio en el cual se cruza el punto donde la aceleracion vale a_0, favoreciendo los modelos de gravedad modificada. Además encontramos que la masa y la dispersión de velocidades asintótica siguen la misma relación Tully- Fisher galáctica. De esta manera se verifica otra de las predicciones de los esquemas de gravedad modificada y se explica el comportamiento asintoticamente constante delperfil de dispersión de velocidades proyectado de los CGs (Hernandez, Jiménez, & Allen 2013a).

En el capítulo cínco exploramos otra consecuencia de los esquemas de gravedad modificada, esta es que cualquier halo isotérmico de partículas de prueba alrededor de una distribución esférica de masa debe adoptar una configuración de equilibrio que en primera aproximación satisface $\rho \propto r^{-3}$. Las observaciones muestran que en efecto esto es así; el halo etelar de la Vía Láctea tiene un perfil de densidad el cual satisface $\rho \propto r^{-3}$, lo mismo ocurre para M31 y las observaciones muestran que la distribución de CGs en la galaxia Andromeda siguen el mismo patrón, además recientemente se ha observado que una población difusa de estrellas en los alrededores de CGs que se extienden más allá de su radio de marea newtoniano siguien la misma distribución. Mientras que en una descripción newtoniana de la gravedad hay diversas explicaciones dependiendo del sistema del que se trate, dentro de la gravedad modificada todas estas observaciones se entienden como consecuencia delcomportamiento de la gravedad en escalas donde

la aceleración es del orden de la aceleración de Milgrom (Hernandez, Jiménez, & Allen 2013b).

Por último, una vez que hemos explorado varios sistemas astrofísicos locales y hemos comprobado que se cumplen las predicciones de los esquemas de gravedad modificada en cada uno de ellos, queremos estudiar las consecuencias cosmológicas de estos modelos. En el capítulo seis exponemos un primer intento, estudiamos la formación de estructura en el régimen lineal en gravedad modificada y mostramos a primer orden es posible formar estructura consistente con la observada hoy en día a partir de las fluctuaciones de materia iniciales cuyo contraste de densidad es el observado en la radiación cósmica de fondo. Mientras que en la gravedad de Einstein o Newton es necesario que las fluctuaciones de materia estén sumergidas en los pozos de potencial ocasionados por fluctuaciones de materia oscura con un contraste de densidad mayor. Además en contraste con el escenario estandar en gravedad modificada no se tiene una dependencia crucial con las condiciones iniciales debido a que se obtiene una solución que converge independientemente de las condiciones iniciales a una solución atractora $\Delta(M, z)$.

En el capítulo siete damos las conclusiones de este trabajo y comentamos el trabajo futuro.

Índice general

Capítulo 1

Introducción

Las anomalías gravitacionales que se observan tanto a escalas galácticas como cosmológicas son consecuencia de que nuestro conocimiento de la naturaleza es incompleto; o bien hay un tipo de materia cuya naturaleza es desconocida y hasta el momento ha logrado evadir toda detección independiente a su efecto gravitacional, o nos falta entender cómo se comporta la fuerza de gravedad en las escalas donde estas anomalías se manifiestan.

En esta tesis exploramos la posibilidad de que nuestro conocimiento de la ley de gravedad sea incompleto y retomamos la propuesta de Milgrom (Milgrom 1983c,a,b) como ha sido replanteada en trabajos recientes Mendoza et al. (2011). llevamos a cabo una prueba de las predicciones de estos modelos en estrellas binarias abiertas y mostramos como dentro de estos esquemas se logra explicar el comportamiento del perfil de dispersión de velocidades asintóticamente plano en cúmulos globulares y en la galaxia elíptica gigante NGC 4649. Por último exploramos la consecuencia del crecimiento de las fluctuaciones primigenias de densidad en el régimen lineal en gravedad modificada y encontramos que a primera aproximación el crecimiento de las fluctuaciones iniciales como se observan en la radiación cósmica de fondo, es consistente con la estructura que se observa hoy en día en el Universo.

A continuación exponemos los aspectos más relevantes de los esquemas de gravedad modificada para este trabajo.

1.0.1. Dinámica modificada (MOND)

Milgrom considera la posibilidad de que en el caso no relativista y en el límite de aceleraciones bajas la fuerza total que actúa sobre un objeto no sea proporcional a la aceleración, sino que depende de ella mediante una función μ. Milgrom supone lo siguiente:
i) La fuerza inercial que experimenta un objeto es proporcional a la masa gravi-

tacional del mismo.
ii)La aceleración que experimenta el objeto depende solo de la fuerza a la posición del objeto, como se deduce en la manera convencional según la distribución de las fuentes.
iii)La fuerza inercial actúa en la dirección de la aceleración.
iv)En el límite de aceleraciones bajas la inercia es proporcional al cuadrado de la aceleración del objeto.
Es decir, Milgrom deja el resto de los supuestos de la física newtoniana intactos y sólo introduce un cambio en escalas donde la aceleración es menor que una constante a_0 (Milgrom 1983c,a,b). De esta manera la fuerza que actúa sobre un objeto de masa m está dada por:

$$ma\mu(\frac{a}{a_0}) = F. \tag{1.1}$$

Donde a_0 es una nueva constante física con unidades de aceleración, μ es una función por determinar que debe tener los siguientes límites; $\mu(\frac{a}{a_0}) = \frac{a}{a_0}$ si $\frac{a}{a_0} \ll 1$ y $\mu(\frac{a}{a_0}) = 1$ si $\frac{a}{a_0} \gg 1$ de manera que para aceleraciones mayores que a_0 obtengamos de nuevo la dinámica newtoniana. Si la única fuerza que actúa sobre la partícula es la gravedad, la aceleración gravitacional modificada estará relacionada con la aceleración gravitacional newtoniana de la siguiente manera:

$$g\mu(g/a_0) = g_n. \tag{1.2}$$

Donde g_n es la aceleración gravitacional newtoniana. En consecuencia para una partícula de prueba orbitando una masa M, si igualamos la aceleración gravitacional g a la aceleración centrípeta de la partícula obtenemos para el régimen de aceleraciones bajas

$$v^4 = GMa_0. \tag{1.3}$$

Con esta modificación se obtienen curvas de rotación asintóticamente planas y la relación Tully-Fisher entre la masa y la velocidad. Siendo esta última consecuencia la principal predicción de este modelo.

En esta fórmula se resume la fenomenología de una gran cantidad de observaciones astronómicas (Famaey & McGaugh 2012). Sin embargo, aplicarla en todo sistema físico puede llevar a inconsistencias, como es el caso del problema de dos cuerpos con diferente masa donde el momento no es conservado (Felten 1984).

Así que la fórmula 1.1 debe considerarse no como una ley universal, sino como una aproximación que es valida en sistemas con una distribución simétrica de masa de una fuerza más general que debe ser derivada de una acción y de un principio variacional.

Milgrom considera la posibilidad de que la dinámica requiera ser modificada sólo cuando hay una fuerza gravitacional involucrada, en este caso es la ley de gravedad la que se modifica y la segunda ley de Newton queda como la conocemos.

En sistemas donde la única fuerza que actúa es la fuerza gravitacional estos dos enfoques son equivalentes. Sin embargo, en general no es así y las implicaciones físicas de considerar una u otra posibilidad son muy distintas.En nuestro trabajo tomaremos el segundo enfoque siguiendo la propuesta de Mendoza et al. (2011).

1.0.2. Gravedad modificada

En el trabajo hecho en esta tesis consideramos la posibilidad de que la fuerza de gravedad sea la que requiera una modificación, usamos la propuesta hecha por Mendoza et al. (2011) donde se propone que la fuerza gravitacional está dada por la siguiente expresión;

$$f(x) = a_0 x \frac{1 - x^n}{1 - x^{n-1}}. \tag{1.4}$$

Donde x es un parámetro a dimensional definido como; $x := \frac{l_M}{r}$ y $l_M := \sqrt{(GM(r)/a_0)}$, vemos que en el límite donde $a \gg a_0$, es decir cuando $x \gg 1$, recobramos la fuerza gravitacional newtoniana:

$$f(x) \longrightarrow a_o x^2 = \frac{GM(r)}{r^2} \tag{1.5}$$

y cuando tenemos $a \ll a_0$, es decir $x \ll 1$ es equivalente a MOND;

$$f(x) \longrightarrow a_o x = \frac{(Ga_0 M(r))^{1/2}}{r} \tag{1.6}$$

Esta propuesta ha demostrado ser consistente con las restricciones observacionales a la dinámica del Sistema Solar, con la curva de rotación estimada para nuestra galaxia y cuenta con una versión relativista (Bernal et al. 2011) que recientemente a mostrado ser consistente con las observaciones de lentes gravitacionales (Mendoza et al. 2012).

1.0.3. Motivación y objetivos de la tesis

Las propuestas de gravedad modificada cuyos límites a velocidades no relativistas y a aceleraciones menores que a_0 son tipo MOND tienen dos predicciones que pueden ser probadas en sistemas astronómicos:

I. En el régimen de aceleraciones bajas, $a < a_0$, donde en el caso de asumir como validas la relatividad general y su límite clásico la dinámica newtoniana se

requiere materia oscura, los sistemas astronómicos se caracterizan por velocidades de equilibrio que no dependen de la distancia.

II. Existe una relación del tipo $M \propto v^4$ ($\sigma^4 \propto M$) (Tully-Fisher)

Es importante notar que no se conoce ningún sistema donde $a >> a_0$ y se necesite materia oscura para explicar la dinámica, ni uno donde $a << a_0$ y no se necesite materia oscura.

En esta tesis pondremos a prueba en estrellas binarias abiertas con separaciones tales que su aceleración relativa es menor que a_0 la predicción de las teorías de gravedad modificada y veremos si la distribución de velocidades relativas de estos sistemas es consistente con un límite superior constante como lo esperan los esquemas de gravedad modificada o es consistente con la tercera ley de Kepler.

Usaremos mediciones recientes en la dispersión de velocidades como función del radio en cúmulos globulares donde las observaciones muestran un perfil que se aplana en escalas donde la aceleración es del orden de a_0 (Scarpa et al. 2011), en el modelo de materia oscura estos objetos tendrían que ser puramente newtonianos y no hay razón para que la dispersión de velocidades permanezca constante en la periferia del cúmulo. Veremos si una ley de gravedad modificada es capaz de explicar el perfil de dispersión de velocidades de estos objetos con las restricciones observacionales existentes.

En la literatura suele explicarse este comportamiento en los CGs en el contexto de la dinámica newtoniana como consecuencia de las fuerzas de marea galácticas, también veremos si está explicación es realmente viable.

Como una prueba de consistencia al modelo hecho para los CGs, lo aplicaremos a una escala de masa y tamaño varios ordenes de magnitud diferentes, lo usaremos para modelar la galaxia elíptica gigante NGC 4649.

Otra consecuencia de los esquemas de gravedad modificada es que cualquier halo isotérmico de partículas de prueba alrededor de una distribución esférica de masa debe adoptar una configuración de equilibrio que en primera aproximación satisface $\rho \propto r^{-3}$, veremos que observaciones en diferentes sistemas astronómicos muestran que esto efectivamente ocurre.

Por último exploraremos un posible escenario de formación de estructura en un contexto de gravedad modificada.

Capítulo 2

Estrellas binarias abiertas

2.1. Resumen

En los esquemas de GM donde se espera un cambio de régimen en la ley de gravedad en lugares donde la aceleración es del orden de $a_0 = 1.2 \times 10^{-8} cm/s^2$, un sistema de estrellas binarias con separaciones mayores a $7000 UA$ y con las masas de sus componentes de alrededor de $1 M_\odot$ representa el sistema más simple donde se puede observar este cambio en el comportamiento de la fuerza de gravedad.

Los sistemas binarios con estas características tienen aceleraciones relativas menores a a_0. Para estos sistemas la gravedad newtoniana predice velocidades relativas que decaen con la raíz cuadrada de la separación entre las estrellas, mientras que en un esquema de GM se espera que esta velocidad sea constante.

Para averiguar cual de las dos descripciones de la fuerza de gravedad es la que se corresponde a las observaciones de los movimientos de las estrellas binarias abiertas en este artículo estudiamos dos muestras independientes de sistemas binarios con separaciones del sistema mayores que $10^4 UA$.

El primer catálogo corresponde a datos del satélite Hipparcos que consiste en 280 sistemas con alrededor de 10 % de falsos positivos y un valor señal a rudo de ~ 2 para los valores de las velocidades relativas. El segundo catalogo es obtenido de datos del satélite Sloan Digital Sky Survey (SDSS), con 1250 sistemas binarios con una relación señal a ruido en sus velocidades relativas de ~ 0.5. Ambos catálogos contienen movimientos propios en dos dimensiones de cada sistema, sus separaciones angulares y sus respectivas distancias. Los datos para construir cada muestra son tomados de manera independiente.

Cada teoría de gravedad espera un resultado distinto, en el caso de la gravedad newtoniana lo que se espera observar es que la distribución de velocidades relativas proyectadas tenga un límite máximo, $\Delta V = 2 \left(\frac{GM}{s} \right)^{1/2}$, para el caso de GM esperamos un límite superior constante de acuerdo con $V = (GMa_0)^{1/4}$.

2. ESTRELLAS BINARIAS ABIERTAS

Tomando en cuenta que la dinámica de un sistema de estrellas binarias puede ser afectada por las fuerzas de marea galácticas, por encuentros con otras estrellas y una serie de otras interacciones propias del ambiente galáctico en el que están sumergidas, estos factores pueden alterar el rango de separaciones y velocidades relativas en el que actualmente se encuentran.

Afortunadamente en trabajo donde (Jiang & Tremaine 2010) se estudia numéricamente la evolución de $50,000$ sistemas binarios de $1M_{\odot}$ en un ambiente galáctico para obtener así la distribución al día de hoy de la velocidad cuadrática media como función de la separación de estos sistemas dentro de la dinámica newtoniana, en este articulo comparamos las observaciones de los dos catálogos que usamos con el modelo de los autores para tener así un análisis adecuado del tipo de ley de gravedad que favorecen las estrellas binarias abiertas que se encuentran en el régimen de aceleración $a < a_0$.

Nuestros resultados muestran que estrellas binarias abiertas con separaciones mayores a $7000UA$ que se encuentran en el régimen donde de aceleración $a < a_0$ la distribución de las velocidades relativas presenta un límite superior constante como lo esperan los esquemas de gravedad modificada y en contradicción con la la tercera ley de Kepler y aún incorporando los efectos debidos a la interacciones que este sistema puede sufrir en su evolución dentro de la galaxia esta tendencia se mantiene.

En este trabajo participe en la extracción de todos los datos necesarios de los catálogos usados para hacer el estudio y en el cálculo de las cantidades involucradas para realizar las gráficas que aparecen en el mismo, también participe en su escritura y en todo el proceso de revisión hasta que fue publicado.

Eur. Phys. J. C (2012) 72:1884
DOI 10.1140/epjc/s10052-012-1884-6

THE EUROPEAN PHYSICAL JOURNAL C

Regular Article - Theoretical Physics

Wide binaries as a critical test of classical gravity

X. Hernandez[a], **M.A. Jiménez**[b], **C. Allen**[c]

Instituto de Astronomía, Universidad Nacional Autónoma de México, AP 70-264, México, Distrito Federal 04510, México

Received: 23 January 2012 / Published online: 21 February 2012

Abstract Modified gravity scenarios where a change of regime appears at acceleration scales $a < a_0$ have been proposed. Since for $1M_\odot$ systems the acceleration drops below a_0 at scales of around 7000 AU, a statistical survey of wide binaries with relative velocities and separations reaching 10^4 AU and beyond should prove useful to the above debate. We apply the proposed test to the best currently available data. Results show a constant upper limit to the relative velocities in wide binaries which is independent of separation for over three orders of magnitude, in analogy with galactic flat rotation curves in the same $a < a_0$ acceleration regime. Our results are suggestive of a breakdown of Kepler's third law beyond $a \approx a_0$ scales, in accordance with generic predictions of modified gravity theories designed not to require any dark matter at galactic scales and beyond.

1 Introduction

Over the past few years the dominant explanation for the large mass to light ratios inferred for galactic and metagalactic systems, that these are embedded within massive dark matter halos, has begun to be challenged. Direct detection of the dark matter particles, in spite of decades of extensive and dedicated searches, remains lacking. This has led some to interpret the velocity dispersion measurements of stars in the local dSph galaxies (e.g. [2, 13]), the extended and flat rotation curves of spiral galaxies (e.g. [19, 24]), the large velocity dispersions of galaxies in clusters (e.g. [21]), stellar dynamics in elliptical galaxies (e.g. [23]), the gravitational lensing due to massive galaxies (e.g. [9, 31]), and even the cosmologically inferred matter content for the universe through CMB and structure formation physics (e.g. [12, 22, 28]), not as indirect evidence for the existence of a dominant dark matter component, but as direct evidence for the failure of the current Newtonian and general relativistic theories of gravity, in the large scale or low acceleration regimes relevant for the above situations.

Numerous alternative theories of gravity have recently appeared (e.g. TeVeS of [3], and variations; [5, 29], F(R) theories e.g. [6, 7, 27], conformal gravity theories e.g. [18]), mostly grounded on geometrical extensions to general relativity, and leading to laws of gravity which in the large scale or low acceleration regime, mimic the MOdified Newtonian Dynamics (MOND) fitting formulae. Similarly, [20] have explored MOND not as a modification to Newton's second law, but as a modified gravitational force law in the Newtonian regime, finding a good agreement with observed dynamics across galactic scales without requiring dark matter. In fact, recently [4] have constructed an $f(R)$ extension to general relativity which in the low velocity limit converges to the above approach.

Whilst classical gravity augmented by the dark matter hypothesis provides a coherent and unified interpretation from galactic to cosmological scales (with the inclusion of dark energy), the very profusion of modified gravity theories, mostly tested in very localised situations, points to the lack of any definitive theoretical contender to classical gravity. Nonetheless, a generic feature of all of the modified gravity schemes mentioned above is the appearance of an acceleration scale, a_0, above which classical gravity is recovered, and below which the dark matter mimicking regime appears. The latter feature results in a general prediction; all systems where $a \gg a_0$ should appear as devoid of dark matter, and all systems where $a \ll a_0$ should appear as dark matter dominated, when interpreted under classical gravity. It is interesting that no $a \gg a_0$ system has ever been detected where dark matter needs to be invoked, in accordance with the former condition. On the other hand, the latter condition furnishes a testable prediction, in relation to the orbits of wide binaries. For test particles in orbit around a $1M_\odot$ star, in circular orbits of radius s, the acceleration is expected to drop below $a_0 \approx 1.2 \times 10^{-10}$ m/s^2 for $s > 7000$ AU $= 3.4 \times 10^{-2}$ pc. The above provides a test for the dark matter/ modified theories of gravity debate; the relative velocities of components

[a] e-mail: xavier@astroscu.unam.mx
[b] e-mail: mjimenez@astro.unam.mx
[c] e-mail: chris@astroscu.unam.mx

of binary stars with large physical separations should deviate from Kepler's third law under the latter interpretation.

More specifically, seen as an equivalent Newtonian force law, beyond $s \approx 7000$ AU the gravitational force should gradually switch from the classical form of $F_N = GM/s^2$ to $F_{\rm MG} = (GMa_0)^{1/2}/s$, and hence the orbital velocity, $V^2/s = F$, should no longer decrease with separation, but settle at a constant value, dependent only on the total mass of the system through $V = (GMa_0)^{1/4}$. That is, under modified gravity theories, binary stars with physical separations beyond around 7000 AU should exhibit "flat rotation curves" and a "Tully–Fisher relation", as galactic systems in the same acceleration regime do.

An interesting precedent in this sense is given by the recent results of [25] and [26] who find evidence for a transition in the dynamics of stars in the outer regions of a series of Galactic globular clusters. These authors report a flattening of the velocity dispersion profile in globular clusters, outwards of the radius where accelerations fall below the a_0 threshold, in accordance with generic predictions of modified gravity schemes. The interpretation under Newtonian dynamics explains the observed flattening as due to tidal heating by the Milky Way, e.g. [17], but the matter is still being debated. We also note the recent results of [16] who point out various discrepancies between standard ΛCDM predictions and structural and dynamical properties of the local group, and suggest solutions to these in the context of modified gravity theories.

In this paper we propose that wide binary orbits may be used to test Newtonian gravity in the low acceleration regime. We apply this test to the binaries of two very recent catalogues containing relative velocities and separations of wide binaries. The two catalogues are entirely independent in their approaches. The first one, [27] uses data from the *Hipparcos* satellite to yield a moderate number of systems (280) relatively devoid of false positives (10%), with a high average signal to noise ratio for the relative velocities of the binaries ($\sim$2). The second, [10] identifies 1,250 wide binaries from the Sloan Digital Sky Survey (SDSS) data base release 7, which, compounded with a detailed galactic stellar distribution model, results in pairs with a very low probability of chance alignment ($<$2%), albeit with a low average signal to noise ratio in their relative velocities ($\sim$0.5).

The paper is organised as follows: Sect. 2 briefly gives the expectations for the distribution of relative velocities as a function of separation for wide binaries, under both Newtonian gravity and generically for modified theories of gravity. In Sect. 3 we show the results of applying the test to the [27] *Hipparcos* catalogue, and to the independent [10] SDSS data. Our conclusions are summarised in Sect. 4.

2 Expected relative velocity distributions for wide binaries

Since orbital periods for $1M_\odot$ binaries with separations in the tens of AU range already extend into the centuries, there is no hope of testing the prediction we are interested in through direct orbital mapping. Fortunately, modern relative proper motion studies do reach binary separations upwards of 10^4 AU, e.g. [1, 8, 10]. The Newtonian prediction for the relative velocities of the two components of binaries having circular orbits, when plotted against the binary physical separation, s, is for a scaling of $\Delta V \propto s^{-1/2}$, essentially following Kepler's third law, provided the range of masses involved were narrow.

In a relative proper motion sample however, only two components of the relative velocity appear, as velocity along the line of sight to the binary leads to no proper motion. Thus, orbital projection plays a part, with systems having orbital planes along the line of sight sometimes appearing as having no relative proper motions. A further effect comes from any degree of orbital ellipticity present; it is hence clear that the trend for $\Delta V \propto s^{-1/2}$ described above, will only provide an upper limit to the distribution of projected ΔV vs. s expected in any real observed sample, even if only a narrow range of masses is included. One should expect a range of measured values of projected ΔV at a fixed observed projected s, all extending below the Newtonian limit, which for equal mass binaries in circular orbits gives

$$\Delta V_N = 2\left(\frac{GM}{s}\right)^{1/2}. \tag{1}$$

The problem is complicated further by the dynamical evolution of any population of binaries in the Galactic environment. Over time, the orbital parameters of wide binaries will evolve due to the effects of Galactic tidal forces. Also, dynamical encounters with other stars in the field will modify the range of separations and relative velocities, specially in the case of wide binaries. To first order, one would expect little evolution for binaries tighter than the tidal limit of the problem, and the eventual dissolution of wider systems.

A very detailed study of all these points has recently appeared, [15]. These authors numerically follow populations of 50,000 $1M_\odot$ binaries in the Galactic environment, accounting for the evolution of the orbital parameters of each due to the cumulative effects of the Galactic tidal field at the solar radius. Also, the effects of close and long range encounters with other stars in the field are carefully included, to yield a present day distribution of separations and relative velocities for an extensive population of wide binaries, under Newtonian gravity. Interestingly, one of the main findings is that although little evolution occurs for separations below the effective tidal radius of the problem, calculated to be of 1.7 pc, the situation for grater separations is much more complex than the simple disappearance of such pairs.

It is found that when many wide binaries cross their Jacobi radius, the two components remain fairly close by in both coordinate and velocity space, drifting in the Galactic potential along very similar orbits. This means that in any real wide binary search a number of wide pairs with separations larger than their Jacobi radii will appear. Finally, [15] obtain the RMS one-dimensional relative velocity difference, ΔV_{1D}, projected along an arbitrary line of sight, for the entire populations of binaries dynamically evolved over 10 Gyr to today, for a distribution of initial ellipticities, as plotted against the projected separation on the sky for each pair. The expected Keplerian fall of $\Delta V_{1D} \propto s^{-1/2}$ for separations below 1.7 pc is obtained, followed by a slight rise in ΔV_{1D} as wide systems cross the Jacobi radius threshold. ΔV_{1D} then settles at RMS values of ≈0.1 km/s.

These authors also explore variation in the initial (realistic) distribution of semi-major axes, and the formation history of the binaries, finding slight differences in the results, which however are quite robust to all the variations in the parameters explored, in the regime we are interested of present day projected separations larger than $\log(s/\mathrm{pc}) > -2$, above very small variations of less than 0.14 in the logarithm. This represents the best currently available estimate of how relative velocities should scale with projected separations for binary stars (both bound and in the process of dissolving in the Galactic tides) under Newtonian gravity.

The testable quantitative prediction of Classical Gravity for the distribution of data in a plot of projected ΔV vs. projected s is clear: one should find a spread of points extending below the limit defined by (1), with an RMS value for ΔV_{1D} given by the results of [15], their Fig. 7.

The recent proliferation of modified gravity models however, implies the absence of a definitive alternative to classical gravity. Further, in many cases, the complex formulations put forth do not lend themselves to straightforward manipulations from which detailed predictions might be extracted for varied applications distinct from the particular problems under which such models are presented. We shall therefore not attempt to test any particular modified gravity theory, but shall only consider the generic predictions such theories make for "flat rotation curves" in the $a < a_0$ regime. That is, the predictions of modified gravity schemes will only be considered qualitatively and generically, to first order, in terms of the upper envelope of observed distributions in projected ΔV vs. s plots to appear flat. For circular orbits one expects:

$$\Delta V_{\mathrm{MG}} = C(GMa_0)^{1/4}, \tag{2}$$

where C is a model-dependent constant expected to be of order unity. A further correction upwards due to departures from circularity, which at this point must be thought of as dependent on the details of the particular modified gravity scheme one might pick, should also be included. This correction will tend to give even larger values of ΔV_{MG}. We note that in the particular case of MOND, the external field effect, the fact that the overall potential of the Galaxy at the solar neighbourhood globally puts local binaries close to the $a = a_0$ threshold, would imply only slight corrections on Newtonian predictions.

We see that all we need is a large sample of relative proper motion and binary separation measurements to test the Newtonian prediction for the RMS values of the 1 dimensional relative velocities of [15], and to contrast the $\Delta V_N \propto s^{-1/2}$ and the $\Delta V_{\mathrm{MG}} = cte.$ predictions for the upper envelope of the ΔV vs. s distributions. It is important to have a sample as free of chance alignments as possible, as the inclusion of non-physical stellar pairs would blur the test, potentially making a conclusion suspect. Also, it is desirable to limit the range of masses of the stars involved, as a spread in mass will also blur any trends expected for the upper limit of the ΔV distributions, although not terribly so, given the small powers to which mass appears in both predictions.

To end this section we briefly recall the first order tidal limit calculation of

$$\left.\frac{dF_{\mathrm{ext}}(R)}{dR}\right|_{R_0} \Delta r = \frac{GM_s^2}{(\Delta r)^2} \tag{3}$$

which leads to the tidal density stability condition of $\rho_s > \overline{\rho}$ for the density of a satellite of extent Δr and mass M_s orbiting at a distance R_0 from the centre of a spherical mass distribution $M(R)$ having an average matter density $\overline{\rho}$ internal to R_0 resulting in a gravitational force $F_{\mathrm{ext}}(R)$, under the assumption $\Delta r \ll R$. The equivalent calculation under the force law given by the $a \ll a_0$ limit of $F_{\mathrm{MG}} = (GMa_0)^{1/2}/R$ is given by

$$\frac{(GM(R)a_0)^{1/2}}{R^2}\Delta r = \frac{(GM_s a_0)^{1/2}}{\Delta r}, \tag{4}$$

leading to

$$\rho_s > \left(\frac{\Delta r}{R}\right)\overline{\rho}, \tag{5}$$

as the equivalent of the classical tidal density criterion, as a first generic approximation under modified gravity. Since the spatial extent of wide binaries will always be much smaller that their Galactocentric radii, (5) shows that under modified gravity, to first order, wide binaries will be much more robust to tides than under Newtonian gravity. In the following section we apply the test we have identified to two recent catalogues of wide binaries which became available over the previous year, the SLoWPoKES catalogue of SDSS wide binaries by [10] and the *Hipparcos* satellite wide binaries catalogue of [27].

3 Observed wide binary Samples

3.1 The Hipparcos wide binaries

The [27] catalogue of very wide binaries was constructed through a full Bayesian analysis of the combined *Hipparcos* data base, the new reduction of the *Hipparcos* catalogue, [30], the Tycho-2 catalogue, [14] and the *Tycho* double star catalogue, [11] mostly, amongst others. There, probable wide binaries are identified by assigning a probability above chance alignment to the stars analysed by carefully comparing to the underlying background (and its variations) in a 5 dimensional parameter space of proper motions and spatial positions. The authors have taken care to account for the distortions introduced by the spherical projection on the relative proper motion measurements, $\Delta\mu$. When angular separations cease to be small, small relative physical velocities between an associated pair of stars might result in large values of $\Delta\mu$. A correction of this effect is introduced, to keep $\Delta\mu$ values comparable across the whole binary separation range studied.

We have taken this catalogue and kept only binaries with a probability of non-chance alignment greater than 0.9. The wide binary search criteria used by the authors requires that the proposed binary should have no near neighbours; the projected separation between the two components is thus always many times smaller than the typical interstellar separation, see [27]. We use the reported distances to the primaries, where errors are smallest, to calculate projected ΔV and projected s from the measured $\Delta\mu$ and $\Delta\theta$ values reported by [27]. Although the use of *Hipparcos* measurements guarantees the best available quality in the data, we have also further pruned the catalogue to remove all binaries for which the final signal to noise ratio in the relative velocities on the plane of the sky was lower than 0.3.

We plot in Fig. 1 a sample of 280 binaries constructed as described above, having distances to the Sun within $6 < d < 100$ in pc. The slanted line gives the Newtonian prediction of (1) to the upper limit expected on the relative velocities shown, which appears in conflict with it, as they are defined by a neat horizontal upper limit, as generically predicted by modified gravity theories, (2). Figure 1 could then be a first direct evidence of the breakdown of classical gravity theories in the low acceleration regime of $a < a_0$.

The average signal to noise ratio for the data in Fig. 2 is 1.7, with an average error on ΔV of 0.83 km/s, which considering a 2σ factor from the top of the distribution to the real underlying upper limit for the sample, results in 3 km/s as our estimate of the actual physical upper limit in ΔV. Comparing with (2), the factor accounting for non-circular orbits in modified gravity comes to 4.5. That this factor is significantly larger than the $\sqrt{2}$ of Newtonian gravity is to be expected, as objects are much more tightly bound in MOND-type schemes.

3.2 The SDSS wide binaries

The Sloan low mass wide pairs catalogue (SLoWPoKES) of [10] contains a little over 1,200 wide binaries with relative proper motions for each pair, distances and angular separations. Also, extreme care was taken to include only physical binaries, with a full galactic population model used to exclude chance alignment stars using galactic coordinates and galactic velocities, resulting in an estimate of fewer than 2% of false positives. As with the *Hipparcos* sample, this last requirement yields only isolated binaries with no neighbours within many times the internal binary separation. We have also excluded all systems with white dwarfs or subdwarf primaries, where distance calibrations are somewhat uncertain. As was also done for the *Hipparcos* sample, all triple systems reported in the catalogue were completely excluded from the analysis.

Given the large range of distances to the SDSS binaries ($46 < d/\mathrm{pc} < 992$), we select only 1/3 of the sample lying within the narrow distance range ($225 < d/\mathrm{pc} < 338$), which forms the most homogeneous set in terms of the errors in ΔV, excluding data with large errors at large distances. Again, we use the reported distances to the primaries, where errors are smallest, to calculate projected ΔV and projected s from the measured $\Delta\mu$, $\Delta\theta$ and d values reported by [10], to plot Fig. 2. The figure shows 417 binaries with average signal to noise ratio and average errors on ΔV of 0.5 and 11.3 km/s, respectively.

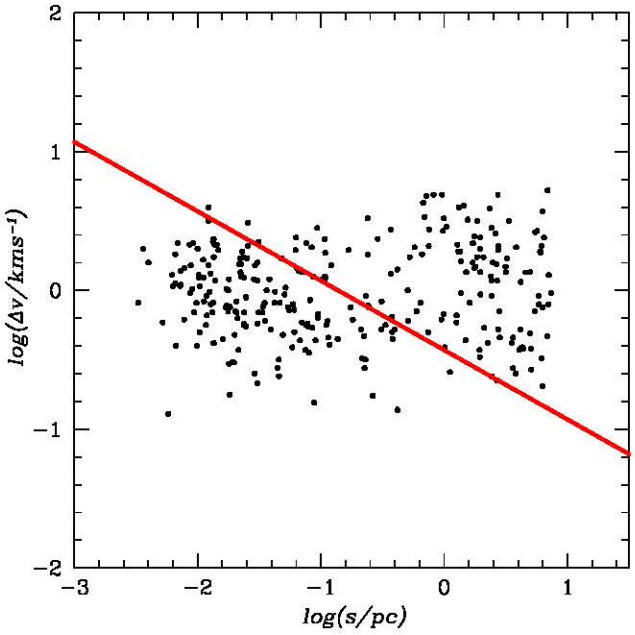

Fig. 1 The figure shows projected relative velocities and separations for each pair of wide binaries from the [27] *Hipparcos* catalogue having a probability of being the result of chance alignment <0.1. The average value for the signal to noise ratio for the sample shown is 1.7. The upper limit shows the flat trend expected from modified gravity theories, at odds with Kepler's third law, shown by the $s^{-1/2}$ *solid line*

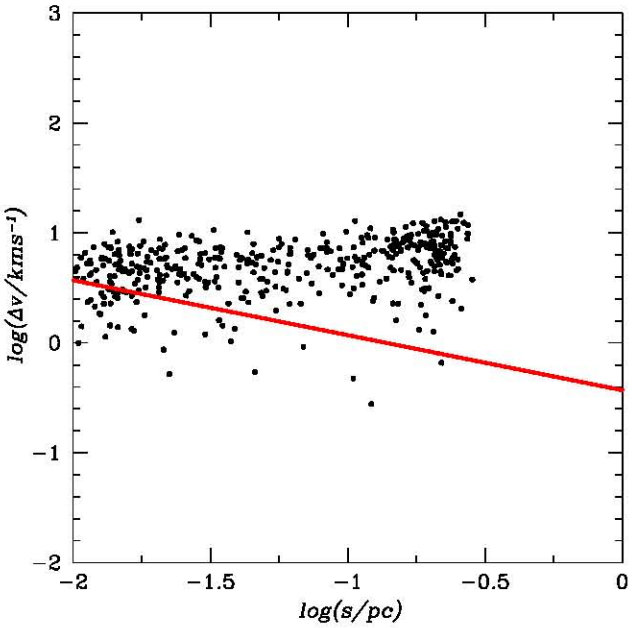

Fig. 2 The figure shows projected relative velocities and separations for each pair of wide binaries from the [10] SDSS catalogue within the distance range ($225 < d/\mathrm{pc} < 338$). The average value for the signal to noise ratio for the sample shown is 0.5. The upper limit shows the flat trend expected from modified gravity theories, at odds with Kepler's third law, shown by the $s^{-1/2}$ *solid line*

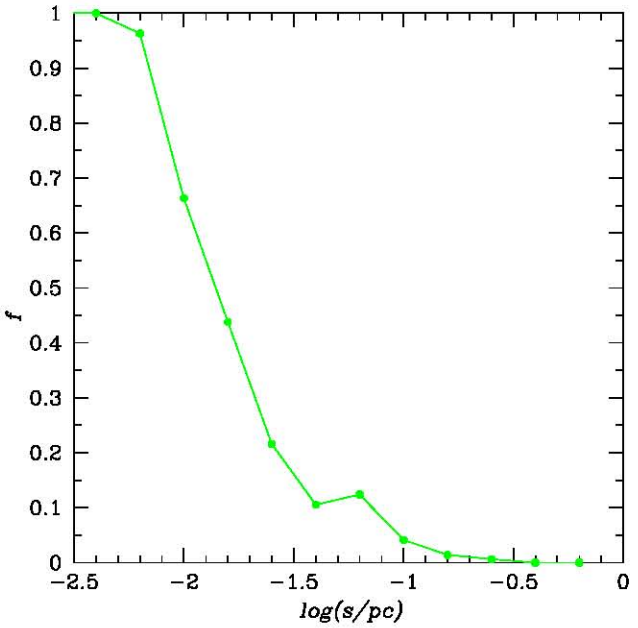

Fig. 3 The figure shows the number of systems with ΔV values below the Newtonian upper limit prediction of (1), as a fraction of the total per bin, for the SDSS data of [10], as a function of projected binary separations

The slanted solid line gives the Newtonian prediction of (1). It is clear that the upper envelope of the distribution of ΔV measurements from the catalogue does not comply with Kepler's third law. As was the case with the *Hipparcos* sample, the upper envelope of the distribution of observed measurements describes a flat line, as expected under modified gravity schemes.

Figure 3 is a plot of the number of SLoWPoKES systems for the full distance range, with ΔV values below the Newtonian prediction of (1), and hence consistent with it, as a fraction of the total per bin, as a function of projected binary separations. We see this fraction starts off being consistent with 1, but begins to decrease on approaching $\log(s/\mathrm{pc}) \approx -2$, after which point it rapidly drops, to end up consistent with 0 on reaching separations of around $\log(s/\mathrm{pc}) \approx -1$. Again, the result matches the qualitative generic expectations of modified gravity schemes, but would call for further explanations under classical gravity.

The average signal to noise values in ΔV for the full distance range of the [10] catalogue is 0.48. The average error on ΔV for the full SDSS sample is 12 km/s, which considering a 2σ factor from the top of the complete distribution to the real underlying upper limit, results in the same 3 km/s as obtained for the [27] *Hipparcos* catalogue.

We end this section with Fig. 4, where we calculate the RMS value of the one-dimensional relative velocity difference for both of the samples discussed, after binning the

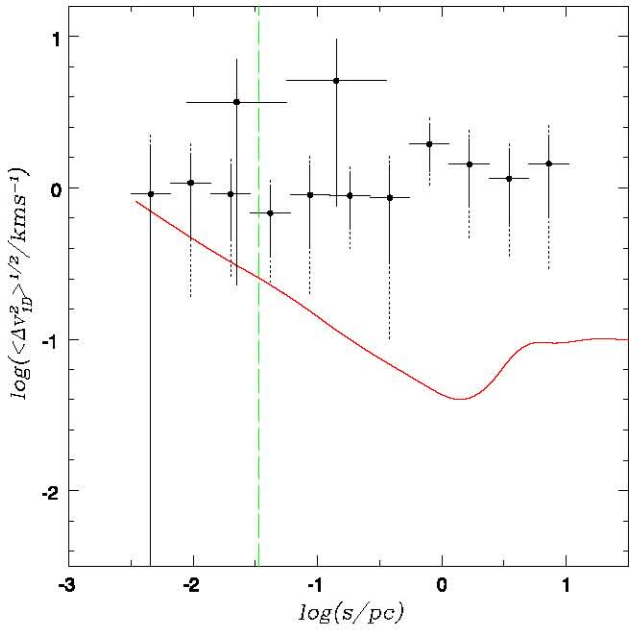

Fig. 4 The *solid curve* gives the RMS values for one dimensional projected relative velocities as a function of projected separations, for the detailed dynamical modelling of large populations of wide binaries evolving in the Galactic environment, taken from [15]. The same quantity for the data from the catalogues analysed is given by the points with error bars; those with narrow $\log(s)$ intervals being from the *Hipparcos* sample of [27], and those two with wide $\log(s)$ intervals coming from the SDSS sample of [10]

data into constant logarithmic intervals in s. This quantity is given by the points, where the error bars simply show the propagation of the errors on $\Delta\mu$ and d, reported by the au-

thors of the catalogues. We construct ΔV_{1D} by considering only one coordinate of the two available from the relative motion on the plane of the sky. Thus, each binary can furnish two ΔV_{1D} measurements, which statistically should not introduce any bias. Indeed, using only $\Delta\mu_l$ or only $\Delta\mu_b$ or both for each binary, yields the same mean values for the points shown. The small solid error bars result from considering an enlarged sample where each binary contributes two ΔV_{1D} measurements, while the larger dotted ones come from considering each binary only once, and do not change if we consider only $\Delta\mu_l$ or only $\Delta\mu_b$. The series of small $\log(s)$ interval data are for the *Hipparcos* catalogue of [27], while the two broader crosses show results for the [10] SDSS sample of Fig. 2. For this last case, the much larger intrinsic errors mean that to compensate through weight of numbers the low signal to noise ratio of this catalogue, imposes the loss of separation resolution through the use of only two bins, with vertical error bars which are only relevant if the sample is doubled, as described above.

The solid curve is the Newtonian prediction of the full Galactic evolutionary model of [15] for a randomly oriented population of wide binaries with a realistic distribution of eccentricities, both bound and in the process of dissolving. Note that the results of this simulation deviate from Kepler's law for s larger than the Newtonian Jacobi radius of the problem of 1.7 pc, whereas the deviation shown by the samples of binaries studied also occur at much smaller separations (see below). Even considering the large error bars, where each binary contributes only one ΔV_{1D} value, we see eight points lying beyond 1σ, making the probability of consistency between this prediction and the observations of less than $(0.272)^8 = 3 \times 10^{-5}$. The only point where this model is slightly at odds with the selection of the *Hipparcos* sample of [27], is that [15] assume $1M_{\odot}$ stars for their binaries, while the typical mass of the stars in the binaries we examine is closer to $0.5M_{\odot}$. This detail would only shift the Newtonian prediction a factor of $2^{1/2}$ further away from the measurements. We obtain an RMS value for ΔV_{1D} compatible with a horizontal line at 1 km/s, in qualitative agreement with expectations from modified gravity schemes. The vertical dashed line marks the $a = a_0$ threshold; we clearly see the data departing from the Newtonian prediction outwards of this line, and not before.

Under Newtonian Gravity one would need to look for an alternative dynamical dissociation and heating mechanism for the binaries we analyse which might result in relative velocities an order of magnitude above the results obtained by [15]. The *Hipparcos* catalogue has been closely studied for over a decade, and not only the values reported, but also the uncertainties in them are now well established. It is highly unlikely that these confidence intervals might have been systematically underestimated by the community by a factor of 3, as would be required for the data in Fig. 4 to be consistent with the Newtonian prediction of [15].

The two SDSS points are clearly consistent with the *Hipparcos* measurements, but given the much larger error bars, they are also marginally consistent with the Newtonian prediction at a 2σ level. A fuller discussion of the robustness of our results to the various sample selection effects and errors involved appears in the appendix.

The consistency of the results obtained from both catalogues provides a check of the physical reality of the trends presented. The two completely independent, very carefully constructed catalogues, each using different sets of selection criteria, each perhaps subject to its own independent systematics, are consistent with the same result, a constant horizontal upper envelope for the distribution of relative velocities on the plane of the sky at an intrinsic value of 3 km/s $\pm$ 1 km/s, extending over three orders of magnitude in s, with a constant RMS ΔV_{1D} value consistent with 1 km/s $\pm$ 0.5 km/s. This supports the interpretation of the effect detected as the generic prediction of modified gravity theories.

Given the relevance of the subject matter discussed, it would be highly desirable to obtain an independent confirmation, ideally using a purposely designed sample including cuts at a variety of stellar masses, in order to test the scaling of the fourth power of the dynamical velocities with mass expected under modified gravity schemes. To include also radial velocity measurements would require sampling over many epochs, as the only way to allow for the effects of nearby companions in these frequently hierarchical systems.

4 Conclusions

We have identified a critical test in the classical gravity/modified gravity debate, using the relative velocities of wide binaries with separations in excess of 7000 AU, as these occupy the $a < a_0$ regime characteristic of modified gravity models. We present a first application of this critical test using the best currently available data; a large sample of wide binaries from the SDSS with low signal to noise on the relative velocities, and a smaller *Hipparcos* satellite sample with signal to noise $\sim$2 on the relative velocities of the binaries sampled.

Results show constant relative RMS velocities for the binary stars in question, irrespective of their separation, in the $a < a_0$ regime sampled. This is quantitatively inconsistent with detailed predictions of Newtonian dynamical models for large populations of binaries evolving in the local galactic environment.

Our results are qualitatively in accordance with generic modified gravity models constructed to explain galactic dynamics in the absence of dark matter, where one expects constant relative velocities for binary stars, irrespective of their separation, in the $a < a_0$ regime sampled.

Acknowledgements The authors wish to thank Arcadio Poveda and Pavel Kroupa for insightful discussions on the subject treated here. Alejandra Jimenez acknowledges financial support from a CONACYT scholarship. Xavier Hernandez acknowledges financial support from UNAM- DGAPA grant IN103011.

Appendix: Calculation of confidence intervals

We begin this section with a discussion of various analyses performed to test for the possibility that our results could have been driven by potential systematics and selection effects in the catalogues.

We first test for the option that the results of Figs. 1 and 2 were distorted from the Newtonian prediction by errors which correlate with the separation of the binaries, increasing as the separation increases, to yield the trends obtained. For the *Hipparcos* sample we ranked the binaries by separation, s, and calculated the average errors on the resulting ΔV in each the tightest third, middle third and widest third of the binaries, yielding values 0.8 (0.4), 0.7 (0.11) and 1.0 (0.4) respectively, in km/s. The numbers in parentheses giving the dispersion of the distributions of errors in each of the three thirds of the sample. It can be seen that there is no increase either in the average values of the errors in ΔV, or in the width of the distributions of errors, with increasing binary separations. For the SDSS sample the average errors in ΔV show only a very slight increase of a factor of 1.3 over the entire range probed. Thus, for both samples, the trends of Figs. 1, 2 and 4 cannot be explained as arising from the Newtonian prediction and an increase in the errors with binary separation. In essence, the data presented are inconsistent with the Newtonian prediction not because of differences in the details of the trends, but because the former presents multiple real detections at a level of 3 km/s $\pm$ 1 km/s, while the latter is smaller by an order of magnitude. The resulting RMS values for the various data points are of $\approx$1 km/s $\pm$ 0.5 km/s, while the Newtonian prediction lies below the detection by about a factor of 10.

We next check against systematics in the catalogues, which would preferentially arise in the lower signal to noise points, or alternatively, in the most distant ones. For the *Hipparcos* sample, we repeat the experiment including only points with a signal to noise ratio on $\Delta V > 1$, and then including only the binaries nearest to earth with $d < 50$ pc. These two sub-samples have 186 and 130 binaries, with average signal to noise ratios on ΔV above the value of 1.7 of Fig. 1, of 2 and 2.2 respectively, and yield results indistinguishable from Figs. 1 and 4. Also, we checked explicitly the results of the SDSS sample for any systematics with distance to the binaries analysed, and found the flat upper envelope to be robust to the choice of distance range taken.

Although no specific cut in resulting ΔV or even on measured $\Delta\mu$ was built into the *Hipparcos* catalogue, the SDSS one includes the selection cut that the signal to noise ratio on $\Delta\mu$ should be <2. We repeat the SDSS analysis tracing the 15% of the points closest to this cut, and find that these, the ones which just made the cut, do not define the flat upper envelope on ΔV. For both the *Hipparcos* and the SDSS samples, any observational bias/truncation would appear in $(\Delta\mu, \Delta\theta)$ space, not in the $(\Delta V, s)$ one.

We end with a detailed description of the calculation of the points in Fig. 4 and their error bars, directly from the data published in the catalogues used. Whenever $z = f(x)$, the error in z is given by $\delta z = |\frac{df}{dx}|\delta x$, where δx is the error in x. If z is a function of several variables $z = f(x_1, x_2, \ldots)$, the absolute error, which we take, is $\delta z = \sum_i |\frac{\partial f}{\partial x_i}|_{x_i}\delta x_i$ which is always greater than the standard deviation $\sigma_z = \sqrt{\sum_i (\frac{\partial f}{\partial x_i}\delta x_i)^2}$.

Following these rules we estimate the absolute error in each ΔV measurement, and in the RMS velocity for the samples studied. For the *Hipparcos* sample we have taken columns 11, 12, 13 and 14 of the online catalogue of [27], which contains the values of the relative motions of each binary and their errors, as well as columns 15 and 16, which contain the distance to the binary, d, and its corresponding error, δd.

For all calculations, we considered the distance to the system as the distance to the primary. For each binary we calculated the projected relative velocity Δv in km/s and its error as

$$\Delta v = 4.74 \times 10^{-3}\Delta\mu d, \tag{A.1}$$

$$\delta(\Delta v) = 4.74 \times 10^{-3}\big(\delta(\Delta\mu)d + \Delta\mu\delta d\big), \tag{A.2}$$

hence, on $(\Delta v)^2$the error is $\delta(\Delta v)^2 = 2\Delta v\delta(\Delta v)$. The RMS velocity is now

$$\Delta v_{\mathrm{RMS}} = \sqrt{\frac{1}{n}\sum_{i=1}^{n}(\Delta v)^2} = \sqrt{\langle(\Delta v)^2\rangle}. \tag{A.3}$$

We then binned the data into constant logarithmic intervals in s with a width of 0.32 and calculated Δv_{RMS} for each bin, n the number of binary systems that fall into each bin. The error in Δv_{RMS} for each bin is now:

$$\delta(\Delta v_{\mathrm{RMS}}) = \frac{1}{2}\frac{\langle\delta(\Delta v)^2\rangle}{\sqrt{\langle(\Delta v)^2\rangle}}. \tag{A.4}$$

To compare with the prediction of the RMS values for the one dimensional projected relative velocities of the evolutionary model of [15] we construct Δv_{RMS} by considering only one coordinate. For the case of the SDSS sample of [10], we have calculated the relative proper motion for each coordinate $\Delta\mu_\alpha = \mu_{\alpha_A} - \mu_{\alpha_B}$ and $\Delta\mu_\delta = \mu_{\delta_A} - \mu_{\delta_B}$ taking columns 18 to 25 of their online catalogue, which contain the proper motions and their errors in equatorial coordinates for each component of the binary system, to estimate the

projected relative velocity we have used column 26 containing the distance to the primary, in this case we consider an error of 15% in the distance and we have followed the same path as in the previous case for calculating the RMS relative velocities and their errors.

References

1. C. Allen, A. Poveda, M.A. Herrera, Astron. Astrophys. **356**, 529 (2000)
2. G.W. Angus, Mon. Not. R. Astron. Soc. **387**, 1481 (2008)
3. J. Bekenstein, Phys. Rev. D **70**, 3509 (2004)
4. T. Bernal, S. Capozziello, J.C. Hidalgo, S. Mendoza, Eur. Phys. J. C **71**, 1794 (2011)
5. J.P. Bruneton, G. Esposito-Farese, Phys. Rev. D **76**, 124012 (2007)
6. S. Capozziello, M. De Laurentis, Phys. Rep. **509**, 167 (2011)
7. S. Capozziello, V.F. Cardone, A. Troisi, Mon. Not. R. Astron. Soc. **375**, 1423 (2007)
8. J. Chaname, A. Gould, Astrophys. J. **601**, 289 (2004)
9. M.C. Chiu, C.M. Ko, Y. Tian, H.S. Zhao, Phys. Rev. D **83**, 06352 (2011)
10. S. Dhital, A.A. West, K.G. Stassun, J.J. Bochanski, Astron. J. **139**, 2566 (2010)
11. C. Fabricius, E. Høg, V.V. Makarov, B.D. Mason, G.L. Wycoff, S.E. Urban, Astron. Astrophys. **384**, 180 (2002)
12. A. Halle, H.S. Zhao, B. Li, Astrophys. J. Suppl. Ser. **177**, 1 (2008)
13. X. Hernandez, S. Mendoza, T. Suarez, T. Bernal, Astron. Astrophys. **514**, A101 (2010)
14. E. Høg et al., Astron. Astrophys. **357**, 367 (2000)
15. Y.F. Jiang, S. Tremaine, Mon. Not. R. Astron. Soc. **401**, 977 (2010)
16. P. Kroupa et al., Astron. Astrophys. **523**, 32 (2010)
17. R. Lane et al., Mon. Not. R. Astron. Soc. **406**, 2732 (2010)
18. P.D. Mannheim, D. Kazanas, Astrophys. J. **342**, 635 (1989)
19. S.S. McGaugh, Phys. Rev. Lett. **106**, 121303 (2011)
20. S. Mendoza, X. Hernandez, J.C. Hidalgo, T. Bernal, Mon. Not. R. Astron. Soc. **411**, 226 (2011)
21. M. Milgrom, R.H. Sanders, Astrophys. J. **678**, 131 (2008)
22. M. Milgrom, Phys. Rev. D **82**, 043523 (2010)
23. N.R. Napolitano, S. Capozziello, A.J. Romanowsky, M. Capaccioli, C. Tortora, Astrophys. J. (2012, in press). arXiv:1201.3363
24. R.H. Sanders, S.S. McGaugh, Annu. Rev. Astron. Astrophys. **40**, 263 (2002)
25. R. Scarpa, G. Marconi, R. Gimuzzi, G. Carraro, Astron. Astrophys. **462**, L9 (2007)
26. R. Scarpa, G. Marconi, G. Carraro, R. Falomo, S. Villanova, Astron. Astrophys. **525**, A148 (2011)
27. E.J. Shaya, R.P. Olling, Astrophys. J. Suppl. Ser. **192**, 2 (2011)
28. C. Skordis, D.F. Mota, P.G. Ferreira, C. Boehm, Phys. Rev. Lett. **96**, 011301 (2006)
29. Y. Sobouti, Astron. Astrophys. **464**, 921 (2007)
30. F. van Leeuwen, Astron. Astrophys. **474**, 653 (2007)
31. H.S. Zhao, B. Famaey, Phys. Rev. D **81**, 087304 (2010)

Capítulo 3

Perfil de dispersión de velocidades asintóticamente plano en cúmulos globulares: modelos con gravedad modificada

3.1. Resumen

Observaciones recientes en cúmulos globulares muestran que la dispersión de velocidades no decrece con la separación al centro del cúmulo como se espera bajo la dinámica newtoniana, sino que se mantiene constante en regiones donde la aceleración es menor que la aceleración de Milgrom $a_0 = 1.2 \times 10^{-8} cm/s^2$. Dentro de un esquema de gravedad modificada se espera tener velocidades de equilibrio constantes cuando la aceleración es del orden de a_0 y qu esta velocidad sea proporcional a la raíz cuarta de la masa bariónica total (relación Tully-Fisher).

En este capítulo construimos modelos de equilibrio dinámico para cúmulos globulares donde el perfil de dispersión de velocidades ha sido medido como función del radio, usamos la ley de fuerza de gravedad modificada propuesta por Mendoza et al. (2011), la cual a mostrado ser consistente con las restricciones impuestas por el sistema solar a una ley de gravedad que se desvie de la newtoniana y con la curva de rotación esperada para nuestra galaxia.

Encontramos que es posible reproducir todas las restricciones observacionales para los cúmulos globulares; el perfil de brillo superficial, la masa total del cúmulo y el perfil de dispersión de velocidades proyectado incluyendo la parte plana. Además usando modelos de síntesis de poblaciones estelares para cada cúmulo estimamos su masa independientemente de cualquier suposición de la dinámica del cúmulo. Como resultado obtenemos que la masa de cada cúmulo globular es pro-

porcional a la cuarta potencia del valor asintótico de la dispersión de velocidades, tal como se espera en los escenarios de gravedad modificada.

Además como una prueba de consistencia de los modelos de equilibrio desarrollados para cúmulos globulares, los aplicamos a la galaxia elíptica gigante NGC 4649, un sistema varios ordenes de magnitud en masa y tamaño mayor que los cúmulos y nuevamente logramos construir modelos de equilibrio para esta galaxia que satisfacen todas las restricciones observacionales incluyendo la parte plana de su perfil de dispersión de velocidades proyectado sin la necesidad de incluir materia oscura. Mientras que los modelos newtonianos requieren un halo de materia oscura con una masa de casi la mitad de la masa total de la galaxia a tres radios efectivos.

Mi participación en estos artículos consistió en desarrollar los modelos de equilibrio y aplicarlos a los cúmulos, y supervisar la elaboración independiente de los mismos modelos del estudiante Gustavo Garcia para que fueran aplicados a NGC 4649, a partir de estos modelos se obtuvieron todos los resultados presentados en el artículo. también participe en la escritura de ambos y en todo el proceso de revisión hasta que fueron publicados.

The Astrophysical Journal, 750:9 (9pp), 2012 May 1 doi:10.1088/0004-637X/750/1/9

THE OUTSKIRTS OF GLOBULAR CLUSTERS AS MODIFIED GRAVITY PROBES

X. Hernandez and M. A. Jiménez
Instituto de Astronomía, Universidad Nacional Autónoma de México, Apartado Postal 70–264, C.P. 04510 México D.F., Mexico; xavier@astroscu.unam.mx
Received 2011 December 6; accepted 2012 February 18; published 2012 April 10

ABSTRACT

In the context of theories of gravity modified to account for the observed dynamics of galactic systems without the need to invoke the existence of dark matter, a prediction often appears regarding low-acceleration systems: wherever a falls below a_0, one should expect a transition from the classical to the modified gravity regime. This modified gravity regime will be characterized by equilibrium velocities that become independent of distance and that scale with the fourth root of the total baryonic mass, $V^4 \propto M$. The two conditions above are the well-known flat rotation curves and Tully–Fisher relations of the galactic regime. Recently, however, a similar phenomenology has been hinted at, at the outskirts of Galactic globular clusters, precisely in the region where $a < a_0$. Radial profiles of the projected velocity dispersion have been observed to stop decreasing along Keplerian expectations and to level off at constant values beyond the radii where $a < a_0$. We have constructed gravitational equilibrium dynamical models for a number of globular clusters for which the above gravitational anomaly has been reported, using a modified Newtonian force law that yields equilibrium velocities equivalent to modified Newtonian dynamics. We find models having an inner Newtonian region and an outer modified gravity regime, which reproduce all observational constraints, surface brightness profiles, total masses, and line-of-sight velocity dispersion profiles, can be easily constructed. Through the use of detailed single stellar population models tuned individually to each of the globular clusters in question, we derive estimates of the total masses for these systems. Interestingly, we find that the asymptotic values of the velocity dispersion profiles are consistent with scaling with the fourth root of the total masses, as expected under modified gravity scenarios.

Key words: globular clusters: general – gravitation – stars: kinematics and dynamics

Online-only material: color figures

1. INTRODUCTION

In the context of modified gravity theories, where the dynamical measurements usually ascribed to the presence of dark matter are interpreted as evidence for a change in the form of gravity, stellar populations in the Galactic halo have proven to be critical test grounds. The relative proximity of many such systems makes them accessible to detailed photometric and spectroscopic kinematical observations, while the total absence of gas in the cases of many dwarf spheroidal satellites (dSph) and globular clusters (GCs) implies these objects present a relatively clean test, as only the measured stellar component must be responsible for the measured dynamics, in the absence of any dark matter.

Galactic dwarf spheroidal satellites appear under classical gravity as the most heavily dark matter dominated systems known and have been modeled extensively under modified Newtonian dynamics (MOND), e.g., Sanchez-Salcedo et al. (2006), Angus (2008), Hernandez et al. (2010), McGaugh & Wolf (2010), and Kroupa et al. (2010) for some recent examples, or equivalently, thinking of MOND as a modified Newtonian force law, rather than a change to Newton's second law, by Mendoza et al. (2011). Sanchez-Salcedo & Hernandez (2007) also studied the problem of the tidal limiting of Galactic GCs and local dSph galaxies comparatively under MOND and dark matter, finding both hypothesis to be consistent with the data, given the present level of observational errors.

One generic prediction of modified gravity theories, designed not to require the hypothesis of dark matter, is that as accelerations fall below $a_0 \approx 1.2 \times 10^{-10}$ m s^{-2}, a transition should occur away from Newtonian gravity (e.g., MOND in Milgrom 1983; TeVeS in Bekenstein 2004; QUMOND, BIMOND in Zhao & Famaey 2010; and modified Newtonian force law in Mendoza et al. 2011). This modified regime will be characterized by equilibrium velocities for test particles orbiting within spherical mass distributions that become constant with distance and that scale with mass as $V^4 \propto M$.

In this sense, the recent studies by Scarpa et al. (2007a, 2007b, 2011) appear particularly exciting, as they find precisely the above-mentioned transition in a number of Galactic GCs, precisely beyond the radius where accelerations fall below a_0.

The modelling of Galactic GCs under modified gravity theories has been studied before, e.g., Baumgardt et al. (2005) study the mean values of the velocity dispersion expected under Newtonian gravity and MOND comparatively, finding larger values are expected in MOND, for GCs in the outer halo of the Milky Way. Moffat & Toth (2008), however, obtain expected values for the mean velocity dispersion of GCs compatible with Newtonian expectations and projected velocity dispersion profiles which fall slower than Newtonian expectations, compatible with the measurements of Scarpa et al. (2007a, 2007b). Haghi et al. (2009) use a MOND N-body code to account for the effects of the external field effect of MOND in the problem and find that the profiles of the projected velocity dispersion of Galactic GCs can serve as a test in constraining modified gravity theories. Using an analytical treatment of the problem under MOND, ignoring the external field effect of MOND, Sollima & Nipoti (2010) construct the MOND equivalent of analytic King profiles, where one limits the extent of the modeled distributions through the Galactic tides, to get models where the velocity dispersion profiles fall to zero. Also, very recently Haghi et al. (2011) again use a numerical MOND N-body code to show that under MOND mean velocity, dispersions of Galactic GCs are expected to be higher than Newtonian.

In this paper, we construct fully self-consistent dynamical models for Galactic GCs using the modified Newtonian force-law formulation of Mendoza et al. (2011) to explore the consistency of that approach. The modeled density profiles are calibrated to match observed surface brightness profiles, projected velocity dispersion radial profiles, and total masses inferred through a careful single stellar population modeling of the GCs in question, taking into account metallicity and age of the relevant stellar populations. We pay particular attention to reproducing the flat outer regions of the velocity dispersion profiles, as recently measured by Drukier et al. (1998), Scarpa & Falomo (2010), and Scarpa et al. (2011).

We find that fully self-consistent equilibrium models can be constructed to match all observational constraints available on Galactic GCs, including the outward flattening of the projected velocity dispersion profiles. To within uncertainties, the same happens under Newtonian gravity (e.g., Drukier et al. 2007; Lane et al. 2010; Küpper et al. 2010), where the kinematics in question are interpreted as evidence of tidal heating by the overall Galactic gravitational field, occurring even in the absence of prominent tidal tails, or contamination of unbound stars. It is interesting that we further find that the masses and asymptotic velocity dispersions of the studied GCs are consistent with a scaling $\sigma^4 \propto M$. This last point strengthens the interpretation of the observed dynamics in the outskirts of Galactic GCs as evidence for modified gravity in general.

In Section 2, we derive the model through which equilibrium profiles for spherically symmetric stellar populations are derived, under the modified Newtonian force law of Mendoza et al. (2011). In Section 3, we show that such models can be easily obtained to satisfy all observed parameters for a sample of eight recently observed Galactic GCs, all clearly showing a flattening of their projected velocity dispersion profiles at large radius. Our conclusions appear in Section 4.

2. NON-ISOTHERMAL GRAVITATIONAL EQUILIBRIUM MODELS

We shall model GCs as populations of self-gravitating stars in spherically symmetric equilibrium configurations (e.g., Sollima & Nipoti 2010), under a modified Newtonian gravitational force law for test particles at a distance r from the centers of spherically symmetric mass distributions $M(r)$:

$$f(x) = a_0 x \left(\frac{1 - x^n}{1 - x^{n-1}} \right). \tag{1}$$

In the above, $x = l_M/r$, where $l_M = (GM(r)/a_0)^{1/2}$. We see that when $a \gg a_0$, $x \gg 1$ and $f(x) \to a_0 x^2$, and one recovers Newton's gravity force law, while when $a \ll a_0$, $x \ll 1$ and $f(x) \to a_0 x$, where an equivalent MOND force law $f = (GM(r)a_0)^{1/2}/r$ is obtained. The index n mediates the abruptness of the transition between the two regimes. Note that for a soft $n = 2$ transition function one recovers the classical MOND μ function of Bekenstein (2004).

This was shown in Mendoza et al. (2011) to yield generalized isothermal gravitational equilibrium configurations with characteristic radii, masses, and velocity dispersions, r_g, M, σ, which smoothly evolve from the classical virial equilibrium of $M = \sigma^2 r_g/G$ to the observed tilt in the fundamental plane of elliptical galaxies, to the $\sigma^4 = (MGa_0)$ scaling of the galactic Tully–Fisher relation, as one goes from $x \gg 1$ to $x \sim 1$ to $x \ll 1$. Also, consistency with solar system observations was found there to constrain the transition to be fairly abrupt, requiring $n > 4$. In Mendoza et al. (2011), it is also proven that a sufficient condition for Newton's theorems for spherically symmetric mass distributions to hold, for any modified force law, is only that f can be written as a function exclusively of the variable x, which we will be using in what follows to construct equilibrium models for GCs. Recently, Bernal et al. (2011) showed this modified force-law model to be the low-velocity limit of a formal generalization to GR of the $f(R)$ type, providing a theoretical basis for the model used.

The equation of hydrostatic equilibrium for a polytropic equation of state $P = K\rho^\gamma$ is

$$K\gamma\rho^{\gamma-2}\frac{d\rho}{dr} = -\nabla\phi. \tag{2}$$

Since $\rho = (4\pi r^2)^{-1} dM(r)/dr$, going to locally Maxwellian conditions $\gamma = 1$ and $K = \sigma^2(r)$, the preceding equation can be written as

$$\sigma(r)^2 \left[\left(\frac{dM(r)}{dr} \right)^{-1} \frac{d^2M(r)}{dr^2} - \frac{2}{r} \right] = -a_0 x \left(\frac{1 - x^n}{1 - x^{n-1}} \right), \tag{3}$$

where $\sigma(r)$ is the isotropic Maxwellian velocity dispersion for the population of stars, which is allowed to vary with radius, as observed in GCs, e.g., Sollima & Nipoti (2010). The above is a generalization of the treatment presented in Hernandez et al. (2010), which we used in the modeling of dSph galaxies, which are characterized by flat velocity dispersion profiles, obtaining mass models consistent with observed velocity dispersions, half-mass radii, and total masses, in the absence of dark matter. Locally Maxwellian models of this type with radially varying volumetric velocity dispersions can be found in, e.g., Ibata et al. (2011), where conditions are further generalized to the inclusion of a varying radial orbital anisotropy, which, for simplicity, we take as zero.

As an illustrative example we can take the limit $f(x) = a_0 x^2$, and recover $-GM(r)/r^2$ for the right-hand side of Equation (3), the Newtonian expression appearing for $a \gg a_0$, or equivalently $r \ll l_M$. If one then imposes isothermal conditions $\sigma(r) \equiv \sigma$ and looks for a power-law solution for $M(r) = M_0(r/r_0)^m$, we get

$$\sigma^2 \left[\frac{m-3}{r} \right] = -\frac{GM_0}{r^2} \left(\frac{r}{r_0} \right)^m, \tag{4}$$

and hence $m = 1$, the standard isothermal halo, $M(r) = 2\sigma^2 r/G$, having a constant centrifugal equilibrium velocity $v^2 = 2\sigma^2$ and infinite extent. At the other limit, $a \ll a_0, r \gg l_M$, Equation (3) yields

$$\sigma^2 \left[\frac{m-3}{r} \right] = -\frac{[GM_0a_0]^{1/2}}{r} \left(\frac{r}{r_0} \right)^{m/2}. \tag{5}$$

In the limit $m = 0$, we obtain $M(r) = M_0$ and $v^2 = 3\sigma^2 = (GM_0a_0)^{1/2}$, the expected Tully–Fisher scaling of the circular equilibrium velocity with the fourth root of the mass, with rotation velocities which remain flat even after the mass distribution has converged, rigorously isothermal halos are naturally limited in extent. It is interesting to note that in this limit the scaling between the circular rotation velocity and the velocity dispersion is only slightly modified as compared to the Newtonian case, the proportionality constant changes from 2 to 3, for the squares of the velocities. In astrophysical units, this

low-acceleration limit for an isothermal halo in gravitational equilibrium yields

$$\sigma = 0.2 \left(\frac{M_0}{M_\odot}\right)^{1/4} \text{km s}^{-1}, \quad (6)$$

$$v = 0.35 \left(\frac{M_0}{M_\odot}\right)^{1/4} \text{km s}^{-1}, \quad (7)$$

for the velocity dispersion and the centrifugal equilibrium velocities of a halo of total mass M_0, respectively.

Also, it must be kept in mind that Galactic GCs are not in isolation, but orbit within the Galactic environment. This leads to a radius beyond which the tidal forces of the Milky Way unbound the outer stars of a GC, which depends on the mass and orbital radius of the GC in question. The above tidal radius can be calculated to first order for a point mass orbiting another point mass by equating the internal gravitational force of the GC to the derivative of the Galactic gravitational force; we briefly recall the first-order tidal limit calculation of

$$\left.\frac{dF_{\text{ext}}(R)}{dR}\right|_{R_0} \Delta r = F_{\text{int}}, \quad (8)$$

which leads to the tidal density stability condition of $\rho_s > \overline{\rho}$ for the density of a satellite of extent Δr and mass M_s orbiting at a distance R_0 from the center of a spherical mass distribution $M(R)$ having an average matter density $\overline{\rho}$ internal to R_0 resulting in a gravitational force $F_{\text{ext}}(R)$, where the internal gravitational force under Newton is $F_{\text{int}} = -GM_s^2/(\Delta r)^2$, under the assumption $\Delta r \ll R$. The equivalent calculation under the force law given by the $a \ll a_0$ limit of $F = -(GMa_0)^{1/2}/R$ is given by

$$\frac{(GM(R)a_0)^{1/2}}{R^2}\Delta r = \frac{(GM_s a_0)^{1/2}}{\Delta r}, \quad (9)$$

leading to

$$\rho_s > \left(\frac{\Delta r}{R}\right)\overline{\rho}, \quad (10)$$

as the equivalent of the classical tidal density criterion. In terms of masses and radii only, we obtain the tidal radius as

$$r_t = R\left(\frac{M_s}{M(R)}\right)^{1/4}. \quad (11)$$

Since the spatial extent of GCs will always be much smaller than their Galactocentric radii, Equation (10) shows that under the modified gravitational force law explored here, GCs will be much more robust to tides than under Newtonian gravity. As an example, for a $3 \times 10^5\, M_\odot$ GC orbiting 10 kpc from a $1.6 \times 10^{11}\, M_\odot$ mass, corresponding through Equation (7) to the 220 km s^{-1} of the Galactic rotation curve, the tidal radius comes to 370 pc. This is relevant as it shows that treating GCs as isolated systems is a self-consistent assumption within the approach of the modified force law being considered. Recent examples of dynamical modeling of Galactic GCs treated as isolated systems can be found in, e.g., Sollima & Nipoti (2010) and Haghi et al. (2011).

Taking initial conditions $M(r) \to 0$, $dM(r)/dr \to 4\pi r^2 \rho_0$, when $r \to 0$, a constant central density ρ_0, we can solve the full second-order differential Equation (3) for $M(r)$ through a numerical finite differences method, once a model for $\sigma(r)$ is adopted.

Solving Equation (3) yields the volumetric profiles for the density and mass, $\rho(r)$, $M(r)$. $\rho(r)$ is then projected along one dimension to obtain a projected surface density mass profile, $\Sigma(R)$. In all that follows we shall use r for radial distances in three dimensions, and R for a projected radial coordinate on the plane of the sky. $\Sigma(R)$ can be compared to observed surface brightness profiles once a mass-to-light ratio is assumed. Given the appearance of mass segregation processes in the dynamically evolved stellar populations of Galactic GCs, volumetrically, the mass-to-light ratio of a real GC will never be strictly constant. However, given the ages of the stellar populations involved, only a narrow range of stellar masses remain, and further, observed surface brightness profiles are projections on the plane of the sky of the volumetric density profiles. Thus, observed surface brightness measurements towards the central regions of GCs imply an integration across the entire foreground and background of any observed cluster. This in turn means that the regions where mass segregation is strongest, the central ones, contribute to the projected surface brightness profiles only after being averaged out over lines of sight traversing entirely the cluster in question. Even after this averaging process, the high densities found toward the center still surely imply M/L values which strictly must be a function of radius, even for the surface brightness profiles $I(R)$. Still, for the reasons described above, it is frequent to compare modelled $\Sigma(R)$ mass surface density profiles directly to observed projected surface brightness profiles through the use of constant M/L values, e.g., Jordi et al. (2009) and Haghi et al. (2011). In what follows, we will also perform such comparisons assuming constant M/L values.

Finally, a projected velocity dispersion profile $\sigma_p(R)$ is constructed through a volume density weighted projection of the volumetric velocity dispersion profile of a model, $\sigma(r)$. Therefore, a proposed model for $\sigma(r)$ does not directly give a projected $\sigma_p(R)$ profile, which the model only yields after having solved for the detailed density structure, and the subsequent mass weighted projection of the proposed $\sigma(r)$.

Observations provide only the density weighted projected profiles of $\sigma(r)$, integrated along the line of sight, $\sigma_p(R)$, not the volumetric $\sigma(r)$ profiles which we require in Equation (3). We shall therefore adopt a parametric form for the volumetric velocity dispersion profile and adjust the parameters to obtain a match to the observed GC properties. For this we use

$$\sigma(r) = \sigma_1 \exp\left(-\frac{r^2}{r_\sigma^2}\right) + \sigma_0. \quad (12)$$

In the above, σ_0 is given directly by the observations as the asymptotic value of the measured projected velocity dispersion profile for each GC, as at large R radii, projection effects tend to zero and $\sigma_p(R) \to \sigma(r)$. This leaves us with three model parameters to determine: ρ_0, σ_1, and r_σ, which we fit to match the observed projected velocity dispersion profiles, as well as central projected velocity dispersion values for each observed GC treated, and comparing the resulting model $\Sigma(R)$ profiles to the observed surface brightness profiles of any given GC, under the requirement that the M/L ratios used be consistent with detailed inferences from the stellar evolutionary and initial mass function (IMF) studies of McLaughlin & van der Marel (2005).

We end this section presenting in Figures 1 and 2, a sample model. In Figure 1 we show the volumetric density profile, which is qualitatively similar to a cored isothermal profile, with the difference that the asymptotic $\rho(r)$ profile at large radii is steeper than the r^{-2} of the Newtonian case. This results in finite total

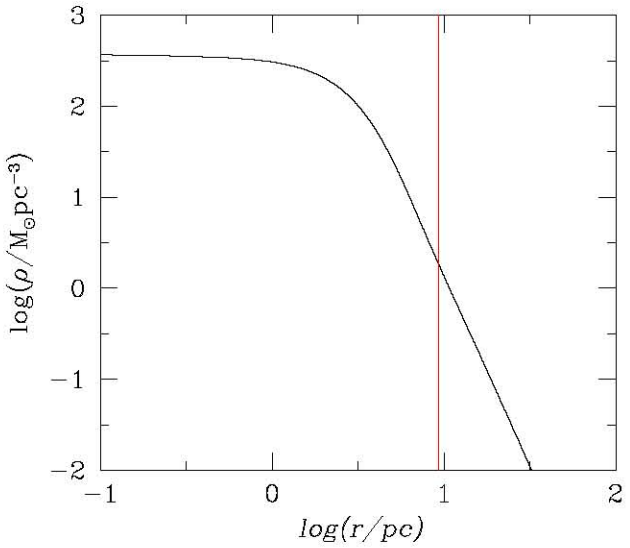

Figure 1. Volumetric density profile for a sample model. The vertical line gives the point where $x = 1$. Note that the asymptotic $\rho(r)$ profile at large radii is steeper than the r^{-2} of the Newtonian case, resulting in a finite total radius and total mass for the configuration.

(A color version of this figure is available in the online journal.)

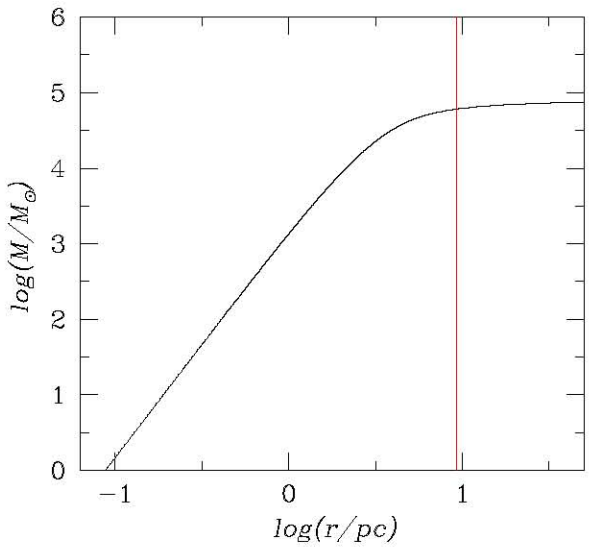

Figure 2. Volumetric mass profile for the same sample model of Figure 1. The vertical line gives the point where $x = 1$. The convergence to a total mass is evident, despite not having introduced any externally determined tidal radius.

(A color version of this figure is available in the online journal.)

masses and finite half-mass radii even for the asymptotically flat $\sigma(r)$ volumetric profiles we adopt, in contrast with the situation in classical gravity, where infinitely extended mass profiles would appear. These finite profiles are also what results under the type of modified gravity laws we are treating, even for rigorously isothermal $\sigma(r) = \sigma_0$ equilibrium configurations, as already pointed out in Hernandez et al. (2010) and Mendoza et al. (2011) and as shown in the developments following Equation (5).

Figure 2 shows the corresponding volumetric radial mass profile for the same sample model, indicating again with a vertical line the threshold where $x = 1$. We see that only 20% of the total model mass lies beyond $x = 1$. This fraction is distributed over a much larger area having much smaller projected mass surface densities than the central regions interior to the $x = 1$ threshold, the ones which are much more easily observed, and over which Newtonian gravity accurately holds.

These two figures illustrate the physical consistency of the model, a positive isothermal volumetric velocity dispersion is assumed, integration of Equation (3) then yields a volumetric density profile essentially consistent with what would appear under Newtonian dynamics in the region interior to $x = 1$, where the force law converges precisely to the standard expression. At large radii however, the density profile increasingly steepens and naturally reaches $\rho(r) = 0$ at a well-defined total radius, as is evident from the convergence seen in Figure 2. Thus, the distribution function is necessarily positive throughout the modeled structure and goes to zero at a well-defined outer radius. In the following section we give best-fit models for eight recently observed Galactic GCs.

3. MODELING OBSERVED GLOBULAR CLUSTERS

We now present best-fit models constructed as described above, optimized to match observed projected surface brightness profiles, under M/L values consistent with the ranges given by McLaughlin & van der Marel (2005) for each individual GC modeled, and projected velocity dispersion measurements for a series of Galactic GCs. The data for the projected velocity dispersion profiles are taken from Drukier et al. (1998), Scarpa et al. (2004, 2007a, 2007b, 2011), and Scarpa & Falomo (2010), and the surface brightness profiles from Trager et al. (1995). We infer the total masses from the integration of the observed surface brightness profiles, assuming again M/L values consistent with the ranges given by McLaughlin & van der Marel (2005) for each individual GC modeled. These author calculate detailed single stellar population models tuned to the inferred ages and metallicities of each of the clusters we model. We checked for consistency through the synthetic H-R diagram construction procedure described in Hernandez & Valls-Gabaud (2008).

For the above-mentioned case, we take the relevant ages and metallicities from the following literature: Salaris & Weiss (2002) and Kraft & Ivans (2003) for NGC 288 and NGC 6341; Salaris & Weiss (2002) and Rutledge et al. (1997) for NGC 6171; Salaris & Weiss (2002), McNamara et al. (2004), and Kraft & Ivans (2003) for NGC 7078; and Samus' et al. (1995) and Harris (1996) for NGC 7099, respectively. In obtaining inferred total masses, confidence intervals were assigned by considering the full catalogue of M/L values given by McLaughlin & van der Marel (2005) for each individual GC, for the full range of plausible stellar models considered in that study, for each of the GCs we treat. The final results for the mass-to-light ratios are shown in Table 1.

The final resulting density weighted projected velocity dispersion profiles, $\sigma_p(R)$, together with the resulting surface brightness profiles for the eight GCs treated appear in Figures 3 and 4, where the vertical line indicates the point where $a = a_0$. The models accurately fit the observed projected surface brightness profiles of the clusters, the central value of the measured projected velocity dispersion, as well as the observed profiles for $\sigma_p(R)$.

We see five cases, NGC 288, NGC 1851, NGC 5139, NGC 6341, and NGC 7099, where the models very accurately reproduce all light distribution and velocity dispersion profiles, which in fact agree with the observations in all cases, to within reported uncertainties. For NGC 1904 and NGC 6171, a very slight mismatch appears between the models and the

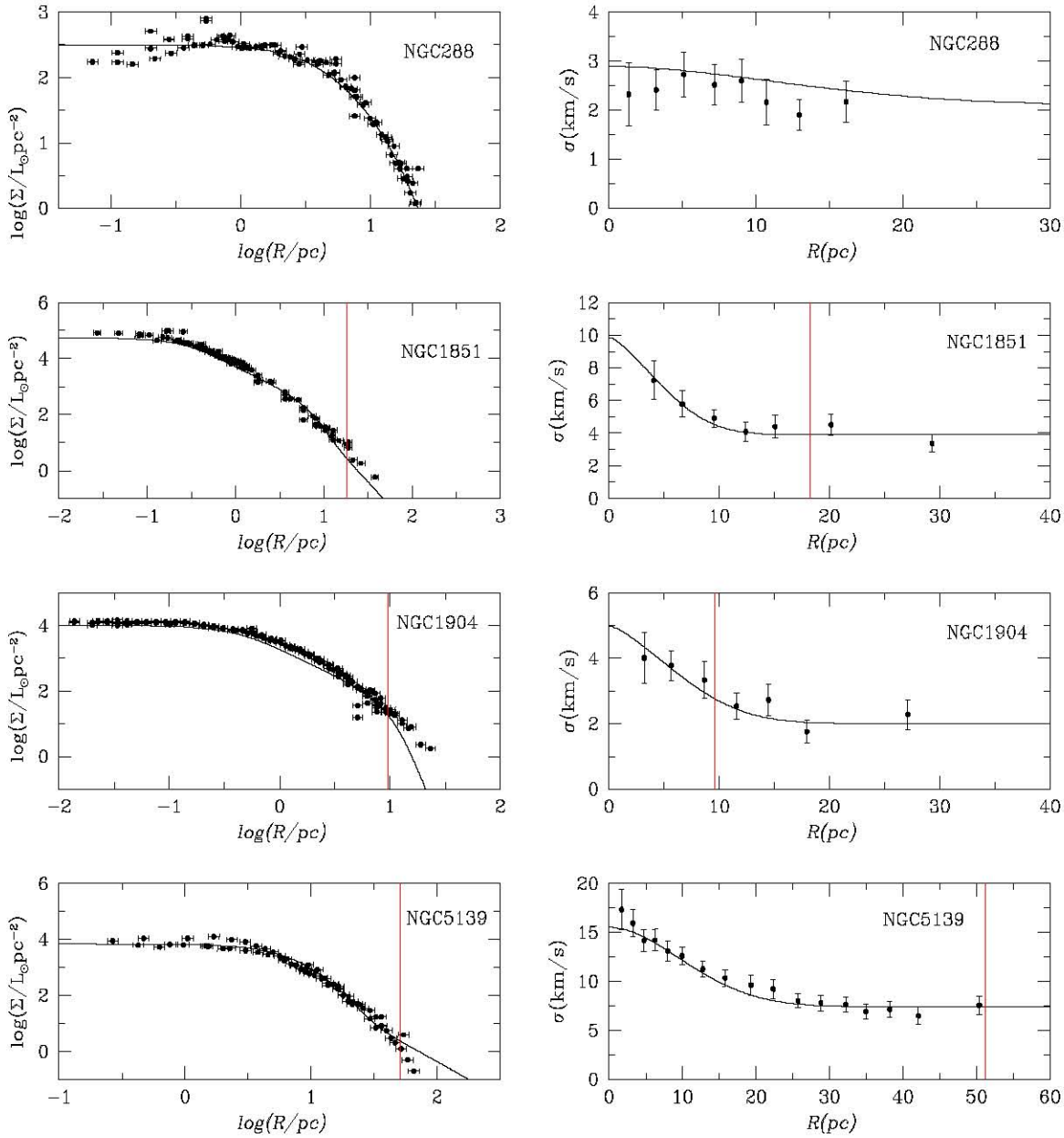

Figure 3. Comparison of the resulting model projected surface brightness profiles and resulting model projected velocity dispersion profiles to the corresponding observed quantities for the first four GCs studied. In all cases, the assumed M/L values were within the ranges given by McLaughlin & van der Marel (2005) for each individual GC through detailed stellar population modeling. The vertical line gives the point where $x = 1$ and the modified force law used shifts from the classical Newtonian form to the MONDian character of Equation (5).

(A color version of this figure is available in the online journal.)

observations of the surface brightness profiles at values of $R \sim$ a few pc, and for NGC 7078, over the outer regions, precisely beyond $x = 1$, the model falls below the observed surface brightness profile. These two last points could be evidence of the failure of some of the assumptions used in these cases, probably the presence of velocity anisotropy in the dynamics of the stars in question. Alternatively, a slight tuning of the assumed volumetric M/L ratios with radius, within entirely plausible ranges, would improve the fits. Rather than introducing a further degree of freedom, we prefer to show that highly adequate fits are easily obtained for the simplest $M/L =$ constant assumption.

We see also the steepening of the surface density brightness profile toward the edge of the clusters, particularly for NGC 288 and NGC 7099. Under Newtonian gravity this feature would be interpreted as a tidal radius, while under the modified force-law scheme treated here, it is a natural consequence of the change in the gravitational regime, leading to finite matter distributions when $a < a_0$ and $\sigma(r)$ tends to a constant, cf. Equation (5).

A model with a degree of radial orbital anisotropy which varies with radius is an entirely plausible alternative, implying the introduction of a further free function that allows us to more accurately reproduce the surface brightness profiles. We have also chosen not to complicate the model with the inclusion of a $\beta(r)$ profile, and preferred to show that under the simplest isotropic construction, the modified force law we test is capable of adequately reproducing all the observations in five of the cases studied, although slight mismatches appear in three other cases. In particular, for NGC 7078, our model requires more mass at large radii, but without an increase in $\sigma(r)$ in that region. This can be trivially accommodated by an increase of kinetic energy

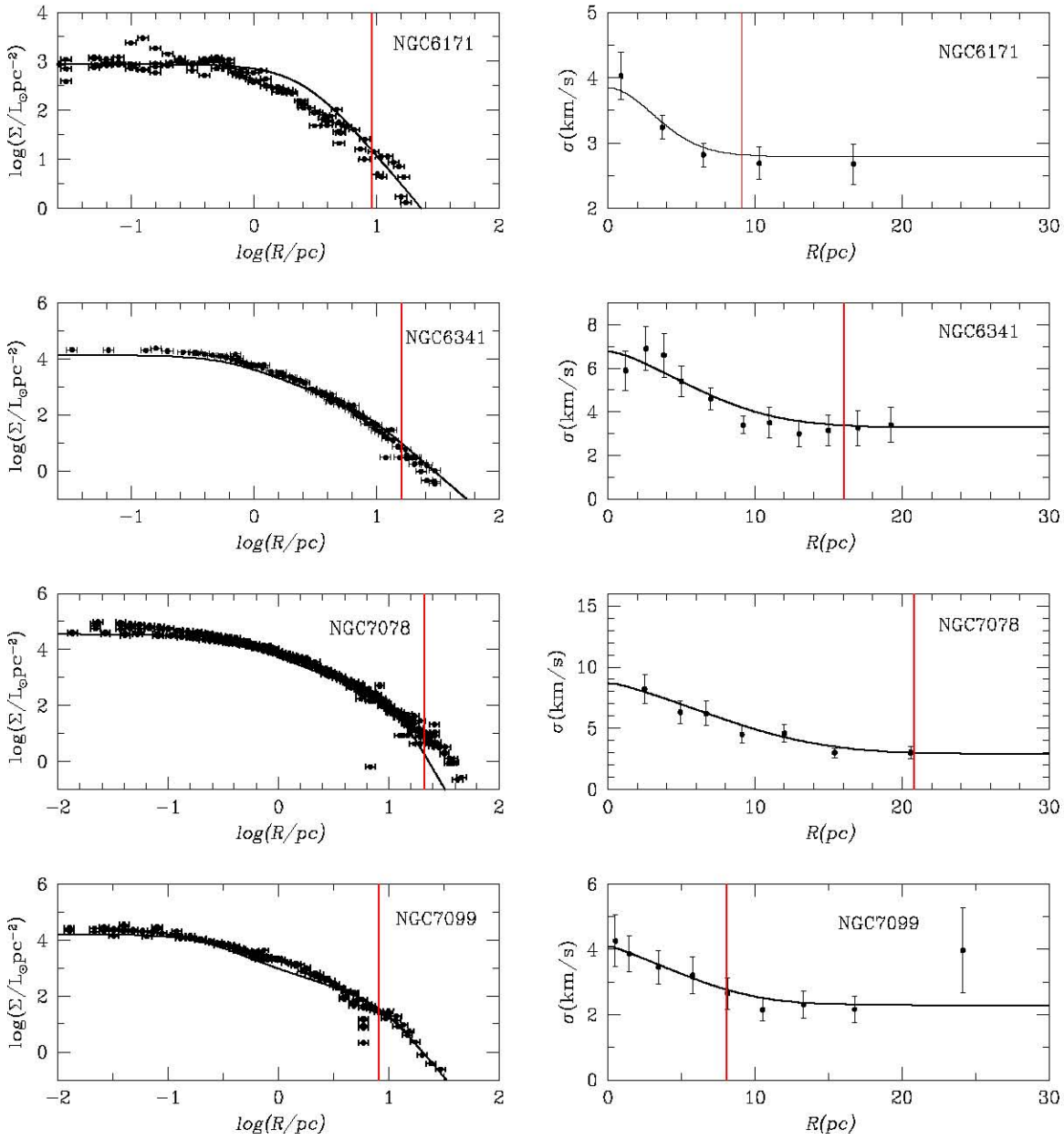

Figure 4. Comparison of the resulting model projected surface brightness profiles and resulting model projected velocity dispersion profiles to the corresponding observed quantities for the last four GCs studied. In all cases, the assumed M/L values were within the ranges given by McLaughlin & van der Marel (2005) for each individual GC through detailed stellar population modeling. The vertical line gives the point where $x = 1$ and the modified force law used shifts from the classical Newtonian form to the MONDian character of Equation (5).

(A color version of this figure is available in the online journal.)

at large radius, which should not be evident in the observed velocity dispersion, through the inclusion of radial motion, a degree of orbital radial anisotropy appearing beyond 20 pc.

Obtaining a good match required taking a high exponent of $n = 10$ in Equation (3), i.e., a relatively sharp transition for the generalized force law, which however, remains continuous and differentiable at all points, by construction. This is in agreement with observed upper limits to deviations from Newtonian dynamics at the solar system, models for the Galactic rotation curve, and equilibrium models for the local dSphs, as shown in Mendoza et al. (2011) to apply for the modified force law tested here, provided $n > 4$. Essentially, this implies that the transition between the Newtonian and the "MONDian" regimes must be fairly abrupt. In fact, given the form of Equation (3), the final model becomes independent of n for any value of n higher than 10.

We now illustrate the dependence of the models obtained to the assumed force-law index n. Figure 5 shows the ratio between the resulting model mass, M, to the observed cluster mass, M_c, as a function of the value of n used, for best-fit models for two illustrative cases, NGC 288 and NGC 6341, the upper and lower curves at the right end, respectively. The shaded region gives the allowed range of GC mass for a particular choice of stellar population parameters in McLaughlin & van der Marel (2005); if the systematic uncertainties were included, the shaded region would extend, but only upward, by a factor of about two. We see that obtaining a total model mass in accordance with direct stellar population studies requires taking a value of $n > 5$ for NGC 288 and $n > 8.5$ for NGC 6341. The particular minimum value of

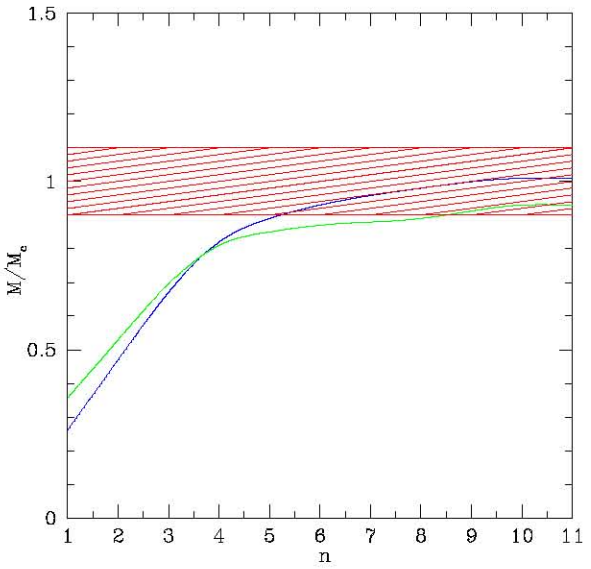

Figure 5. Dependence of resulting model mass on the value of the force-law index n. The ratio of the model mass to the inferred GC mass is shown for two representative clusters, with the shaded region giving the range allowed by direct stellar population studies of the clusters shown, NGC 288 and NGC 6341. This illustrates the need for a sharp transition in the force law used.

(A color version of this figure is available in the online journal.)

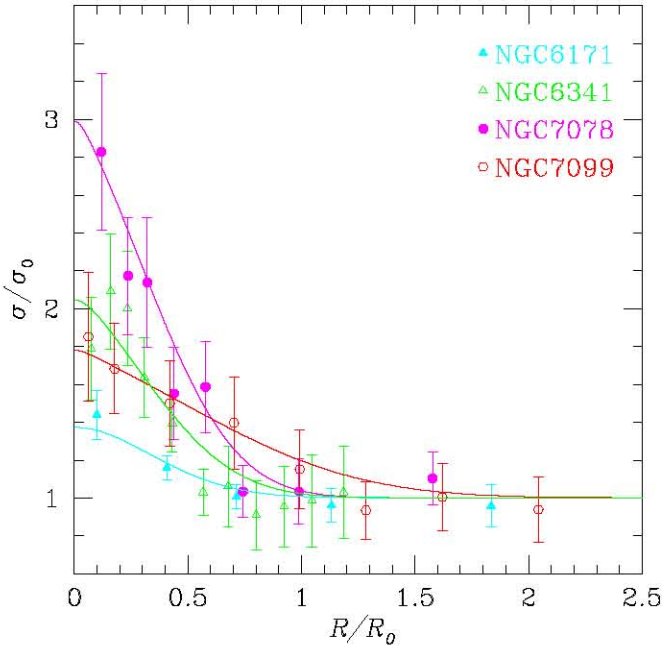

Figure 6. Projected velocity dispersion profiles normalized to σ_0 and to R_0 of our models for four representative examples.

(A color version of this figure is available in the online journal.)

Table 1
Model Parameters for the Globular Clusters Treated

Globular Cluster	$\log(\rho_0)$	σ_1	σ_0	r_σ	$(M/L)_M$	$(M/L)_{GC}$
NGC 288	2.15	0.83	2.1	18.0	2.0	3.03 ± 1.12
NGC 1851	5.65	6.00	3.9	7.0	2.0	3.00 ± 1.19
NGC 1904	4.70	3.00	2.0	9.0	1.73	2.73 ± 1.00
NGC 5139	3.60	8.90	7.4	15.0	2.0	2.68 ± 0.98
NGC 6171	3.52	1.20	2.8	5.0	2.5	3.20 ± 1.20
NGC 6341	4.68	3.50	3.3	9.0	1.63	2.55 ± 0.95
NGC 7078	4.98	5.80	2.9	11.0	1.7	2.51 ± 0.90
NGC 7099	4.92	1.80	2.3	8.0	1.65	2.60 ± 0.90

Notes. ρ_0 gives the central values of the stellar density used in each model in units of $M_\odot$ pc^{-3}, while σ_0, σ_1 and r_σ give the parameters of the volumetric velocity dispersion profile used, in units of km s^{-1} and pc, respectively. $(M/L)_M$ gives the mass-to-luminosity ratios used in each model, and $(M/L)_{GC}$ gives the corresponding values reported by McLaughlin & van der Marel (2005) for each cluster through single stellar population modeling using age and metallicity parameters as appropriate for each.

n required for the other clusters in the sample varies somewhat, although most require values $n > 8$–9 to reach the minimum inferred masses. As this parameter cannot be expected to change from cluster to cluster, we have taken $n = 10$ in all cases.

Note that this value results in an equivalent MOND μ transition function that is fairly abrupt. For comparison, most MOND transition functions proposed imply a softer transition from the Newtonian to the MONDian regimes, e.g., the μ function of Bekenstein (2004) corresponds exactly to the force law treated here, with $n = 2$. A similar result has recently been presented by Qasem (2011), who analyzes laser lunar ranging data to constrain the allowed departures from Newtonian gravity at the scale studied and finds that the data rule out most proposed MOND transition functions, while our proposal of Mendoza et al. (2011) remains consistent with the test performed. This completely independent study supports the constraints of Figure 5, implying that the transition from the Newtonian regime to the MONDian one is probably steeper than commonly thought.

Figure 6 now shows the radial profiles of $\sigma_p(R)$ for four of the Galactic GCs in the sample, where we have normalized the velocity dispersions to their asymptotic values, and the radial coordinate to the values where the condition $x = 1$ ($a = a_0$) is met in each of the models, R_0. Measurements with confidence intervals appear represented by different symbols for each GC. We again see that $\sigma_p(R)$ profiles consistent with observations are easily obtained, while fitting simultaneously surface brightness profiles, to within the error bars, where we have also assumed a 20% uncertainty in all distance determinations. The four clusters included in this figure illustrate the range of behaviors found, from NGC 7078 which shows a very large variation in $\sigma_p(R)$ from the center to the outskirts, implying a large Newtonian inner region and only a slight MONDian outer zone, to clusters with only small variations in $\sigma_p(R)$ like NGC 6171 and NGC 7099. An extreme case is NGC 288 with a $\sigma_p(R)$ profile which is also consistent with observations, but which cannot be plotted in Figure 6, as that low-density cluster lies in the $a < a_0$ regime throughout, and therefore R_0 is not defined for it.

Note that no external field effect of MOND was included in the dynamical modeling performed, as was also not included in, e.g., Sollima & Nipoti (2010). The fact that accurate mass and velocity dispersion models can be thus constructed is suggestive of a modified gravity formulation where no such effect appears.

Finally, in Figure 7 we plot inferred values of the total masses and asymptotic values of projected velocity dispersions for the eight GCs we study, with their corresponding confidence intervals. The solid line shows the best-fit power-law dependence for this plot, excluding Omega Cen from the fit. Note that the quantities plotted here are completely independent of any dynamical modeling, being merely measured velocity dispersion values in the outskirts of the clusters in question, and total masses as

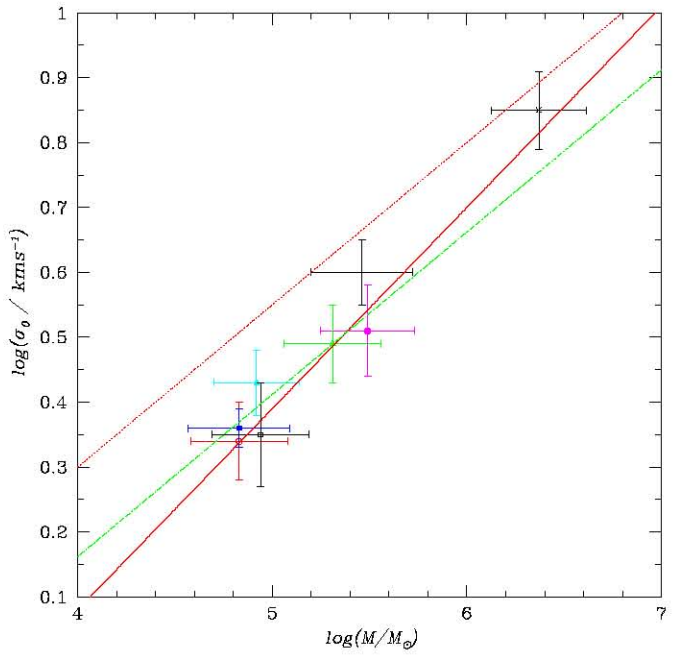

Figure 7. Points with error bars represent the values of σ_0 and total stellar mass for the eight GCs we study. The solid line gives the best-fit power law, having a slope of 0.31 ± 0.06, excluding Omega Cen from the fit. If Omega Cen is included in the fit, the slope comes to 0.32 ± 0.04. The dotted curve shows the prediction of Equation (6) for isothermal systems fully in the $a \ll a_0$ regime, while the dashed line gives the best slope 1/4 fit.

(A color version of this figure is available in the online journal.)

inferred from total luminosities and models of their observed stellar populations.

Despite the small ranges in parameters covered by the clusters studied, it is clear that the data are consistent with the generic modified gravity prediction of $\sigma_0 \propto M^{1/4}$, the slope of the solid line being statistically determined to be 0.31 ± 0.06. For comparison, the dashed line gives the best slope 1/4 fit, as the numbers above show, a consistent description of the data. Omega Cen was excluded from the fit, as it is usually acknowledged to be an outlier. The complex stellar populations it presents, its abnormally high mass, together with the possible presence of an intermediate mass black hole in its center probably indicate a complex dynamical formation history. Still, its inclusion in the power-law fit of Figure 7 only slightly modifies the resulting slope to 0.32 ± 0.04.

Figure 7 lends credibility to the interpretation of the outer flattening of the observed velocity dispersion profiles as evidence for modifications in the law of gravity. Under classical gravity, one needs to invoke further causal correlations to account for the clear trend appearing in Figure 7, a more contrived scenario than simply the natural consequence of a shift toward MONDian dynamics in GCs at scales where $a < a_0$. As a comparison, the dotted line in Figure 7 shows the prediction of Equation (6) for isothermal systems fully in the $a \ll a_0$ regime.

That the GCs treated lye somewhat below the prediction of Equation (6) is not surprising, as they are by no means structures fully in the $a \ll a_0$ regime; most of the mass is partly in the Newtonian regime, or in the transition between both, hence the asymptotic velocity dispersions are slightly off the results of Equation (6).

We acknowledge that with the number of the assumptions going into the modeling remain as such, it is entirely plausible that some might not strictly apply. As already discussed, the case of NGC 7078 could be indicative of a certain degree of orbital radial anisotropy appearing toward the outskirts of some of these systems. Also, the projected M/L values might have some radial variations, or the flattening of the projected velocity dispersion profiles might simply reflect the presence of contaminating unbound stars, or the effects of tidal heating, as assumed under Newtonian interpretations of GC structure, e.g., Drukier et al. (2007) or Lane et al. (2010). Under Newtonian dynamics, perfectly self-consistent models can be constructed, often leading to fits even better than those resulting from modified gravity approaches, e.g., Ibata et al. (2011). It is the new results of Figure 7, which are independent of any gravitational modeling, which we find most suggestive of the modified gravity interpretation; as under the standard approach, further mechanisms must be invoked to explain the appearance of a "Tully–Fisher" relation for GCs.

We conclude this section with Table 1, which summarizes the observed parameters used and the model parameters fitted for each of the eight Galactic GCs in this paper. We also note that the models are relatively insensitive to small changes in the values of ρ_0 used; only changes of factors $\sim$3 and above in this model parameter result in significant changes.

4. CONCLUSIONS

We show that for Galactic GCs, spherically symmetric equilibrium models can be constructed using a modified Newtonian force law which reproduces the MOND phenomenology, which naturally satisfies all observational constraints available.

The resulting models are typically characterized by a Newtonian inner region, which smoothly transitions to a modified gravity outer region upon approaching the $a = a_0$ threshold. The resulting internal velocity dispersion profiles correspondingly transit from an inner radially decaying region to an outer flat velocity dispersion one.

By comparing against careful single stellar population modeling of the GCs studied to derive total stellar mass estimates, we show that the asymptotic values of the measured velocity dispersion profiles, $\sigma_p(R \to \infty)$, and total masses for these systems, M, are consistent with the generic modified gravity prediction for a scaling $\sigma_p^4(R \to \infty) \propto M$.

The authors acknowledge the constructive criticism of an anonymous referee as valuable toward reaching a clearer and more complete manuscript. X.H. acknowledges financial assistance from UNAM DGAPA grant IN103011-3. A.J. acknowledges financial support from a CONACYT scholarship.

REFERENCES

Allen, C., Poveda, A., & Herrera, M. A. 2000, A&A, 356, 529
Angus, G. W. 2008, MNRAS, 387, 1481
Baumgardt, H., Grebel, E. K., & Kroupa, P. 2005, MNRAS, 359, L1
Bekenstein, J. D. 2004, Phys. Rev. D, 70, 083509
Bernal, T., Capozziello, S., Hidalgo, J. C., & Mendoza, S. 2011, Eur. Phys. J. C, 71, 1794
Drukier, G. A., Cohn, H. N., Lugger, P. M., et al. 2007, AJ, 133, 1041
Drukier, G. A., Slavin, S. D., Cohn, H. N., et al. 1998, AJ, 115, 708
Haghi, H., Baumgardt, H., & Kroupa, P. 2011, A&A, 527, A33
Haghi, H., Baumgardt, H., Kroupa, P., et al. 2009, MNRAS, 395, 1549
Harris, W. E. 1996, AJ, 112, 1487
Hernandez, X., Mendoza, S., Suarez, T., & Bernal, T. 2010, A&A, 514, A101
Hernandez, X., & Valls-Gabaud, D. 2008, MNRAS, 383, 1603
Ibata, R., Sollima, A., Nipoti, C., et al. 2011, ApJ, 738, 186
Jordi, K., Grebel, E. K., Hilker, M., et al. 2009, AJ, 137, 4586
Kraft, R. P., & Ivans, I. I. 2003, PASP, 115, 143

Kroupa, P., Famaey, B., de Boer, K. S., et al. 2010, A&A, 523, 32
Küpper, A. H. W., Kroupa, P., Baumgardt, H., & Heggie, D. C. 2010, MNRAS, 407, 2241
Lane, R., Kiss, L. L., Lewis, G. F., et al. 2010, MNRAS, 406, 2732
McGaugh, S. S., & Wolf, J. 2010, ApJ, 722, 248
McLaughlin, D. E., & van der Marel, R. P. 2005, ApJS, 161, 304
McNamara, B. J., Harrison, T. E., & Baumgardt, H. 2004, ApJ, 602, 264
Mendoza, S., Hernandez, X., Hidalgo, J. C., & Bernal, T. 2011, MNRAS, 411, 226
Milgrom, M. 1983, ApJ, 270, 365
Moffat, J. W., & Toth, V. T. 2008, ApJ, 680, 1158
Qasem, E. 2011, arXiv:1112.4652
Rutledge, G. A., Hesser, J. E., Stetson, P. B., et al. 1997, PASP, 109, 883
Salaris, M., & Weiss, A. 2002, A&A, 388, 492
Samus', N. N., Ipatov, A. P., Smirnov, O. M., et al. 1995, Astron. Lett., 21, 810
Sanchez-Salcedo, F. J., & Hernandez, X. 2007, ApJ, 667, 878
Sanchez-Salcedo, F. J., Reyes-Iturbide, J., & Hernandez, X. 2006, MNRAS, 370, 1829
Scarpa, R., & Falomo, R. 2010, A&A, 523, 43
Scarpa, R., Marconi, G., Carraro, G., Falomo, R., & Villanova, S. 2011, A&A, 525, A148
Scarpa, R., Marconi, G., & Gilmozzi, R. 2004, in Proc. Baryons in Dark Matter Halos, Novigrad, Croatia, 2004 October 5–9, ed. R. Dettmar, U. Klein, & P. Salucci (Proceedings of Science; SISSA), 55.1, http://pos.sissa.it
Scarpa, R., Marconi, G., Gilmozzi, R., & Carraro, G. 2007a, A&A, 462, L9
Scarpa, R., Marconi, G., Gilmozzi, R., & Carraro, G. 2007b, Messenger, 128, 41
Sollima, A., & Nipoti, C. 2010, MNRAS, 401, 131
Trager, S. C., King, I. R., & Djorgovski, S. 1995, AJ, 109, 218
Zhao, H., & Famaey, B. 2010, Phys. Rev. D, 81, 087304

The Astrophysical Journal, 768:142 (6pp), 2013 May 10 doi:10.1088/0004-637X/768/2/142

THE MASSIVE ELLIPTICAL GALAXY NGC 4649 FROM THE PERSPECTIVE OF EXTENDED GRAVITY

M. A. Jiménez[1], G. Garcia[1], X. Hernandez[1], and L. Nasser[2]
[1] Instituto de Astronomía, Universidad Nacional Autónoma de México, Apartado Postal 70–264 C.P. 04510 México D.F., Mexico; mjimenez@astro.unam.mx
[2] Department of Science and Mathematics, Columbia College, Chicago, 1L 60605, USA
Received 2013 January 28; accepted 2013 March 18; published 2013 April 24

ABSTRACT

Elliptical galaxies are systems where dark matter is usually less necessary to explain observed dynamics than in the case of spiral galaxies; however, there are some instances where Newtonian gravity and the observable mass are insufficient to explain their observed structure and kinematics. Such is the case of NGC 4649, a massive elliptical galaxy in the Virgo cluster for which recent studies report a high fraction of dark matter, 0.78 at 4 R_e. However, this galaxy has been studied within the MOdified Newtonian Dynamics (MOND) hypothesis, where a good agreement with the observed values of velocity dispersion is found. Using a MONDian gravity force law, here we model this galaxy as a self-consistent gravitational equilibrium dynamical system. This force law reproduces the MOND phenomenology in the $a < a_0$ regime, and reduces to the Newtonian case when $a > a_0$. Within the MONDian $a < a_0$ scales, centrifugal equilibrium or dispersion velocities become independent of radius, and show a direct proportionality to the fourth root of the total baryonic mass, $V^4 \propto (MGa_0)$. We find that the recent detailed observations of the surface brightness profile and the velocity dispersion profile for this galaxy are consistent with the phenomenology expected in MONDian theories of modified gravity, without the need to invoke the presence of any hypothetical dark matter.

Key words: galaxies: general – galaxies: individual (NGC 4649) – galaxies: structure

Online-only material: color figures

1. INTRODUCTION

The flat rotation curves of spiral galaxies have been well known for decades (e.g., Bosma 1981; Rubin et al. 1982); assuming the validity of the Newtonian law of gravity throughout, this results in a discrepancy between the dynamical mass and the luminous mass of spiral galaxies. Other types of galaxies exhibit mass discrepancies as well: the most remarkable is the case of dwarf spheroidal (dSph) galaxies for which the velocity dispersion is well known and the mass inferred from their internal dynamics greatly exceeds the visible mass by factors reaching into the thousands (e.g., Simon & Geha 2007). On the other hand, bright giant elliptical galaxies exhibit small mass discrepancies (e.g., Romanowsky et al. 2003). Usually these facts are commonly interpreted as the manifestation of the dark matter halo in which the different galaxies are immersed. This halo dominates the dynamics of extended galaxies with low surface brightness, and its presence is less significant in more centrally concentrated galaxies with larger surface brightness values (e.g., McGaugh & de Blok 1998).

Alternatively, the discrepancy between observable mass in galaxies and their dynamics can be interpreted as direct evidence for the failure of the current Newtonian and general relativistic theories of gravity, rather than the existence of a dark matter component. As examples, in spiral galaxies the flat rotation curve has been successfully interpreted assuming a modification of Newtonian dynamics (MOND) (e.g., Sanders & McGaugh 2002), or equivalently an extended Newtonian force law (e.g., Mendoza et al. 2011); the projected surface density profiles and observational parameters of the local dSph galaxies are in agreement with a description in MOND (e.g., Hernandez et al. 2010; McGaugh & Wolf 2010; Kroupa et al. 2010). Similarly, modified gravity approaches have been successful in explaining the general shape of the observed rotation curves of many dwarf and low surface brightness galaxies (e.g., Swaters et al. 2010), and many other astronomical systems have been interpreted in this context, such as globular clusters (GCs) (e.g., Sollima & Nipoti 2010; Haghi et al. 2011; Hernandez & Jiménez 2012), the relative velocity of wide binaries in the solar neighborhood (e.g., Hernandez et al. 2012), the infall velocity of the two components of the Bullet cluster (e.g., Moffat & Toth 2010), and the gravitational lensing of elliptical galaxies (e.g., Mendoza et al. 2012).

Modified gravity proposals not requiring any dark matter generically predict that for accelerations below $a_0 \approx 1.2 \times 10^{-10}\,\mathrm{m\,s^{-2}}$, one should transit away from Newtonian gravity, e.g., MOND in Milgrom (1983), TeVeS in Bekenstein (2004), QUMOND and BIMOND in Zhao & Famaey (2010), the extended Newtonian force law in Mendoza et al. (2011) or its relativistic version in Bernal et al. (2011). Regardless of the details, within $a < a_0$ scales velocities for test particles about spherical mass distributions will become independent of radius, and show a mass scaling coinciding with that of the galactic Tully–Fisher relation of $V^4 \propto M$.

To test the predictions of modified gravity schemes in elliptical galaxies, one needs to know the kinematics and mass distribution of these systems. Elliptical galaxies are dynamically hot systems with little or no cold gas where determining their kinematics is more difficult than for spiral galaxies. Their orbital structure is thought to be the result of their evolution through a complex formation process. For determining their dynamics several tracers have been used, such as X-ray gas, GCs, and planetary nebulae (PNe). Massive elliptical galaxies are usually surrounded by hot and low-density gas evident through its X-ray glow. A tool to determine the mass distribution in these systems is to model their X-ray spectra to obtain density and temperature profiles for the gas. If we assume hydrostatic equilibrium for this component, we can then obtain the mass distribution and then an estimate of the brightness profile to be compared to the photometrically observed one (e.g., Das et al. 2010).

The problem of modeling the luminosity profile and kinematics of elliptical galaxies has been treated before; e.g., Kormendy et al. (2009) modeled the brightness profiles of all known elliptical galaxies in the Virgo cluster using Sérsic profiles $\log I \propto r^{1/n}$; they develop a mechanism to calculate a realistic error in the Sérsic parameters and identify departures from these profiles that are diagnostic of galaxy formation processes. Teodorescu et al. (2011) studied the kinematics of PNe in the Virgo giant elliptical galaxy NGC 4649 (M60). Assuming Newtonian gravity, they conclude that the kinematics of this object are consistent with the presence of a dark matter halo around M60; this halo is almost one-half of the total mass of the galaxy within 3 R_e. In De Bruyne et al. (2001), three-integral axisymmetric models for NGC 4649 and NGC 7097 are considered, concluding that the kinematic data of NGC 4649 are consistent with a dynamical model with a moderate amount of dark matter; Das et al. (2010) create a dynamical model of NGC 4649 using the NMAGIC code and kinematic constraints to infer a dark matter mass fraction in NGC 4649 of ∼0.78 at 4 R_e. In Samurović & Ćirković (2008a, 2008b), the GC dynamics of NGC 4649 are used as mass tracers and the Jeans equation is solved for Newtonian and MOND models, finding that both are consistent with the values of the observed velocity profile of the galaxy, although considering the light distribution only to first approximation, as a radial power law for the surface brightness profile.

Along the same lines, we here treat the massive elliptical galaxy NGC 4649 assuming the modified Newtonian force law formulation of Mendoza et al. (2011) through fully consistent self-gravitating models, as a test of the above ideas. The free parameters of the galactic model are calibrated to match the details of the observed surface brightness and projected velocity dispersion profiles. This becomes a valuable test of the physical modeling introduced in Hernandez & Jiménez (2012) to the modeling of light and velocity dispersion profiles in Galactic GCs, as the same scheme is now applied to a system which lies orders of magnitude above the GCs in size and mass.

We obtain equilibrium models which satisfy all observed parameters of the galaxy in question, including crucially, the flattening of the projected velocity dispersion evident at large radii, in the absence of any unseen dark component. Under a purely Newtonian framework, any accurate modeling of this galaxy requires the inclusion of a substantial amount of dark matter.

In Section 2 we present the modeling used to construct equilibrium models for self-gravitating spherically symmetric stellar populations using the modified Newtonian force law of Mendoza et al. (2011). We then show in Section 3 specific models satisfying all observational constraints available for NGC 4649. Section 4 gives our conclusions.

2. SELF-GRAVITATING EQUILIBRIUM MODELING

In the same way as done for GCs in Hernandez & Jiménez (2012), we have modeled the massive elliptical galaxy NGC 4649 as a population of self-gravitating stars in a spherically symmetric equilibrium configuration, under a modified Newtonian gravitational force law. For a test particle a distance r from the center of a spherically symmetric mass distribution $M(r)$, the force per unit mass is given by

$$f(x) = a_0 x \left(\frac{1-x^n}{1-x^{n-1}}\right). \quad (1)$$

In the equation above, $x = l_M/r$, where $l_M = (GM(r)/a_0)^{1/2}$. Notice that for $a \gg a_0$ ($x \gg 1$), $f(x) \to a_0 x^2$ and we recover the standard force law, while for $a \ll a_0$ ($x \ll 1$), $f(x) \to a_0 x$ and the corresponding MONDian force law of $f = (M(r)Ga_0)^{1/2}/r$ ensues. The abruptness of the transition between the two limits is regulated by the index n, which satisfies $n > 1$.

In Mendoza et al. (2011), the above force law was proven to result in generalized isothermal gravitational equilibrium configurations having well defined and finite r_g, M, and σ values, radii, masses, and velocity dispersion, which evolve smoothly from the classical virial equilibrium scaling of $M = \sigma^2 r_g/G$ to the observed tilt in the fundamental plane of elliptical galaxies, to the $\sigma^4 = (MGa_0)$ Tully–Fisher relation, in going from $x \gg 1$ to $x \sim 1$ to $x \ll 1$. In that paper it was also shown that solar system constraints will not be violated, provided that the transition in Equation (1) is sufficiently abrupt, $n > 4$, and also that Newton's theorems for spherically symmetric mass distributions will continue to be valid, provided only that f depends exclusively on the variable x.

Recently, in Hernandez & Jiménez (2012) we showed that constructing similarly successful models for GCs requires $n \geqslant 10$ to obtain best fits to brightness and velocity dispersion profiles; here we use $n = 10$ to construct equilibrium models for the elliptical galaxy NGC 4649. Notice also that given the form of the proposed force law, any other larger value of n results in only marginal differences from $n = 10$. Since any feasible modified force law at the Newtonian level evidently requires the form of the force law to be fully fixed across astrophysical systems and scales, here we do not treat n as a free parameter, but use always a fixed $n = 10$ value. A theoretical grounding for the above modified force law appeared in Bernal et al. (2011), who provided an $f(R)$ formal generalization to general relativity which has as its low velocity limit precisely the MONDian force law of Equation (1) in the $a \ll a_0$ range.

Taking the derivative of the kinematic pressure, the equation of hydrostatic equilibrium for a polytropic equation of state $P = K\rho^\gamma$ is

$$\frac{d(K\rho^\gamma)}{dr} = -\rho\nabla\phi. \quad (2)$$

In going to locally isotropic Maxwellian conditions, $\gamma = 1$ and $K = \sigma(r)^2$, and we get

$$2\sigma(r)\frac{d\sigma(r)}{dr} + \frac{\sigma^2(r)}{\rho}\frac{d\rho}{dr} = -\nabla\phi. \quad (3)$$

Since $\rho = (4\pi r^2)^{-1} dM(r)/dr$, the preceding equation can be written as

$$2\sigma(r)\frac{d\sigma(r)}{dr} + \sigma(r)^2\left[\left(\frac{dM(r)}{dr}\right)^{-1}\frac{d^2M(r)}{dr^2} - \frac{2}{r}\right] = -a_0 x\left(\frac{1-x^n}{1-x^{n-1}}\right), \quad (4)$$

with $\sigma(r)$ the isotropic Maxwellian velocity dispersion for the population of stars. This is hence an application of the treatment developed in Hernandez & Jiménez (2012), where we modeled eight GCs in our Galaxy under the same modified force law used here. In that paper we showed that using a plausible parametric $\sigma(r)$ function, self-gravitating models can be easily constructed to accurately reproduce all observational constraints.

Once a specific $\sigma(r)$ is chosen, using a numerical finite differences scheme and the initial condition of a fixed central

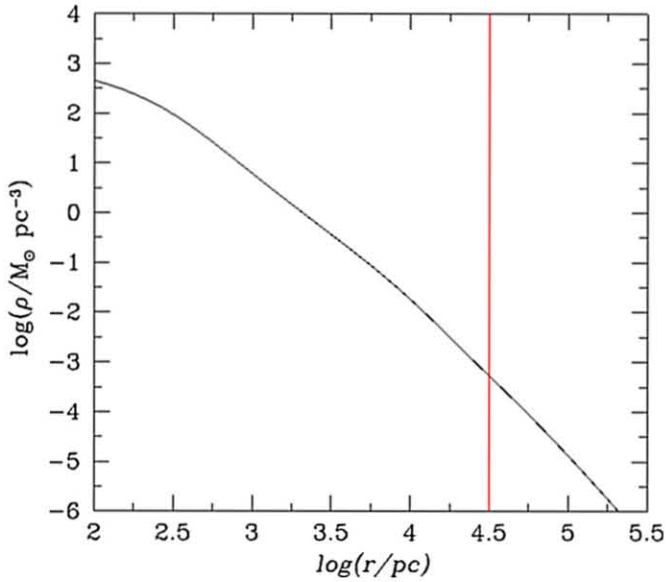

Figure 1. Volumetric density profile for the best-fit model for NGC 4649. The point where $x = 1$, $a = a_0$, is shown by the vertical line. Notice that at large radii $\rho(r)$ becomes steeper than the r^{-2} of the Newtonian case, which yields a finite total radius and mass for the model.

(A color version of this figure is available in the online journal.)

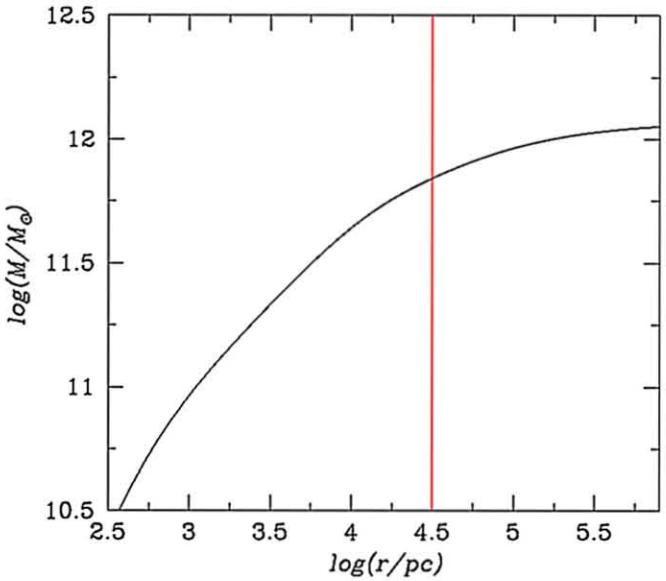

Figure 2. Volumetric mass profile for the best-fit model for NGC 4649. The point where $x = 1, a = a_0$, is shown by the vertical line. Notice the convergence of the mass appearing at large radii.

(A color version of this figure is available in the online journal.)

density ρ_0, i.e., $M(r) \to 0$, $dM(r)/dr \to 4\pi r^2 \rho_0$, for $r \to 0$, the second-order differential equation (Equation (4)) can be solved. This solution gives $\rho(r)$ and $M(r)$, volumetric profiles for the density and mass. Projecting $\rho(r)$ along one direction then yields the corresponding $\Sigma(R)$, a projected surface density mass profile, which, assuming a mass-to-light ratio (M/L), can then be compared against an observed surface brightness profile. We use r for radial distances in three dimensions, and R as a projected radial coordinate on the plane of the sky.

Lastly, a volume density weighted projection of $\sigma(r)$ yields $\sigma_p(R)$, the corresponding projected velocity dispersion profile. Thus, it is only after solving for the complete density structure that a $\sigma_p(R)$ is obtained. Notice that existing observations only give $\sigma_p(R)$, the density weighted projected profiles of $\sigma(r)$, and never $\sigma(r)$ itself. To solve Equation (4), we assume a parametric form for $\sigma(r)$, with parameters which will be adjusted to yield full projected models in surface brightness and $\sigma_p(R)$ in accordance with the properties of the observed galaxy. We shall use

$$\sigma(r) = \sigma_1 \exp\left(-\frac{r}{r_\sigma}\right)^m + \sigma_\infty. \quad (5)$$

Notice that σ_∞ will be given directly by the observations, since at large radial distances the effects of projection tend to zero and $\sigma(R) \to \sigma(r)$. Therefore, σ_∞ can be obtained from the asymptotic value of the observed projected velocity dispersion profile for the galaxy in question, in this case $\approx 200\,\mathrm{km\,s^{-1}}$, following Das et al. (2011). The remaining four free parameters, ρ_0, σ_1, r_σ, and m, will be fitted to yield projected velocity dispersion and surface brightness profiles (following Bridges et al. 2006, we take $M/L = 8.0$) in accordance with the corresponding observed quantities.

3. MODELING ELLIPTICAL GALAXY NGC 4649

We begin this section by presenting in Figures 1 and 2 our best-fit NGC 4649 model. The volumetric density profile is shown in Figure 1, and appears similar to a cored isothermal density distribution, with the difference that at large radii $\rho(r)$ becomes steeper than the Newtonian r^{-2}. The consequence of this steepening is a finite total mass and radius, even using asymptotically flat $\sigma(r)$ profiles, e.g., Milgrom (1984). This contrasts with the Newtonian case where classical isothermal spheres of infinite extent appear. As already pointed out by Hernandez et al. (2010) and Mendoza et al. (2011), these finite profiles also appear for the modified gravity law we are using, even under rigorously isothermal $\sigma(r) = \sigma_0$ equilibrium configurations. The vertical line shows the radius where the condition $x = 1$ is crossed, i.e., the point beyond which $a < a_0$, and hence the departure of the force law used from the Newtonian value toward the MONDian regime, consequently the point where the density profile steepens away from the $1/r^2$ of Newtonian gravity, toward the convergence of the MONDian regime.

The corresponding volumetric radial mass profile is given in Figure 2, where the vertical line again shows the $x = 1$ threshold. This clearly shows the departure from the linear growth of the total mass within the approximately isothermal Newtonian region, toward convergence to a finite total mass in the MONDian $a < a_0$ regime. We see that 40% of the mass of the modeled galaxy falls outside of the $x = 1$ threshold. This mass appears spread out over large areas, and hence presents much smaller surface densities than those appearing in the central regions interior to the $a > a_0$, $x = 1$ limit, the more easily observed Newtonian central parts.

The consistency of the model is shown in Figures 1 and 2; having assumed a positive isotropic Maxwellian velocity distribution function, the physical modeling results in a mass density profile in accordance with what a Newtonian modeling would have yielded for the inner $a > a_0$ region, where the force law used reproduces Newton's expression. In going to larger radii, $\rho(r)$ steepens increasingly to eventually reach $\rho(r) = 0$ at a finite total radius, as can be seen from the convergence of the mass profile given in Figure 2. The distribution function is thus positive throughout the model, going to zero at the outer edge.

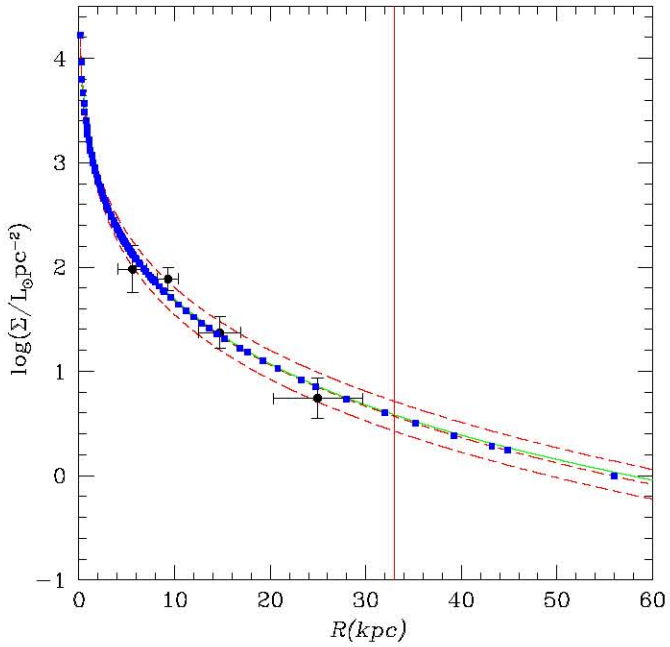

Figure 3. Comparison of the resulting model projected surface brightness for NGC 4649 (continuous line) with the corresponding observed quantities and the best-fit Sérsic function with the central (dashed line), maximum, and minimum values consistent with the reported confidence intervals for the Sérsic parameters, flanking curves. The squares correspond to data in Kormendy et al. (2009), and the points with error bars to PNe data (Teodorescu et al. 2011). Following Bridges et al. (2006), we take $M/L_V = 8$, which coincides with the stellar population studies of Shen & Gebhardt (2010). The point where $a = a_0$ and the modified force law used changes from the Newtonian form to the outer MONDian behavior is shown by the vertical line.

(A color version of this figure is available in the online journal.)

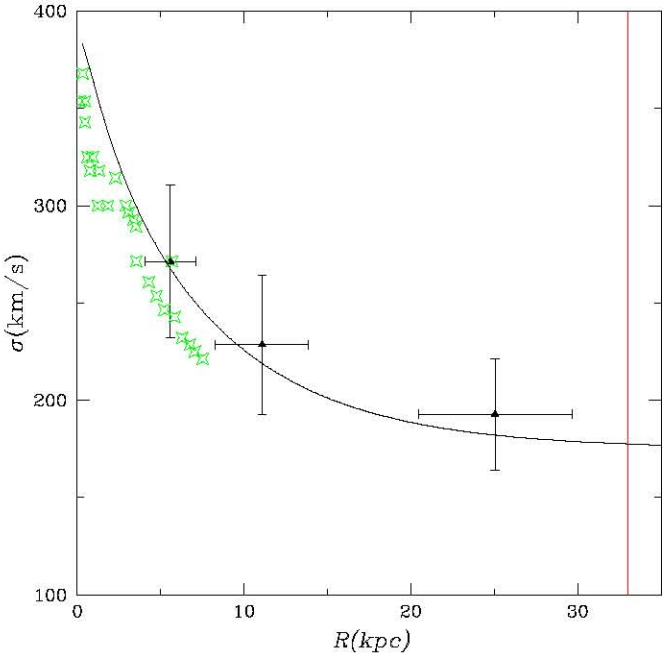

Figure 4. Comparison of the resulting model projected velocity dispersion profile for NGC 4649 (continuous line) with the corresponding observed quantities; stars for long-slit observations in Pinkney et al. (2003) and the points with error bars for PNe data. The point where $a = a_0$ and the modified force law used changes from the Newtonian form to the outer MONDian behavior is shown by the vertical line.

(A color version of this figure is available in the online journal.)

The optimum model shown was fitted to agree with the observed projected velocity dispersion and surface brightness profile for NGC 4649, assuming a constant M/L_V value; see below. We take the surface brightness profile observations from photometry in Kormendy et al. (2009) and the number density calculated from PNe in Teodorescu et al. (2011) as scaled in Das et al. (2011), and projected velocity dispersion measurements from Pinkney et al. (2003) adopted from De Bruyne et al. (2001). Following Bridges et al. (2006) we take $M/L_V = 8$, which coincides with the central value reported by Shen & Gebhardt (2010), determined directly from stellar population synthesis models.

The final resulting surface brightness profile and its corresponding volume density weighted projected velocity dispersion profile $\sigma_p(R)$ for galaxy NGC 4649 are presented in Figures 3 and 4 for $M/L_V = 8$. The parameters for the best fit in Equation (5) are $\sigma_\infty = 175\,\mathrm{km\,s^{-1}}$, $\sigma_1 = 230\,\mathrm{km\,s^{-1}}$, $r_\sigma = 8.5\,\mathrm{kpc}$, and $m = 1$; the central density that we have assumed is $\rho_0 = 1.5 \times 10^2\,M_\odot\,\mathrm{pc^{-3}}$.

Regarding the free parameters of the model, m, σ_1, r_σ, and ρ_0, we began with $m = 1$ as used in our GC study of Hernandez & Jiménez (2012), and with a trial r_σ at the effective radius of the galaxy, and a trial σ_1 at the $\sigma_p(R = 0) = \sigma_1 + \sigma_\infty$ condition. We then performed a least-squares fit to the well-established projected surface density profile to obtain an optimal ρ_0 value. The projected $\sigma(R)$ profile was then visually examined, and the procedure ended if the model agreed with these more uncertain observations to within their reported error bands. If not, the procedure is repeated with r_σ and σ_1 re-adjusted to yield a larger or smaller central $\sigma_p(R = 0)$ value, or a faster or slower decay in the $\sigma_p(R)$ curve. Only at the lowest M/L range were solutions with $m = 1$ slightly less good than the ones presented, so the procedure was repeated with slight variations in m. We do not claim the models obtained to be unique, neither did we set out to find final values for our parameters which could be definitively associated to NGC 4649, merely working models intended to show the plausibility of the force law examined. We do note, however, that the full observed and Sérsic fit to the projected surface density profile can be reproduced, not only within the observed uncertainties, but actually to an almost indistinguishable level, giving us confidence that some of the physics of the problem has been captured by the modeling presented. At the same time, the more uncertain projected velocity dispersion profile has also been adequately reproduced, to within the observational confidence intervals.

In the figures, the vertical line indicates the point where $a = a_0$; we can see that the model accurately fits the observed projected surface brightness profiles of the galaxy and the central value of the measured projected velocity dispersion $\sigma_p(R = 0) = 400\,\mathrm{km\,s^{-1}}$, as well as the observed profiles for $\sigma_p(R)$.

We see that both the surface brightness and velocity dispersion profiles are in agreement with photometry and PNe observations, to within reported uncertainties. Under Newtonian gravity, this requires invoking a large amount of dark matter to reproduce the structure and kinematics of this galaxy; using the proposed modified force law, however, it is natural that once the change in the gravitational regime appears, $\sigma(r)$ will tend to a constant once the mass distribution has converged.

Although the projected surface brightness profile of the model shown in Figure 3 is in excellent accordance with the observed one, a value of $M/L_V = 8$ might appear as somewhat excessive. Indeed, from Figure 4 we see that the projected

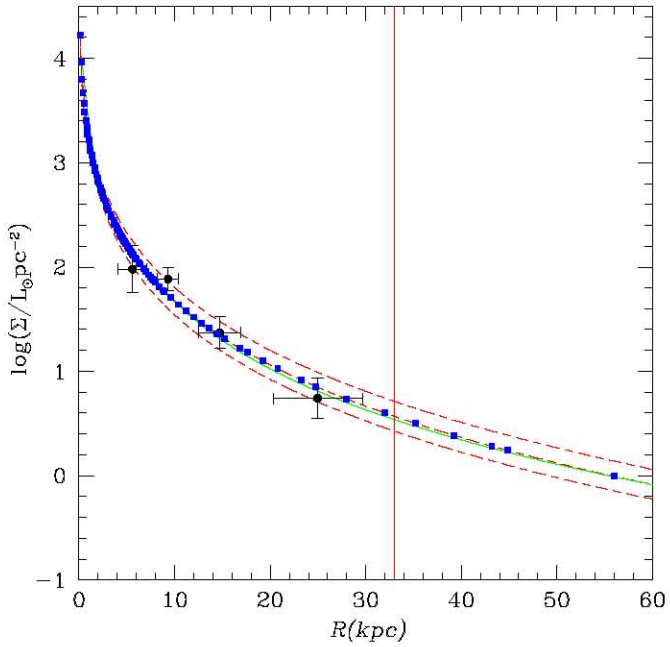

Figure 5. Same as Figure 3 but using $M/L_V = 6$.
(A color version of this figure is available in the online journal.)

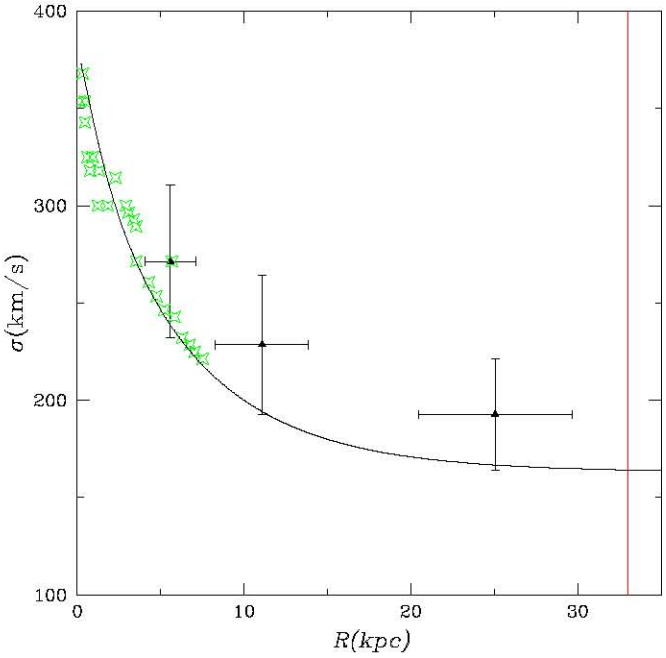

Figure 6. Same as Figure 4 but using $M/L_V = 6$.
(A color version of this figure is available in the online journal.)

velocity dispersion of the model systematically exceeds the measurements from long-slit observations, and is more in accordance with the more crude PNe inferences. To test the range of values in M/L_V that the physical modeling can accommodate, we repeated the experiment, taking this time a lower value of $M/L_V = 6$. The results are presented in Figures 5 and 6, which are analogous to Figures 3 and 4. We see a similarly excellent accordance for the projected surface brightness profile in Figure 5, and a projected velocity dispersion profile in Figure 6 which this time closely follows the more detailed data of the long-slit observations, and lies slightly below the PNe inferences. The parameters of this second model are $\sigma_\infty = 163\,\mathrm{km\,s^{-1}}$, $\sigma_1 = 233\,\mathrm{km\,s^{-1}}$, $r_\sigma = 6.6\,\mathrm{kpc}$, and $m = 0.95$, with $\rho_0 = 2.3 \times 10^2\,M_\odot\,\mathrm{pc}^{-3}$.

M/L ratios higher than 8 appear unphysical from the point of view of pure stellar populations, while models with values lower than 6 result in $\sigma(R)$ curves which fall below the observed values. The range $6 < M/L_V < 8$ thus brackets the models which can yield accurate simultaneous fits to both the observed surface brightness profile and the observed velocity dispersion profile of NGC 4649.

The total mass we obtain from the dynamical modeling described is consistent with what results from the integration of the surface brightness profile assuming a constant M/L_V. The mass obtained for the dynamical model to NGC 4649 is $1.09 \times 10^{12}\,M_\odot$, and the luminosity that results from integrating the V-band light profile is $1.36 \times 10^{11}\,L_\odot$, implying a mass of $1.08 \times 10^{12}\,M_\odot$ from using $M/L_V = 8$ as determined directly from the stellar population studies of Shen & Gebhardt (2010). Also, notice that the asymptotic value of the velocity dispersion is $195.0 \pm 30.36\,\mathrm{km\,s^{-1}}$ in consistency with the $\sigma = 0.2\,(M/M_\odot)^{1/4} = 203.9\,\mathrm{km\,s^{-1}}$ prediction of Hernandez & Jiménez (2012) for $1.08 \times 10^{12}\,M_\odot$, and $190.09\,\mathrm{km\,s^{-1}}$ for the $8.16 \times 10^{11}\,M_\odot$ of the $M/L_V = 6$ case.

Models including a degree of orbital anisotropy, constant or with radial variations, are also possible, as are ones considering also some degree of sub-dominant rotation, as often observed in elliptical galaxies. Introducing more free functions would clearly allow even finer fits to the observed restrictions. We have chosen not to increase the complexity of the modeling in this way, as our aim here is merely to prove that for the simplest isotropic, non-rotating construction, reproducing all the available observational constraint is easily achieved under the modified force tested. As already mentioned, the models presented are not intended as unique definitive fittings to any of the parameters used, merely as examples of plausible models showing the viability of the force law used.

4. CONCLUSIONS

We show that for the massive elliptical galaxy NGC 4649, fully self-consistent spherically symmetric equilibrium models can be constructed using a modified Newtonian force law which smoothly transits from the Newtonian value when $a > a_0$, toward the MONDian phenomenology in the $a < a_0$ regime, which naturally satisfy all observational constraints available for the central, asymptotic, and radial profiles for projected surface brightness and velocity dispersion measurements. All this, without the need to invoke any hypothetical and as yet undetected dark matter component.

We obtain models which show a Newtonian inner region, smoothly evolving outward toward a MONDian solution on crossing the $a = a_0$ limit. The corresponding velocity dispersion profiles similarly evolve from an internal "Keplerian" region to an external constant velocity dispersion regime.

We show that the asymptotic value of the observed velocity dispersion profile, $\sigma_p(R \to \infty)$, and the total mass for this system, M, are consistent with the generic modified gravity prediction for $\sigma_p(R \to \infty) = 0.2\,(M/M_\odot)^{1/4}$.

The authors wish to thank an anonymous referee for comments leading to a clearer and more complete final version. Xavier Hernandez acknowledges financial assistance from UNAM DGAPA grant IN103011-3. Alejandra Jimenez acknowledges financial support from a CONACYT scholarship.

REFERENCES

Bekenstein, J. D. 2004, PhRvD, 70, 083509
Bernal, T., Capozziello, S., Hidalgo, J. C., & Mendoza, S. 2011, EPJC, 71, 1794
Bosma, A. 1981, AJ, 86, 1825
Bridges, T., Gebhardt, K., Sharples, R., et al. 2006, MNRAS, 373, 157
Das, P., Gerhard, O., Churazov, E., & Zhuravleva, I. 2010, MNRAS, 409, 1362
Das, P., Gerhard, O., Mendez, R. H., Teodorescu, A. M., & de Lorenzi, F. 2011, MNRAS, 415, 1244
De Bruyne, V., Dejonghe, H., Pizzella, A., Bernardi, M., & Zeilinger, W. W. 2001, ApJ, 546, 903
Haghi, H., Baumgardt, H., & Kroupa, P. 2011, A&A, 527, A33
Hernandez, X., & Jiménez, M. A. 2012, ApJ, 750, 9
Hernandez, X., Jiménez, M. A., & Allen, C. 2012, EPJC, 72, 1884
Hernandez, X., Mendoza, S., Suarez, T., & Bernal, T. 2010, A&A, 514, A101
Kormendy, J., Fisher, D. B., Cornell, M. E., & Bender, R. 2009, ApJS, 182, 216
Kroupa, P., Famaey, B., de Boer, K. S., et al. 2010, A&A, 523, A32
McGaugh, S. S., & de Blok, W. J. G. 1998, ApJ, 499, 41
McGaugh, S. S., & Wolf, J. 2010, ApJ, 722, 248
Mendoza, S., Bernal, T., Hernandez, X., Hidalgo, J. C., & Torres, L. A. 2012, arXiv:1208.6241
Mendoza, S., Hernandez, X., Hidalgo, J. C., & Bernal, T. 2011, MNRAS, 411, 226
Milgrom, M. 1983, ApJ, 270, 365
Milgrom, M. 1984, ApJ, 287, 571
Moffat, J. W., & Toth, V. T. 2010, arXiv:1005.2685
Pinkney, J., Gebhardt, K., Bender, R., et al. 2003, ApJ, 596, 903
Romanowsky, A. J., Douglas, N. G., Arnaboldi, M., et al. 2003, Sci, 301, 1696
Rubin, V. C., Ford, W. K., Jr., Thonnard, N., & Burstein, D. 1982, ApJ, 261, 439
Samurović, S., & Ćirković, M. M. 2008a, A&A, 488, 873
Samurović, S., & Ćirković, M. M. 2008b, SerAJ, 177, 1
Sanders, R. H., & McGaugh, S. S. 2002, ARA&A, 40, 263
Shen, J., & Gebhardt, K. 2010, ApJ, 711, 484
Simon, J. D., & Geha, M. 2007, ApJ, 670, 313
Sollima, A., & Nipoti, C. 2010, MNRAS, 401, 131
Swaters, R. A., Sanders, R. H., & McGaugh, S. S. 2010, ApJ, 718, 380
Teodorescu, A. M., Méndez, R. H., Bernardi, F., et al. 2011, ApJ, 736, 65
Zhao, H., & Famaey, B. 2010, PhRvD, 81, 087304

3. PERFIL DE DISPERSIÓN DE VELOCIDADES ASINTÓTICAMENTE PLANO EN CÚMULOS GLOBULARES: MODELOS CON GRAVEDAD MODIFICADA

Capítulo 4

¿Gravedad modificada o mareas newtonianas en cúmulos globulares?

4.1. Resumen

Observaciones hechas en años recientes muestran que el perfil de dispersión de velocidades proyectado sobre la linea de visión de cúmulos globulares de nuestra galaxia sufre un aplanamiento a partir de cierto radio. La dispersión de velocidades conforme aumenta la distancia al centro del cúmulo ya no decrece sino que tiende a un valor constante σ_∞.

En el contexto de la gravedad newtoniana este comportamiento tiende a explicarse como consecuencia del calentamiento de las fuerzas de marea sobre las estrellas en la periferia del cúmulo ocasionado por el potencial de la Vía Láctea.

En gravedad modificada en cambio, se espera un aplanamiento del perfil de dispersión de velocidades en el lugar donde la aceleración es menor que a_0, ya que es aquí donde ocurre la transición de una dinámica newtoniana a una dinámica MONDiana donde las velocidades de equilibrio dejan de ser función del radio. En este capitulo contrastamos estas dos posibles explicaciones desde un análisis puramente empírico.

Calculamos el radio de marea de los cúmulos globulares utilizando el estudio detallado de (Allen & Santillan 1991) de la órbita de 54 cúmulos globulares, para los cuales se conocen sus movimientos propios y sus velocidades sobre la linea de visión. En este estudio se utiliza un modelo de masa $3D$ axisimétrico (bulbo, disco, halo de materia oscura que se extiende hasta $100kpc$) para nuestra galaxia así como un modelo con barra, los 16 CGs de nuestra muestra están incluidos, las masas de los cúmulos son obtenidas por modelos de síntesis de poblaciones

estelares que son independientes de cualquier supuesto dinámico.

Encontramos que el radio de marea en el punto de la órbita del cúmulo más cercano al centro galáctico es en general mayor que el radio en el cual el perfil se aplana, este hecho hace que la explicación de que las fuerzas de marea newtonianas son las responsables del aplanamiento del perfil de dispersión de velocidades inadecuado. Por otro lado se observa que el radio al cual el perfil se aplana coincide en promedio con el radio en el cual se cruza el umbral de aceleración a_0 y que σ_∞ resulta proporcional a la raíz cuarta de la masa (relación Tully - Fisher), es decir se observa lo esperado en un contexto de gravedad modificada.

Para este artículo realice los ajustes del perfil de dispersión de velocidades, Compare estos ajustes con los existentes en la literatura en el contexto newtoniano, realice las comparaciones entre R_f y R_T y entre R_f y R_a y junto con los demás autores participe en todo el proceso de revisión hasta lograr la publicación del trabajo.

MNRAS **428,** 3196–3205 (2013) doi:10.1093/mnras/sts263

Flattened velocity dispersion profiles in globular clusters: Newtonian tides or modified gravity?

X. Hernandez,⋆ M. A. Jiménez and C. Allen

Instituto de Astronomía, Universidad Nacional Autónoma de México, Apartado Postal 70–264 C.P. 04510 D.F., Mexico

Accepted 2012 October 22. Received 2012 October 18; in original form 2012 June 21

ABSTRACT

Over the past couple of years, a number of observational studies have confirmed the flattening of the radial velocity dispersion profiles for stars in various nearby globular clusters. As the projected radial coordinate is increased, a radius appears beyond which, the measured velocity dispersion ceases to drop and settles at a fixed value, σ_∞. Under Newtonian gravity, this is explained by invoking tidal heating from the overall Milky Way potential on the outer, more loosely bound stars of the globular clusters in question. From the point of view of modified gravity theories, such an outer flattening is expected on crossing the critical acceleration threshold a_0, beyond which, a transition to MONDian dynamics is expected, were equilibrium velocities cease to be a function of distance. In this paper, we attempt to sort out between the above competing explanations, by looking at their plausibility in terms of an strictly empirical approach. We determine Newtonian tidal radii using masses accurately calculated through stellar population modelling, and hence independent of any dynamical assumptions, distances, size and orbital determinations for a sample of 16 globular clusters. We show that their Newtonian tidal radii at perigalacticon are generally larger that the radii at which the flattening in the velocity dispersion profiles occurs, by large factors of 4, on average. While this point makes the Newtonian tidal explanation suspect, it is found that the radii at which the flattening is observed on average correlate with the radii where the a_0 threshold is crossed, and that σ_∞ values scale with the fourth root of the total masses, all features predicted under modified gravity theories.

Key words: gravitation – stars: kinematics and dynamics – globular clusters: general – Galaxy: kinematics and dynamics.

1 INTRODUCTION

The central values of the stellar velocity dispersion, projected on the plane of the sky, for many Galactic globular clusters (GCs) have been well known for decades, and are known to accurately correspond to the expectations of self-consistent dynamical models under Newtonian gravity, e.g. King models (e.g. Binney & Tremaine 1987; Harris 1996). Recently, a number of studies (e.g. Scarpa & Falomo 2010; Scarpa et al. 2007a,b, 2011; Lane et al. 2009, 2010a,b, 2011, henceforth the Scarpa et al. and Lane et al. groups, respectively) have performed measurements of the projected velocity dispersion along the line of sight for stars in a number of Galactic GCs, but as a function of radius, and reaching in many cases out to radial distances larger than the half-light radii of the clusters by factors of a few.

The surprising result of the above studies has been that radially, although velocity dispersion profiles first drop along Newtonian expectations, after a certain radius, settle to a constant value which varies from cluster to cluster. This behaviour is what is expected under MOND (Milgrom 1983), where equilibrium velocities tend to a constant value when below a critical acceleration, a_0. In fact, such a result is fairly generic to modified theories of gravity designed to explain galactic rotation curves in the absence of any dark matter, e.g. Milgrom (1994), Bekenstein (2004), Zhao & Famaey (2010), Bernal et al. (2011), Mendoza et al. (2011), Capozziello & De Laurentis (2011). As already noted by Scarpa et al. (2011), it is suggestive of a modified gravity scenario that the point where the velocity dispersion profiles flatten, approximately corresponds to the point where average stellar accelerations drop below a_0. Several recent studies have shown dynamical models for self-gravitating populations of stars under MOND or other modified gravity variants (e.g. Moffat & Toth 2008; Haghi et al. 2009; Sollima & Nipoti 2010; Haghi, Baumgardt & Kroupa 2011; Hernandez & Jiménez 2012) which accurately reproduce not only the observed velocity

⋆ E-mail: xavier@astro.unam.mx

dispersion profiles, but also the observed surface brightness profiles of GCs.

A recent study reaching the same conclusions, but at a significantly distinct scale, can be found in our work (Hernandez, Jiménez & Allen 2012), where we show that the relative velocity of wide binaries in the solar neighbourhood is in conflict with predictions from full galactic dynamical simulations of the systems observed, and actually shows also velocities which cease to drop with distance, precisely on crossing the same a_0 threshold. Along the same lines, Lee & Komatsu (2010) show that the infall velocity of the two components of the Bullet cluster, as required to account for the hydrodynamical shock observed in the gas, is inconsistent with expectations of full cosmological simulations under standard Λ cold dark matter (ΛCDM) assumptions. This has recently been confirmed in greater detail by Thompson & Nagamine (2012), and can in fact be seen as a failure not only of the ΛCDM model, but of standard gravity, as the required collisional velocity is actually larger than the escape velocity of the combined system. We note also the recent reviews by Kroupa et al. (2010), Famaey & McGaugh (2012) and Kroupa (2012) and references therein, detailing a number of observations in tension with standard ΛCDM assumptions.

From the point of view of assuming Newtonian gravity to be exactly valid at all low-velocity regimes, it has also been shown that both velocity dispersion and surface brightness profiles for Galactic GCs can be self-consistently modelled. Under this hypothesis, it is dynamical heating due to the overall Milky Way potential that is responsible for the flattening of the velocity dispersion profiles e.g. Drukier et al. (2007), Küpper et al. (2010), Lane et al. (2010a). The constant velocity dispersion observed at large radii merely shows the contribution of unbound stars in the process of evaporating into the Milky Way halo. In attempting to sort between these two contrasting scenarios, here we take a fully empirical approach. We critically examine the plausibility of both gravitational scenarios by looking through the data for other correlations which each suggest.

For the Newtonian case, we examine the best-available inferences for the tidal radius of each cluster at closest galactocentric passage, and compare it to the observed point where the velocity dispersion flattens. Here, we find the former to generally exceed the latter by factors of 4 on average, making the Newtonian interpretation suspect. Also, we take all the clusters which the Lane et al. group have claimed show no indication of a modified gravity phenomenology, based on the fact that their velocity dispersion profiles can be modelled using Plummer profiles, and show that the fits with the generic asymptotically flat profiles we use are actually slightly better, in all cases.

From the point of view of MONDian-modified gravity theories, we reexamine in greater detail the correlation between the crossing of the a_0 threshold and the point where the velocity dispersion flattens, already suggested by Scarpa et al. (2011). We shall use the term MONDian to refer to any modified theory of gravity which reproduces the basic phenomenology of MOND in the low-velocity limit for accelerations below a_0, of flat equilibrium velocities and a Tully–Fisher relation, regardless of the details of the fundamental theory which might underlie this phenomenology.

In consistency with the expectations of such theories, we find that mostly systems almost fully within the $a < a_0$ threshold show almost fully flat velocity dispersion profiles, while those which only reach this threshold at their outskirts present a significant Newtonian region, with a large fall in their velocity dispersion profiles. The above correlations are actually what would be expected generically under modified gravity schemes. We confirm our previous results with a much smaller sample of Hernandez & Jiménez (2012), showing that the asymptotic values of the velocity dispersion profiles are consistent with scaling with the fourth root of the total masses, a Tully–Fisher relation for GCs. Our results support the interpretation of the observed phenomenology as evidence for a change in regime for gravity on crossing the a_0 threshold.

In Section 2, we present the detailed velocity dispersion fitting procedure, and show the best-fitting profiles, including a comparison with the Plummer models used by the Lane et al. group, which are slightly worse than the asymptotically flat profiles we use. A description of the tidal radii derivations and the calculation of the confidence intervals for all the GC parameters used is also given. Section 3 shows a comparison of the tidal radii against the radii at which the velocity dispersion becomes flat, as a test of the plausibility of Galactic tides under a Newtonian scenario as responsible for the observed outer flattening of the velocity dispersion profiles. In Section 4, we present a number of scalings between the structural parameters of the observed GCs, showing these systems to be consistent with MONDian gravity expectations, in terms of a change towards a modified regime on crossing the a_0 threshold. Our conclusions are summarized in section 5.

2 EMPIRICAL VELOCITY DISPERSION MODELLING

We begin by modelling the observed projected radial velocity dispersion profiles, $\sigma_{\rm obs}(R)$, in the GCs in our sample, listed in Table 1. As seen from the Scarpa et al. and Lane et al. data, the observed velocity dispersion profiles show a central core region where the velocity dispersion drops only slightly, followed by a 'Keplerian' zone where the drop is more pronounced. These first two regions are in accordance with standard Newtonian King profiles, but they are then followed by a third outermost region where the velocity dispersion profiles cease to fall along Keplerian expectations, and settle to fixed values out to the last measured point. As some of us showed in Hernandez & Jiménez (2012), an accurate empirical modelling for these velocity dispersion profiles can be achieved through the function

$$\sigma(R) = \sigma_1 {\rm e}^{-(R/R_\sigma)^2} + \sigma_\infty. \quad (1)$$

In the above equation σ_∞ is the asymptotic value of $\sigma(R)$ at large radii, R_σ a scale radius fixing how fast the asymptotic value is approached, and σ_1 a normalization constant giving $\sigma(R=0) = \sigma_1 + \sigma_\infty$.

We now take the observed data points $\sigma_{\rm obs}(R_i)$ along with the errors associated with each data point, to determine objectively through a maximum likelihood method the best-fitting values for each of the three parameters in equation (1), for each of the 16 observed GCs. Assuming the errors to have a Gaussian distribution, the likelihood function will be

$$\mathcal{L}(\sigma_\infty, \sigma_1, R_\sigma; \sigma_{\rm obs}(R_i)) = \prod_{i=1}^{n} \frac{\exp\left[-(\sigma_{\rm obs}(R_i) - \sigma(R_i))^2/2\Delta_i^2\right]}{\Delta_i}, \quad (2)$$

where Δ_i is the error on the ith data point, and $\sigma(R)$ is a particular model resulting from a given choice of the three model parameters. Thus, for any choice of the three model parameters, the likelihood function can be calculated for a given data set $\sigma_{\rm obs}(R_i)$ with its errors. For each observed GC, we calculate the likelihood function over a 100^3 grid in parameter space, and then select the point where this function is maximized, to identify the optimal set of parameters for each observed velocity dispersion profile, $(X_{1,0}, X_{2,0}, X_{3,0})$. As it

Table 1. Parameters for the GCs treated.

GC	σ_1 (km s^{-1})	σ_∞ (km s^{-1})	R_σ (pc)	R_a (pc)	$R_{1/2}$ (pc)	$R_{\rm T}$ (pc)	$\log_{10}$ (M/M$_\odot$)	b	$\Delta V_{\rm r}$ (km s^{-1})
NGC 104[b]	4.5 ± 0.4	5.0 ± 0.1	14.8 ± 0.9	23.6 ± 1.3	8.7 ± 1	93.5 ± 11.1	6.3 ± 0.2	-45.20	-18.7
NGC 288[a, b]	2.3 ± 1.4	0.2 ± 0.8	24.0 ± 5.8	4.8 ± 1.2	5.9 ± 1	33.8 ± 4.2	4.8 ± 0.2	-89.38	-46.6
NGC 1851[a]	4.2 ± 3.0	3.9 ± 0.4	7.9 ± 2.4	13.6 ± 4.5	2.4 ± 1	60.9 ± 10.7	5.6 ± 0.2	-35.03	320.5
NGC 1904[a]	2.4 ± 0.3	2.0 ± 0.1	10.3 ± 2.9	8.4 ± 2.6	2.7 ± 1	55.8 ± 9.4	4.9 ± 0.2	-29.35	206.0
NGC 4590[b]	1.5 ± 0.6	0.8 ± 0.4	18.1 ± 5.0	3.9 ± 1.1	8.0 ± 1	49.8 ± 6.0	5.7 ± 0.2	35.8	-94.3
NGC 5024[b]	2.4 ± 1.5	2.4 ± 0.5	24.0 ± 3.8	12.3 ± 2.2	7.8 ± 1	184.1 ± 22.2	5.6 ± 0.2	79.3	-62.9
NGC 5139[a]	8.0 ± 1.0	7.2 ± 0.4	16.8 ± 2.1	41.9 ± 5.6	7.2 ± 1	55.3 ± 8.9	6.4 ± 0.2	14.97	232.3
NGC 6121[b]	1.3 ± 1.0	2.9 ± 0.6	5.9 ± 4.6	8.0 ± 8.0	3.8 ± 1	9.6 ± 1.3	4.9 ± 0.2	15.38	70.7
NGC 6171[a]	1.4 ± 0.6	2.7 ± 0.2	3.8 ± 1.1	6.4 ± 1.5	3.2 ± 1	30.8 ± 5.2	4.9 ± 0.2	23.01	-33.6
NGC 6218[b]	3.3 ± 0.9	1.4 ± 0.5	4.7 ± 1.2	4.9 ± 1.4	1.8 ± 1	34.5 ± 4.4	4.9 ± 0.2	-42.20	25.71
NGC 6341[a]	3.8 ± 0.7	3.1 ± 0.2	6.8 ± 2.4	10.0 ± 2.0	3.2 ± 1	20.6 ± 3.4	5.3 ± 0.2	34.86	-120.3
NGC 6656[b]	3.8 ± 1.3	3.3 ± 0.8	7.4 ± 1.7	11.1 ± 2.9	2.7 ± 1	58.6 ± 7.0	5.4 ± 0.2	-8.15	-146.3
NGC 6752[b]	3.5 ± 0.8	2.0 ± 0.3	10.7 ± 1.4	5.5 ± 0.9	3.7 ± 1	63.9 ± 7.8	4.9 ± 0.2	-23.87	174.7
NGC 6809[b]	1.1 ± 0.8	1.6 ± 0.5	16.0 ± 5.8	5.5 ± 2.0	2.7 ± 1	28.6 ± 3.6	4.9 ± 0.2	-29.35	206.0
NGC 7078[a]	5.1 ± 1.6	3.0 ± 0.3	8.7 ± 1.4	12.0 ± 1.7	3.2 ± 1	127.5 ± 21.0	5.5 ± 0.2	-27.31	-107.0
NGC 7099[a, b]	2.1 ± 0.4	2.0 ± 0.2	6.8 ± 1.1	6.7 ± 2.4	2.1 ± 1	53.4 ± 8.3	4.8 ± 0.2	-46.80	-185.0

The first three entries give the parameters of the fits to the observed projected velocity dispersion profiles and their confidence intervals to data from the Scarpa et al. group[a] and the Lane et al. group[b]. The fourth column gives an empirical estimate of the point where the average stellar acceleration drops below a_0. Columns 5–7 give the half-light radius calculated from the surface density light profiles, the Newtonian tidal radius from the Galactic mass model and orbital calculations derived from observed proper motions by Allen et al. (2006), and the total masses derived from the M/L values inferred through stellar population modelling by McLaughlin & van der Marel (2005) for each cluster, with corresponding confidence intervals. The last two columns give the Galactic latitude of the clusters, and the radial velocity difference with respect to the Sun.

is customary, we work with the logarithm of the likelihood function. The confidence intervals for each of the three parameters are then obtained by looking through the full likelihood matrix to identify the largest and smallest values for a particular parameter which satisfy the condition $\ln\mathcal{L}(X_{\rm lim}, X_2, X_3) - \ln\mathcal{L}(X_{1,0}, X_{2,0}, X_{3,0}) = 0.5$, i.e. the full projection of the error ellipsoid is considered, without imposing any marginalization. This last point allows us to properly account for any correlations between the three fitted parameters when calculating any quantity derived from combinations of them, as will be constructed in what follows.

Taking $\sigma_{\rm obs}(R_i)$ data from Drukier et al. (1998), Scarpa, Marconi & Gilmozzi (2004), Scarpa et al. (2007a,b, 2010, 2011), Lane et al. (2009, 2010a,b, 2011) and half-light radii, $R_{1/2}$, from integrating the surface density brightness profiles of Trager, King & Djorgovski (1995), we perform a maximum likelihood fit as described above for all the 16 GCs studied.

Fig. 1 shows the observed projected velocity dispersion profiles for the six GCs from the Scarpa et al. group, which are not also part of the Lane et al. total sample, denoted by points with error bars. The radial coordinate has been normalized to the $R_{1/2}$ radius of each of the clusters. The continuous curves show the maximum likelihood fits for each cluster, which are clearly good representations of the data. We can now give $R_{\rm f} = 1.5R_\sigma$ as an adequate empirical estimate of the radius beyond which the dispersion velocity profile becomes essentially flat. In terms of equation (1), which can be seen to be highly consistent with the observed velocity dispersion profiles, $R_{\rm f}$ is the radius such that $\sigma(R_{\rm f}) = 0.1\sigma_1 + \sigma_\infty$, a good representation of the transition to the flat behaviour, as can be checked from Fig. 1, where the arrows give $R_{\rm f}$, with the horizontal lines on the arrows showing the 1σ confidence intervals on these fitted parameters. An empirical definition of the radius where the typical acceleration felt by stars drops below a_0 can now be given as R_a, where

$$\frac{3\sigma(R_a)^2}{R_a} = a_0. \tag{3}$$

Using the above definition, we can now identify R_a for each of the GCs studied. The vertical lines in Fig. 1 show R_a for each cluster, also normalized to the half-light radius of each. In the figure, clusters have been ordered by their $R_a/R_{1/2}$ values, with the smallest appearing at the top, and $R_a/R_{1/2}$ growing towards the bottom of the figure.

The Lane et al. sample comprises 10 clusters, two of which are also part of the Scarpa et al. sample. Fig. 2 is analogous to Fig. 1, and shows velocity dispersion profiles for five clusters from the Lane et al. sample not having any overlap with the Scarpa et al. group. Here, we have added also the best-fitting Plummer models to the data, with parameters taken from the Lane et al. papers, and shown by the dashed curves. It is obvious that both functional forms provide good representations to the data, which qualitatively, display an asymptotically flat region at large radii. At large radii, the line-of-sight velocity dispersion profiles for the Plummer models fall to zero, but only very slowly, as $R^{-1/2}$. This allows good fits to data which qualitatively tend to constant values. The good fits allowed by the Plummer models are clearly not sufficient to dismiss a modified gravity interpretation, as the asymptotically flat projected dispersion velocity fits of the type used for full dynamical modelling under modified gravity (Hernandez & Jiménez 2012) are equally consistent with the data.

Fig. 3 completes the fits to the Lane et al. sample, where NGC 6121, NGC 6218 and NGC 6752 are analogous to the ones shown in Fig. 2. Again, the dashed and solid curves are essentially equivalent. The remaining two clusters in this figure give the two examples which have been studied by both groups of observers, NGC 7099 and NGC288, where the triangles and dots with error bars give the Scarpa et al. and Lane et al. data, respectively. In these last two cases, the dashed lines give the best-fitting Plummer models from the Lane et al. papers, and the solid lines the best-fitting models from equation (1), considering joint data samples from both groups. An equation (1) fit limited to the Lane et al. data for these last two clusters was also performed, for the comparison shown in the following figure. For the last two clusters, we see that the two independent data samples are consistent with a fixed underlying distribution, and also, that the fits to the added samples from equation (1) represent the data as well as the Plummer models.

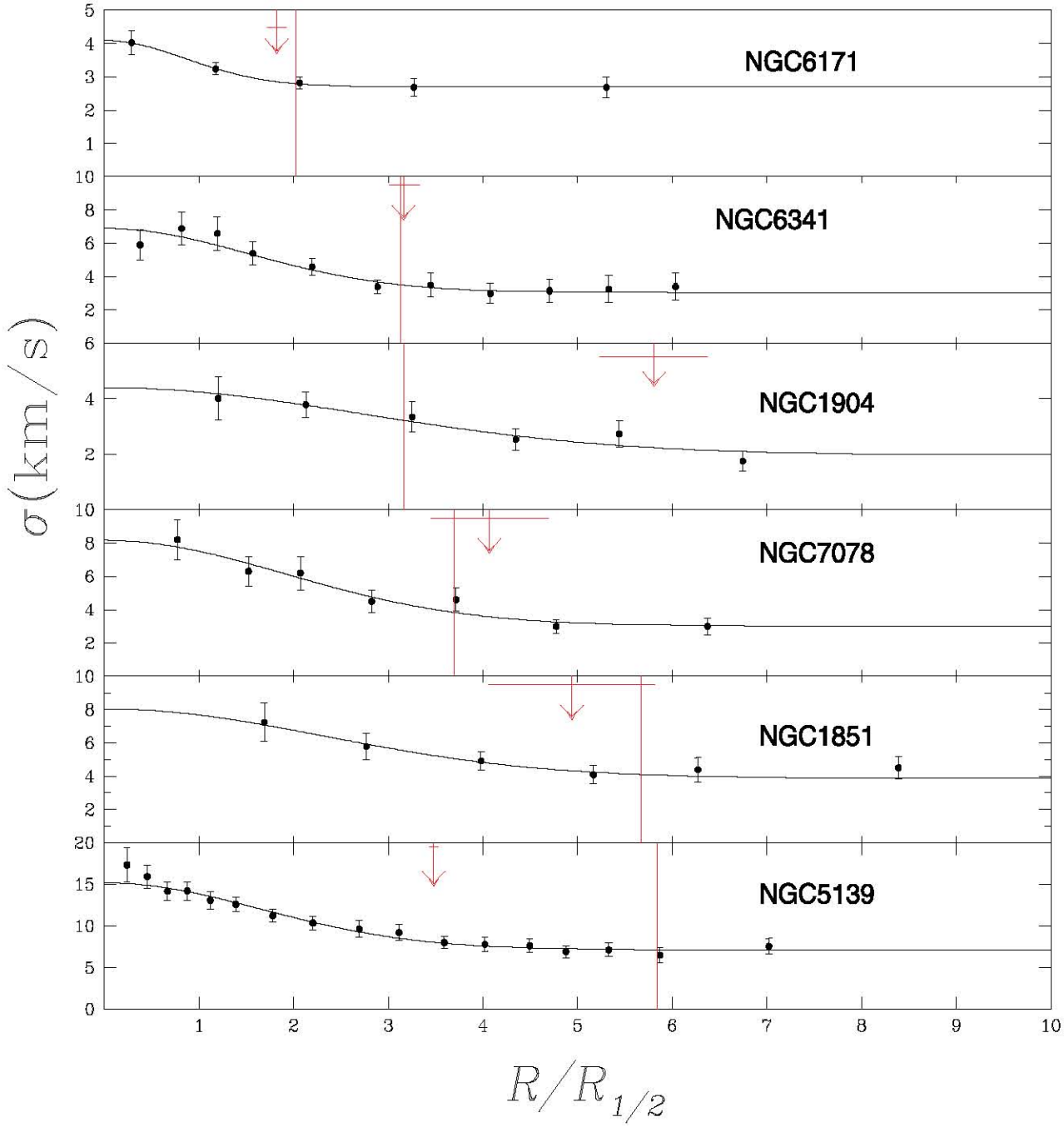

Figure 1. The observed projected velocity dispersion profiles for six GCs in the Scarpa et al. sample, points with error bars, as a function of the radial coordinate, normalized to the half-light radius of each. The solid curves indicate the maximum likelihood fits to the asymptotically flat $\sigma(R)$ model of equation (1), seen to be accurate descriptions of the data. The vertical lines indicate the $a = a_0$ threshold, and the arrows the point where the profiles flatten, a priori independent features, in most cases seen to occur at approximately the same region; see the text for details.

It is interesting at this point to notice a first correlation, the smaller the value of $R_a/R_{1/2}$, the larger the fraction of the cluster which lies in the $a < a_0$ regime, and interestingly, the flatter the velocity dispersion profile appears. At the top of the figures we see clusters where stars experience acceleration below a_0 almost at all radii, and it so happens that it is only in these systems that the velocity dispersion profile appears almost flat throughout. Towards the bottom, we see systems where only at the outskirts accelerations fall under a_0. Over most of their extents, these clusters lie in the Newtonian $a > a_0$ regime, and indeed, it is exclusively these that show a clear Keplerian decline in the projected velocity dispersion profiles over most of their extents. Also, note that on average, R_f and R_a approximately coincide, as already previously noticed by Scarpa et al. (2007a), the flattening in the velocity dispersion profiles seems to appear on crossing the a_0 threshold.

We end this section with Fig. 4 which compares the χ^2 values for the Plummer fits to the Lane et al. data to the χ^2 values for the equation (1) fits to the same data. As it was already obvious from Figs 2–3, both functional forms provide fits of very similar quality, although a rigorous statistical assessment actually shows the fits to

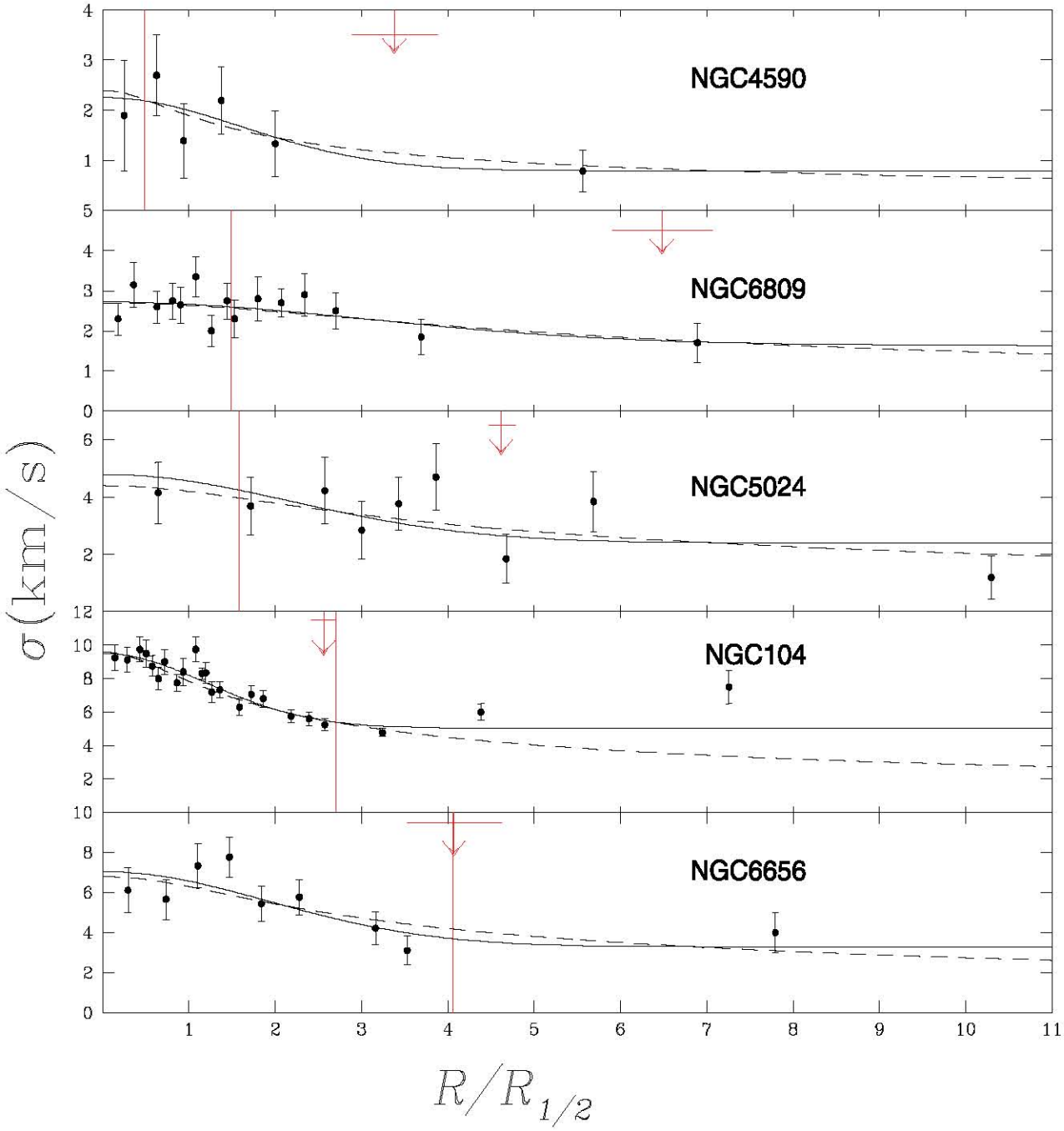

Figure 2. The observed projected velocity dispersion profiles for five GCs in the Lane et al. sample, points with error bars, as a function of the radial coordinate, normalized to the half-light radius of each. The solid curves indicate the maximum likelihood fits to the asymptotically flat $\sigma(R)$ model of equation (1), seen to be accurate descriptions of the data. The dashed lines indicate the best-fitting Plummer models from the Lane et al. papers, also fair representations of the data. The vertical lines indicate the $a = a_0$ threshold, and the arrows the point where the profiles flatten, a priori independent features, in most cases seen to occur at approximately the same region; see the text for details.

profiles which are asymptotically flat at large radii to better represent the data than the Plummer models, which slowly tend to zero. NGC 104, which results in the poorest fits under both functional forms tested, falls off the range shown in Fig. 4. For the asymptotically flat profile suggested by MONDian gravity schemes, this cluster yields a χ^2 value of 28.55, while for the Newtonian Plummer profile of Lane et al., a χ^2 of 51.14 results. This cluster is in fact the one for which the difference in χ^2 values is greatest, in the sense of further supporting the conclusions presented, but was omitted from the figure to allow greater detail in the region where the majority of the clusters lie.

3 TESTING THE NEWTONIAN EXPLANATION

In order to test the validity of the explanation for the outer flattening of the observed velocity dispersion profiles under Newtonian gravity, that these indicate dynamical heating due to the tides of the Milky Way system (bulge plus disc plus dark halo), we need

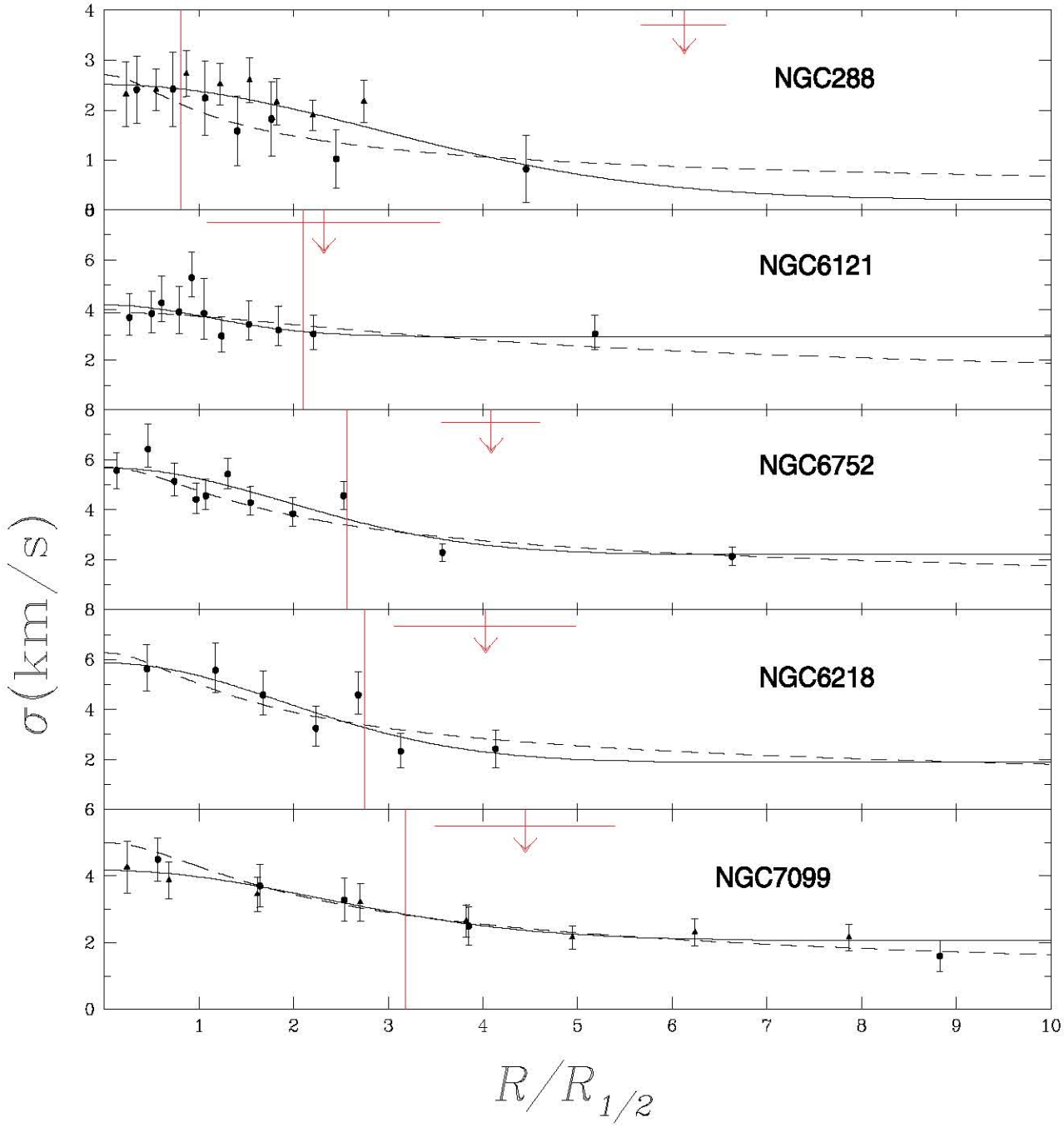

Figure 3. The observed projected velocity dispersion profiles for the remaining five GCs in the Lane et al. sample, points with error bars, as a function of the radial coordinate, normalized to the half-light radius of each. The solid curves indicate the maximum likelihood fits to the asymptotically flat $\sigma(R)$ model of equation (1), seen to be accurate descriptions of the data. The dashed lines indicate the best-fitting Plummer models from the Lane et al. papers, also fair representations of the data. NGC 288 and NGC 7099 are common to both samples; dots and triangles show the Lane et al. and Scarpa et al. data, respectively. The vertical lines indicate the $a = a_0$ threshold, and the arrows the point where the profiles flatten, a priori independent features, in most cases seen to occur at approximately the same region; see the text for details.

accurate estimates of the Newtonian tidal radii for the clusters studied. One of us in Allen, Moreno & Pichardo (2006, 2008) performed detailed orbital studies for 54 GCs for which absolute proper motions and line-of-sight velocities exist. In that study, both a full 3D axisymmetric Newtonian mass model for the Milky Way and a model incorporating a Galactic bar were used to compute precise orbits for a large sample of GCs, which fortunately includes the 16 of our current study. The Galactic mass models used in those papers are fully consistent with all kinematic and structural restrictions available. Having a full mass model, together with orbits for each GC, allows the calculation of the Newtonian tidal radius, not under any 'effective mass' approximation, but directly through the calculation of the derivative of the total Galactic gravitational force, including also the evaluation of gradients in the acceleration across the extent of the clusters, at each point along the orbit of each studied cluster.

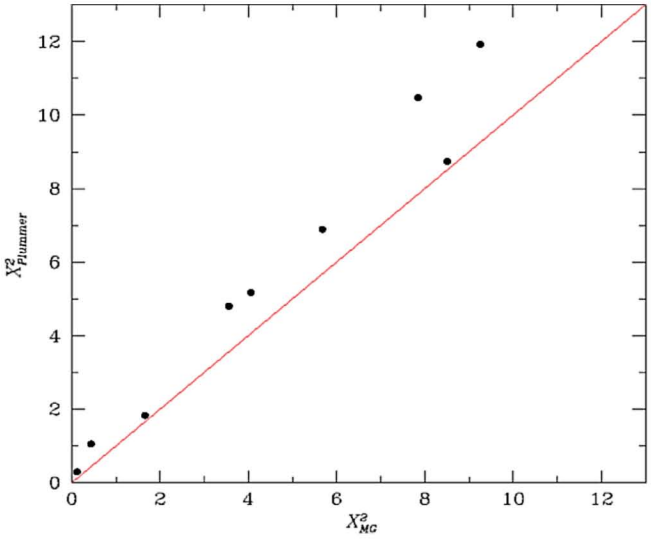

Figure 4. A comparison of the χ^2 values for the best-fitting asymptotically flat $\sigma(R)$ model of equation (1), and the optimum Plummer model fits from the Lane et al. papers to the same data samples. Although both fits are comparable as representations of the observed projected velocity dispersion profiles, the asymptotically flat model suggested by modified gravity schemes provides, in all cases, a slightly better description of the data.

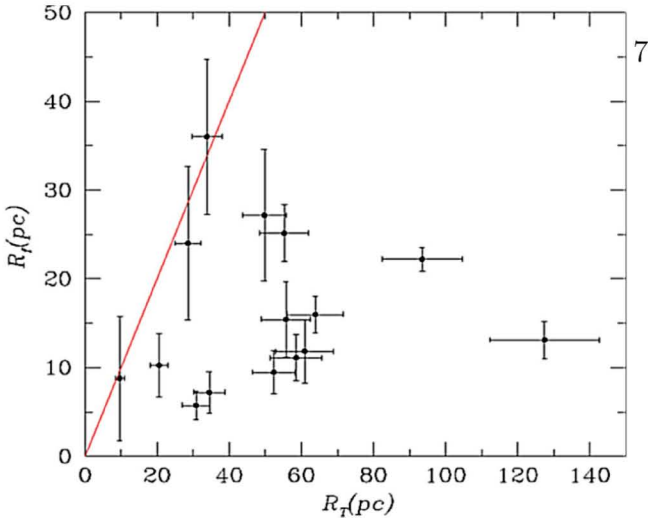

Figure 5. The relation between the point where the velocity dispersion flattens, R_f, and the Newtonian tidal radius, R_T, for each cluster. Even considering the large errors involved on both quantities, on average points fall far to the right of the identity line shown, making the Newtonian explanation for the flattened velocity dispersion profiles, rather suspect.

The Newtonian tidal radii we take for our clusters, R_T, are actually the values which result in the largest dynamical heating effect upon the clusters studied, those at perigalacticon. As the distance of closest approach to the centre of the Galaxy might vary from passage to passage, as indeed it often does, detailed orbital integration is used to take R_T as an average for perigalactic passages over the last 1 Gyr.

We update the tidal radii published in Allen et al. (2006, 2008), by considering revised total masses from the integration of the observed *V*-band surface brightness profiles for our clusters (Trager et al. 1995), and using the *V*-band stellar M/L values given in McLaughlin & van der Marel (2005) and accompanying electronic tables. For each individual GC, detailed single stellar population models tuned to the inferred ages and metallicities of each of the clusters we model were constructed in that study, using various standard population synthesis codes, and for a variety of assumed initial mass functions (IMFs). In this way, present stellar M/L values in the *V* band were derived, which we use here. As we do not in any way use the dynamical mass estimates of McLaughlin & van der Marel (2005), the total masses we use are independent of any dynamical modelling or assumption regarding the law of gravity, as they are derived through completely independent surface brightness profile measurements and stellar population modelling. The confidence intervals in our tidal radii include the full range of stellar M/L values given by McLaughlin & van der Marel (2005), through considering a range of ages, metallicities and IMFs consistent with the observed HR diagrams for each cluster. These uncertainties dominate the error budget on R_T, as those introduced by the observational uncertainties in the orbital determinations are much smaller. This last can be seen from the range in R_T values given in Allen et al. (2006) which are extreme in being derived from taking all four orbital parameters at their 1σ extremes, something with a probability of $(0.318)^4 = 1$ per cent, and are hence about 2.58σ ranges. Although sub-dominant, the corresponding 1σ errors on R_T have also been added. In what follows, we shall make use of total stellar masses derived as explained above, including as confidence intervals the full uncertainties in these results associated with the various IMFs assumed by McLaughlin & van der Marel (2005), and not the much narrower confidence intervals resulting from taking a fixed IMF.

In Fig. 5, we show values of R_f for our clusters, plotted against their corresponding R_T values, both in units of pc. The error bars in R_f come from the full likelihood analysis described in the fitting process of equation (1) to $\sigma_{obs}(R)$, which guarantees that confidence intervals in both of the quantities plotted are robust 1σ ranges. The solid line shows an $R_f = R_T$ relation. It is obvious from the figure that the onset of the flat velocity dispersion regime occurs at radii substantially smaller than the tidal radii, for all of the GCs in our sample. Even under the most extreme accounting of the resulting errors, only three of the clusters studied are consistent with $R_T \approx R_f$ at 1σ. Actually, the average values are closer to $R_T = 4R_f$, with values higher than 8 appearing. One of the clusters, NGC 5024, does not appear, as it has values of $R_T = 184.12$, $R_f = 36$, which puts it out of the plotted range, but consistent with the description given above. Given the R^3 scaling of Newtonian tidal phenomena, even a small factor of less than 2 inwards of the tidal radii, tides can be safely ignored, e.g. in Roche lobe overflow dynamics, the stellar interior is largely unaffected by the tidal fields, until almost reaching the tidal radius. It therefore appears highly unlikely under a Newtonian scheme that Galactic tides could be responsible for any appreciable dynamical heating of the velocity dispersion of the studied clusters.

We note that Lane et al. (2010a) and Lane, Küpper & Heggie (2012) find that Newtonian tidal heating can explain the observed velocity dispersion profile of their GC sample. However, it is important to note that in Lane et al. (2010a, 2012) total masses were calculated directly from the observed velocity dispersion observations, under the assumption that Newtonian dynamics hold. If that assumption is to be tested, the importance of deriving total masses through an independent method, not based on stellar dynamics, is evident. Our results do not imply that the Newtonian explanation might not apply to other GCs, e.g. the theoretically constructed ones of Küpper et al. (2010) and Küpper, Lane & Heggie (2012), which show the Newtonian explanation to hold *in principle*, although no real GCs were included in those studies. A potential caveat of all

the above studies is the use of strictly axisymmetric potentials for the Milky Way, given that in Allen et al. (2006, 2008) it is shown that the orbital dynamics of Galactic GCs with orbits probing the regions where the Galactic bar is present, as many in our sample do, can be strongly affected by its presence.

Note also that most of the clusters in our sample are problematic for a Newtonian gravity scheme, even without the recent observations of an outer flat velocity dispersion profile. As remarked already in Allen et al. (2006), the clusters in our sample have Newtonian tidal radii larger than the observed truncation radii of their light distribution, the sole exceptions being Omega Cen (NGC 5139) and M92 (NGC 6341), two rather anomalous clusters. Whereas a full dynamical modelling under an extended gravity force law of these clusters, Hernandez & Jiménez (2012), naturally yielded an outer truncation for the light profile, under a Newtonian hypothesis, the observed truncation in the light profile of the clusters in our sample cannot be explained as arising from interaction with the tidal field of the Milky Way.

Furthermore, note that we have taken $R_{\rm T}$ at perigalacticon, where tides are at their most severe over the clusters orbit, any other orbital occupation averaging would result in substantially larger $R_{\rm T}$ values. Note also that as shown by Allen et al. (2006, 2008), the inclusion of a realistic massive Galactic bar potential, in the case of the clusters in our sample, results generally in negligible changes in the resulting $R_{\rm T}$ values, or in some cases, a slight increase in these values. Hence, even taking the fullest non-axisymmetric Galactic mass model under Newtonian gravity, with precise orbits derived from 3D velocity measurements for the clusters studied, together with total mass determinations tuned to the individual stellar populations of them, yields tidal radii as shown in Fig. 2.

Regarding a comparison to the expectations under Newtonian gravity, an interesting dynamical effect appears when a stellar halo object is near its apocentre. As shown in e.g. Niederste-Ostholt, Belokurov & Evans (2012), near apocentre tidal tails are compressed into what might look like a high dispersion velocity halo. We have checked the position of the clusters studied along their orbits, and found that only in the case of NGC 6121 is the cluster near apocentre, checked explicitly from the orbits for the clusters in question from Allen et al. (2006, 2008). Note that this case also follows the MONDian expectations of Fig. 7, see below. It is also important to note that the piling up of tidally stripped stars near apocentre has not been proven to hold for more chaotic orbits, and probably does so to a much smaller degree than what shown in Niederste-Ostholt et al. (2012) for a pure axisymmetric potential. This is relevant, as the orbits of clusters lying within the region of influence of the Galactic bar, as many of the ones in our sample do, become substantially chaotic, with no well-defined periodic apocentre distance, as shown in the Allen et al. papers mentioned.

4 TESTING A MODIFIED GRAVITY EXPLANATION

We begin this section by testing the correlation between R_a and $R_{\rm f}$. As already noticed by Scarpa et al. (2011), the flattening in the observed velocity dispersion profiles seems to appear at the point where the a_0 threshold is crossed. Here, we use the much more careful and objective modelling of the observed velocity dispersion curves of the previous section to test this point, shown in Fig. 6.

We see nine GCs in the sample falling within 1σ of the identity line shown, a further three lying within 2σ of this same line and the remaining four appearing as outliers. Thus, the correlation appears stronger than in Figs 1–3, where errors on $R_f/R_{1/2}$ appear and only

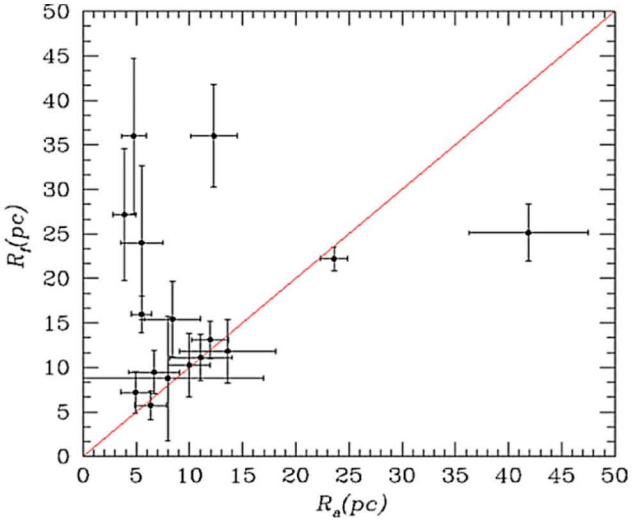

Figure 6. The relation between the radius where the velocity dispersion flattens, $R_{\rm f}$, and the point where average stellar accelerations fall below the a_0 threshold, R_a.

a qualitative comparison is implied, not including the confidence intervals in R_a. A quantitative test of the correlation being explored is possible, since the careful modelling of the velocity dispersion profiles we performed naturally yields objective confidence intervals for the parameters of the fit. Of the outliers, NGC 288 presents an almost entirely flat velocity dispersion profile, and is hence a case where the parameter R_σ is only poorly constrained. In this figure, we thus quantify the correlation between the point where the velocity profile flattens and the crossing of the a_0 threshold, as expected under MONDian schemes, which is seen to hold on average. One could think of adding a point at (0,0) in Fig. 6, corresponding to the local dSph galaxies, systems with fully isothermal observed velocity dispersion profiles, lying fully within the $a < a_0$ condition, e.g. Angus (2008), Hernandez et al. (2010). A possible caveat is the use of only a coarse definition for Ra, which relies only on projected quantities which are integrals along the line of sight. More detailed dynamical structure modelling of the type as found in Hernandez & Jiménez (2012), requiring fixing on a particular modified gravity model, something which we expressedly avoid in this study, might reveal slight differences from the current Fig. 6, perhaps with no outliers.

As already noticed in Figs 1–3, a correlation is evident in that the further out, in units of the cluster half-light radius, the a_0 threshold is reached, the larger the relative drop in the observed velocity dispersion profile. This is expected under MONDian gravity schemes, since when the Newtonian $a > a_0$ region is larger within a particular cluster, the larger the 'Keplerian' fall before the $a < a_0$ modified regime is reached.

We end this section with Fig. 7, which shows the relation between the measured asymptotic velocity dispersion, σ_∞, and the total mass of the clusters in question. The mass was calculated as described in Section 3, and therefore represents the best current estimate of the stellar mass for each of the clusters in the sample, including its corresponding confidence intervals. As with all the other correlations and data presented in Figs 1–6, there is no dynamical modelling or modified gravity assumptions going into the data presented in Fig. 7, merely observable quantities. We see, as already pointed out in Hernandez & Jiménez (2012), that the GCs observed comply with a scaling of $\sigma \propto M^{1/4}$, the Tully–Fisher law of galactic systems 'embedded within massive dark haloes'.

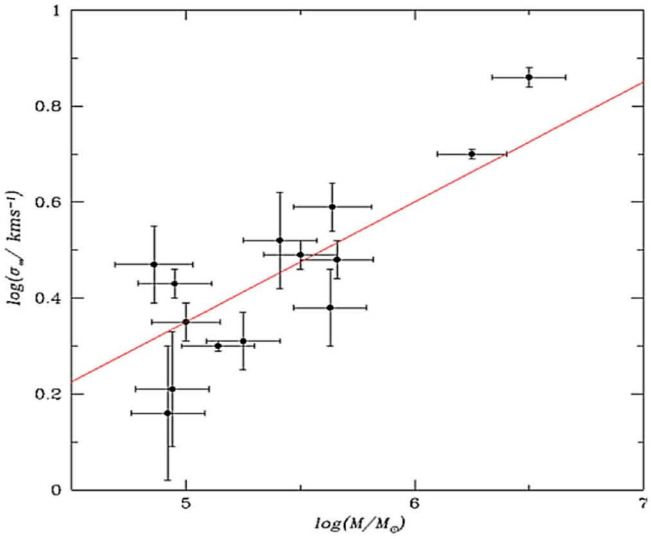

Figure 7. The relation between the observed asymptotic dispersion velocity measurements and the total mass of each cluster. The line indicates the best-fitting $\sigma \propto M^{1/4}$ scaling for the data, and is consistent with the galactic scale Tully–Fisher relation.

From this last figure two clusters have been excluded, NGC 288 and NGC 4590 which have very poorly determined σ_∞ values, with uncertainties so large that these clusters provide little information in terms of Fig. 7. Regarding NGC 288, both the Scarpa et al. and the Lane et al. data are noisier than for the others. Also, taking only one set of data yields significantly distinct answers, although still barely within their respective errors, a low asymptotic velocity for the Lane et al. sample and a high value from the Scarpa et al. data. This does not happen with the other common GC, NGC 7099, where both data samples are in complete agreement. Although Sollima, Bellazzini & Lee (2012) recently reported a velocity dispersion profile for NGC 288, this is equally noisy, and does not help to clear the case, their data are actually consistent, to their respective errors, with both the Lane et al. or the Scarpa et al. data. Given the current level of observational uncertainties we prefer to exclude NGC 288 from any consideration regarding its asymptotic velocity value, until a clearer picture emerges from the observational point of view.

The straight line shows the best-fitting $\sigma \propto M^{1/4}$ scaling, and actually falls only a factor of 1.3 below the modified gravity prediction for systems lying fully within the low-acceleration regime (e.g. Hernandez & Jiménez 2012), for the same value of $a_0 = 1.2 \times 10^{-10}\,\mathrm{m\,s^{-1}}$ used here, as calibrated through the rotation curves of galactic systems. This small offset is not surprising, since the GCs treated here are not fully within the $a < a_0$ condition, most have an inner Newtonian region encompassing a substantial fraction of their masses. Note also that from an statistical point of view, consistency of a set of data points with a model does not require for all data points to lie within 1σ of the proposed model. Probabilistically, one actually expects about $1/3$ of the points to lie between 1σ and 2σ of the model, with $1/100$ expected between 2σ and 3σ, even for data actually extracted from a given model. Given the size of our sample, finding five GCs without 1σ, but within 2σ of the proposed model is then well within expected random noise, inasmuch as we have taken care to ensure that the error bars given are real 1σ confidence intervals. Further, as many of the GCs in our sample have not reached acceleration values significantly below a_0 at their last measured point, while other have, a certain intrinsic scatter would be expected in Fig. 7 from a MONDian gravity perspective.

From a Newtonian point of view, if Galactic tides were responsible for the observed outer flattening of the velocity dispersion profiles studied, given the narrow range of half-light radii these present, and given the inverse scaling of Newtonian tides with the density of the satellite, a slight downward trend for decreasing asymptotic velocity dispersion with increasing mass would be expected in Fig. 7. This would of course be blurred significantly by the range of perigalacticon distances inferred for the GCs in our sample. It is clear from the figure that a blurred decreasing trend is not what the data show; rather, consistency with the $\sigma \propto M^{1/4}$ of MONDian gravity, including the normalization, is evident. A preliminary version of this last figure appeared already in Hernandez & Jiménez (2012); we reproduce here an updated version using now the extended sample of clusters treated, and σ_∞ values and their confidence intervals as derived through the careful velocity dispersion fitting procedure introduced.

Given that the inclusion of even a few high-velocity contaminating stars can bias the velocity dispersion measurements significantly, e.g. Giersz & Heggie (2011), it is important to assess the robustness of the velocity dispersion profiles we use to this possibility. The stars from the Lane et al. group were selected through the requirement of four stellar parameters, ensuring membership through requiring simultaneously a ΔV_r, and also Ca, g and $[m/H]$ membership criteria. These make it unlikely that contamination issues might have degraded the velocity dispersion profiles reported by the Lane et al. group. Regarding the Scarpa et al. results, only a ΔV_r membership criteria was used. However, as can be seen from the table, only one of their clusters, NGC 6171, has $|b| < 45$ and $\Delta V_\mathrm{r} < 100\,\mathrm{km\,s^{-1}}$, showing that with this only possible exception, contamination of field stars is unlikely to affect the derived velocity dispersion determinations we use. It is also reassuring of the reliability of the Scarpa et al. results that of the two clusters which have also been studied by the Lane et al. group, NGC 7099 has reported velocity dispersion profiles which are fully consistent when comparing the data samples from the two groups of observers. The case of NGC 288 has already been discussed, although both data samples are still consistent to within their respective errors, a definitive trend appears for large and small asymptotic velocity dispersion values for the Scarps et al. and Lane et al. groups, respectively.

To summarize, we have tested the Newtonian explanation of Galactic tides as responsible for the observed $\sigma(R)$ phenomenology, and found it to be in tension with the observations, given the tidal radii (at perigalacticon) which the GCs in our sample present are generally larger than the points where $\sigma(R)$ flattens, on average, by factors of 4, with values higher than 8 also appearing. An explanation under a MONDian gravity scheme appears probable, given the correlations we found for the clusters in our sample, all in the expected sense, and shown in Figs 1–7. Table 1 gives the parameters of velocity dispersion fits and their confidence intervals. The errors in σ_∞ are uncorrelated with those in the other two parameters, which, as it is easy to see from the model, are perfectly anticorrelated amongst themselves. The masses come from integrating the observed surface density light profiles, and using the M/L values, and their uncertainties, calculated using detailed stellar population modelling on a cluster by cluster basis by McLaughlin & van der Marel (2005).

5 CONCLUSIONS

From a purely empirical perspective, we test the Newtonian explanation of Galactic tides as responsible for the observed flattening of the velocity dispersion profiles in the GCs studied. These

clusters can be shown to have Newtonian tidal radii at closest Galactic passage larger than the points where $\sigma(R)$ flattens, by large factors of 4 on average, making the explanation under the Newtonian hypothesis suspect.

Through a careful modelling of the observed velocity dispersion profiles, we corroborate an average correlation between the appearance of a flat region in $\sigma(R)$ and the crossing of the a_0 threshold, as expected under modified gravity schemes.

By including results from careful stellar population modelling of the GCs studied to derive total mass estimates, we show that the asymptotic values of the measured velocity dispersion profiles, σ_∞, and total masses for these systems, M, are consistent with the generic modified gravity prediction for a scaling $\sigma_\infty^4 \propto M$.

Although individual velocity dispersion profiles can be adequately fitted with either Newtonian Plummer models or MONDian asymptotically flat ones to equivalent accuracy, the large Newtonian tidal radii sometimes found and the 'Tully–Fisher' mass–velocity scaling observed show that the phenomenology of the velocity dispersion profiles of the GCs studied is consistent with a qualitative change in gravity in the low-acceleration regime, as predicted by MONDian gravity theories.

ACKNOWLEDGMENTS

The authors thank an anonymous referee for a thorough reading of a previous version of the paper, leading to a helpful report abundant in constructive criticism. XH acknowledges financial assistance from UNAM DGAPA grant IN103011. MAJ acknowledges financial support from a CONACYT scholarship.

REFERENCES

Allen C., Moreno E., Pichardo P., 2006, ApJ, 652, 1150
Allen C., Moreno E., Pichardo P., 2008, ApJ, 674, 237
Angus G. W., 2008, MNRAS, 387, 1481
Bekenstein J. D., 2004, Phys. Rev. D, 70, 083509
Bernal T., Capozziello S., Hidalgo J. C., Mendoza S., 2011, Eur. Phys. J. C, 71, 1794
Binney J., Tremaine S., 1987, Galactic Dynamics. Princeton Univ. Press, Princeton, NJ
Capozziello S., De Laurentis M., 2011, Phys. Rep., 509, 167
Drukier G. A., Cohn H. N., Lugger P. M., Slavin S. D., Berrington R. C., Murphy B. W., 2007, AJ, 133, 1041
Famaey B., McGaugh S., 2012, Living Reviews in Relativity, 15, 10
Giersz M., Heggie D. C., 2011, MNRAS, 410, 2698
Haghi H., Baumgardt H., Kroupa P., Grebel E. K., Hilker M., Jordi K., 2009, MNRAS, 395, 1549
Haghi H., Baumgardt H., Kroupa P., 2011, A&A, 527, A33
Harris W. E., 1996, AJ, 112, 1487
Hernandez X., Jiménez M. A., 2012, ApJ, 750, 9
Hernandez X., Mendoza S., Suarez T., Bernal T., 2010, A&A, 514, A101
Hernandez X., Jiménez M. A., Allen C., 2012, Eur. Phys. J. C, 72, 1884
Kroupa P., 2012, PASA, 29, 395
Kroupa P. et al., 2010, A&A, 523, 32
Küpper A. H. W., Kroupa P., Baumgardt H., Heggie D. C., 2010, MNRAS, 407, 224
Küpper A. H. W., Lane R. R., Heggie D. C., 2012, MNRAS, 420, 2700
Lane R. R., Kiss L. L., Lewis G. F., Ibata R. A., Siebert A., Bedding T. R., Szkely P., 2009, MNRAS, 400, 917
Lane R. R. et al., 2010a, MNRAS, 406, 2732
Lane R. R., Kiss L. L., Lewis G. F., Ibata R. A., Siebert A., Bedding T. R., Szkely P., 2010b, MNRAS, 401, 2521
Lane R. R., Kiss L. L., Lewis G. F., Ibata R. A., Siebert A., Bedding T. R., Székely P., Szabó G. M., 2011, A&A, 530, A31
Lane R. R., Küpper A. H. W., Heggie D. C., 2012, MNRAS, 423, 2845
Lee J., Komatsu E., 2010, ApJ, 718, 60
McLaughlin D. E., van der Marel R. P., 2005, ApJS, 161, 304
Mendoza S., Hernandez X., Hidalgo J. C., Bernal T., 2011, MNRAS, 411, 226
Milgrom M., 1983, ApJ, 270, 365
Milgrom M., 1994, ApJ, 429, 540
Moffat J. W., Toth V. T., 2008, ApJ, 680, 1158
Niederste-Ostholt M., Belokurov V., Evans N. W., 2012, MNRAS, 422, 207
Scarpa R., Falomo R., 2010, A&A, 523, 43
Scarpa R., Marconi G., Gilmozzi R., 2004, in Dettmar R., Klein U., Salucci P., eds, Proc. Science, Baryons in Dark Matter Haloes. SISSA, Novigrad, p. 55.1
Scarpa R., Marconi G., Gimuzzi R., Carraro G., 2007a, A&A, 462, L9
Scarpa R., Marconi G., Gimuzzi R., Carraro G., 2007b, The Messenger, 128, 41
Scarpa R., Marconi G., Carraro G., Falomo R., Villanova S., 2011, A&A, 525, A148
Sollima A., Nipoti C., 2010, MNRAS, 401, 131
Sollima A., Bellazzini M., Lee J. W., 2012, ApJ, 755, 156
Thompson R., Nagamine K., 2012, MNRAS, 419, 3560
Trager S. C., King I. R., Djorgovski S., 1995, AJ, 109, 218
Zhao H., Famaey B., 2010, Phys. Rev. D, 81, 087304

This paper has been typeset from a TEX/LATEX file prepared by the author.

4. ¿GRAVEDAD MODIFICADA O MAREAS NEWTONIANAS EN CÚMULOS GLOBULARES?

Capítulo 5

Perfiles de densidad

5.1. Resumen

.

Es un hecho conocido que el halo estelar de la Vía Láctea tiene un perfil de densidad el cual a primera aproximación satisface $\rho \propto r^{-3}$. , Lo mismo ocurre para M31 y las observaciones muestran que la distribución de CGs en la galaxia Andrómeda siguen el mismo patrón. Recientemente se ha observado que una población difusa de estrellas en los alrededores de CGs que se extiende más allá de su radio de marea newtoniano sigue la misma distribución.

En un esquema de gravedad modificada cualquier halo isotérmico de partículas de prueba alrededor de una distribución esférica de masa debe adoptar una configuración de equilibrio que en primera aproximación satisface $\rho \propto r^{-3}$.

En una descripción newtoniana de la gravedad hay diversas explicaciones para cada caso dependiendo del sistema del que se trate, dentro de la gravedad modificada en cambio todas estas observaciones se entienden como consecuencia del comportamiento de la gravedad en escalas donde la aceleración es del orden de la aceleración de Milgrom.

En este trabajo participe en la deducción de la relación $\rho \propto r^{-3}$ en un esquema de gravedad modificada, en la búsqueda de registros en la literatura donde se documentara este comportamiento en diferentes sistemas astrofísicos y junto con los demás autores participe en todo el proceso de revisión hasta lograr la publicación del trabajo.

The Astrophysical Journal, 770:83 (6pp), 2013 June 20 doi:10.1088/0004-637X/770/2/83

ISOTHERMAL DISTRIBUTIONS IN MONDian GRAVITY AS A SIMPLE UNIFYING EXPLANATION FOR THE UBIQUITOUS $\rho \propto r^{-3}$ DENSITY PROFILES IN TENUOUS STELLAR HALOS

X. Hernandez, M. A. Jiménez, and C. Allen
Instituto de Astronomía, Universidad Nacional Autónoma de México, Apartado Postal 70-264, C.P. 04510 México D.F., Mexico; xavier@astro.unam.mx
Received 2013 January 17; accepted 2013 April 11; published 2013 May 28

ABSTRACT

That the stellar halo of the Milky Way has a density profile which, to first approximation, satisfies $\rho \propto r^{-3}$ and has been known for a long time. More recently, it has become clear that M31 also has such an extended stellar halo, which approximately follows the same radial scaling. Studies of distant galaxies have revealed the same phenomenology. Also, we now know that the density profiles of the globular cluster systems of our Galaxy and Andromeda to first approximation follow $\rho \propto r^{-3}$, $\Sigma \propto R^{-2}$ in projection. Recently, diffuse populations of stars have been detected spherically surrounding a number of Galactic globular clusters, extending much beyond the Newtonian tidal radii, often without showing any evidence of tidal features. Within the standard Newtonian and general relativity scenario, numerous and diverse particular explanations have been suggested, individually tailored to each of the different classes of systems described above. Here we show that in a MONDian gravity scenario any isothermal tenuous halo of tracer particles forming a small perturbation surrounding a spherically symmetric mass distribution will have an equilibrium configuration which to first approximation satisfies a $\rho \propto r^{-3}$ scaling.

Key words: galaxies: kinematics and dynamics – galaxies: star clusters: general – gravitation – stars: kinematics and dynamics

1. INTRODUCTION

Progress in the debate between the hypothetical physical reality of astrophysical dark matter and the option of modifying gravity at the low acceleration regime will hinge upon the exploration of as many independent lines of enquiry as possible. Whereas the rotation curves of galaxies can be adequately reproduced from either point of view (Milgrom 1983, 1994; Sanders & McGaugh 2002; Swaters et al. 2010), a variety of recent studies have shown results in tension with the standard scale-invariant gravity plus dark matter paradigm, and being more in line with generic MONDian gravity approaches.

We shall use the term MONDian to refer to modified gravity theories in which, in the low velocity limit, the force per unit mass between a test particle and a spherical mass distribution will shift from the Newtonian expression of GM/r^2 to an $(GMa_0)^{1/2}/r$ behavior for acceleration scales below Milgrom's a_0, independently of the fundamental underlying theory of gravity which might lead to such a behavior, e.g., Bekenstein (2004), Moffat & Toth (2008), Zhao & Famaey (2010), Bernal et al. (2011), Mendoza et al. (2011), Capozziello & De Laurentis (2011), and Famaey & McGaugh (2012). The most salient features of such schemes are equilibrium velocities which become independent of distances at a value $\approx (GMa_0)^{1/4}$.

In Lee & Komatsu (2010) and Thompson & Nagamine (2012) it has been shown that the infall velocity of the two components of the Bullet cluster is incompatible with expectations of full ΛCDM predictions, and is actually a challenge to the standard gravity theory, as it surpasses the escape velocity of the combined system. Recently, Kroupa (2012) has shown that tidal dwarf galaxies, which, under the standard scenario, are transient tidal clumps of galactic material having out of equilibrium dynamics, actually fall on the same Tully–Fisher relation as all dwarf galaxies. This appears as an uncanny coincidence from the standard gravity perspective, where the dynamics of normal dwarfs are thought to be determined by their dominant dark matter halos. The result is expected under MONDian gravity schemes, where, once the baryonic mass of the system is fixed, the dynamics will uniquely follow, as it is indeed observed.

Along the same lines, in Haghi et al. (2011), Scarpa et al. (2011), Hernandez & Jiménez (2012), and Hernandez et al. (2013), it has been shown that the velocity dispersion profiles of a number of Galactic globular clusters stop falling radially along Keplerian expectations and settle to finite asymptotic values on crossing the $a < a_0$ threshold. The standard gravity explanation for these profiles, that it is the tides of the Milky Way (MW) that dynamically heat the outskirts of the clusters observed, e.g., Lane et al. (2010), appears suspect, as the Newtonian tidal radii can be shown to exceed the points where the velocity dispersion profiles flatten by large factors, and because the total globular cluster masses and asymptotic velocity dispersion values follow the galactic Tully–Fisher relation, as expected under MONDian gravity schemes. Finally, in Hernandez et al. (2012) we showed that the relative velocities of extremely wide binaries do not follow the expectations of full galactic dynamical Newtonian simulations, but diverge from the Keplerian decline with radius to settle also at finite relative velocities on crossing the $a < a_0$ threshold of MONDian gravity proposals.

In this paper we show that the density profile of an isothermal population of trace particles surrounding a spherical mass distribution in MONDian gravity will naturally follow an approximately $\rho \propto r^{-3}$ profile. Under standard gravity approaches, the ubiquitous nature of $\rho \propto r^{-3}$ profiles has to be addressed through a variety of highly specific explanations, individually tailored to each of the diverse classes of systems where these profiles have been observed. Examples of the above are mergers and tidal dissolution of accreted substructure for the tenuous stellar halos surrounding our Galaxy, M31, and also the recently detected ones around external galaxies (e.g., Bullock et al. 2001; Abadi et al. 2006), and the compression of tidal tails at apocenter or disk shock heating for the "extra tidal" features surrounding Galactic globular clusters, e.g., Da Costa (2012).

The above situation contrasts with the appearance of a direct equilibrium solution for tracer populations having the

simplest isotropic and isothermal Maxwellian distribution function, which, to first order, yields $\rho \propto r^{-3}$ profiles under MONDian gravity schemes, which we show here. We suggest that this is one further piece of evidence pointing in the direction of the necessity of a modified gravity regime at low acceleration scales.

In Section 2 we derive the first order predictions for equilibrium tenuous stellar halos under a MONDian gravity scheme, and also under Newtonian gravity within dark matter halos, and under Newtonian gravity in the absence of dark matter halos. In Section 3 we compare the theoretical estimates with the observed profiles for a variety of systems, finding the MONDian prediction a good fit to the observed situation, over a wide variety of scales and classes of astronomical systems. Section 4 presents a final discussion of our results.

2. FIRST ORDER DYNAMICAL EXPECTATIONS

We shall model the physical situation which applies generically for a MONDian scenario, where in the $a \ll a_0$ limit, the force between a test particle and a spherically symmetric mass distribution becomes $-(GM(r)a_0)^{1/2}/r$, when one introduces no modifications to Newton's second law, e.g., Hernandez et al. (2010) and Mendoza et al. (2011).

Assuming spherical symmetry, and taking the derivative of the kinematic pressure, the equation of hydrostatic equilibrium for a polytropic equation of state $P = K\rho^{\gamma}$ is

$$\frac{d(K\rho^{\gamma})}{dr} = -\rho\nabla\phi. \tag{1}$$

In going to isothermal conditions, $\gamma = 1$ and $K = \sigma^2$, e.g., Binney & Tremaine (1987), and we get

$$\frac{\sigma^2}{\rho}\frac{d\rho}{dr} = -\nabla\phi. \tag{2}$$

Writing $\rho = (4\pi r^2)^{-1} dM(r)/dr$, the above equation can be written as

$$\sigma^2\left[\left(\frac{dM(r)}{dr}\right)^{-1}\frac{d^2M(r)}{dr^2} - \frac{2}{r}\right] = -\nabla\phi(r) \tag{3}$$

where σ is the isotropic Maxwellian velocity dispersion for the population of stars. The above treatment is common, and can be found in, e.g., Hernandez et al. (2010), where we used it in the modeling of dSph galaxies, systems characterized by flat velocity dispersion profiles, obtaining mass models consistent with observed velocity dispersion, half mass radii and total masses, in the absence of dark matter. Other recent examples of similar treatments can found in, e.g., Drukier et al. (2007), Sollima & Nipoti (2010), and Hernandez & Jiménez (2012), all modeling stellar populations using isotropic Maxwellian distribution functions.

As an illustrative example we can take $\nabla\phi(r) = GM(r)/r^2$ for the right-hand side of Equation (3), the Newtonian expression appearing for $a \gg a_0$. Looking for a power law solution for $M(r) = M_0(r/r_0)^m$, we get

$$\sigma^2\left[\frac{m-3}{r}\right] = -\frac{GM_0}{r^2}\left(\frac{r}{r_0}\right)^m, \tag{4}$$

and hence $m = 1$, the standard isothermal halo, $M(r) = 2\sigma^2 r/G$, having a constant centrifugal equilibrium velocity $v^2 = 2\sigma^2$ and infinite extent. In going to the MONDian limit of $a \ll a_0$, $\nabla\phi(r) = (GM(r)a_0)^{1/2}/r$, Equation (3) yields

$$\sigma^2\left[\frac{m-3}{r}\right] = -\frac{[GM_0a_0]^{1/2}}{r}\left(\frac{r}{r_0}\right)^{m/2}. \tag{5}$$

In this limit $m = 0$, we obtain $M(r) = M_0$ and $v^2 = 3\sigma^2 = (GM_0a_0)^{1/2}$, the expected Tully–Fisher scaling of the circular equilibrium velocity with the fourth root of the mass, with rotation velocities that remain flat even after the mass distribution has converged, thus, rigorously isothermal halos are naturally limited in extent, as already shown by Milgrom (1984). It is interesting that in this limit the scaling between the circular rotation velocity and the velocity dispersion is only slightly modified as compared to the Newtonian case, with the proportionality constant changing from 2 to 3, for the squares of the velocities. Note also that a fuller asymptotic analysis (Milgrom 1984) not imposing a power law solution shows that the factor of three obtained above will in general lie in the range 3–4.5.

We can now look for the behavior of a tenuous stellar halo in the MONDian regime, and hence at large distances, around a mass distribution which has essentially converged, by looking at Equation (2) and writing the right-hand side as $-(GM_{\rm tot}a_0)^{1/2}/r$, where $M_{\rm tot}$ is the total mass of the galactic or stellar system. The ρ in the left-hand side of this same equation now refers to the density distribution of essentially test particles making up a trace population, e.g., a stellar galactic halo, the globular cluster distribution around a large galaxy, or the faint halos of "extra-tidal" stars surrounding Galactic globular clusters. Using also the result of Equation (5) of $3\sigma^2 = (GM_0a_0)^{1/2}$, Equation (2) yields

$$\frac{d\rho}{dr} = -3\frac{\rho}{r}, \tag{6}$$

which can then be integrated directly to yield

$$\rho(r) = \rho_0(r_0/r)^3. \tag{7}$$

In deriving Equation (7) we have introduced the assumptions of a tracer population and the results of having forced a power law solution in Equation (5), which significantly simplify the calculations with respect to a full numerical solution (e.g., Milgrom 1984 or Hernandez & Jiménez 2012), or even with respect to the asymptotic analysis of Milgrom (1984). The above assumptions will certainly never be strictly valid in a real astrophysical system, still, provided they are approximately valid, the solution of Equation (7) will represent a first order description. Our simplified approach, however, allows a transparent handling of the physics, and permits a clear understanding for the generic appearance of a $\rho(r) \propto r^{-3}$ region, a feature already noted in the numerical solutions presented in Milgrom (1984), and apparent in many astrophysical systems, as discussed in the following section. The volumetric distribution of Equation (7) can be projected analytically along one direction to yield the projected surface density profile

$$\Sigma(R) = \frac{\pi\rho_0 r_0^3}{2R^2}. \tag{8}$$

Of course, $\rho \propto r^{-3}$ is an approximation which will only be valid over a limited radial range. In fact, mass profiles for isothermal solutions converge to finite total masses and radii, as

shown in, e.g., Milgrom (1984) and Hernandez et al. (2010). In closer detail, the density profiles will steepen beyond r^{-3} as one moves farther out as the total mass converges, e.g., as seen in the broken power law fits for the Galactic stellar halo reported by Sesar et al. (2011).

Under the Newtonian expression of $\nabla\phi = GM(r)/r^2$, the equivalent development for a trace population in the halo of a galaxy having the same rotation curve as the one leading to Equation (6), $M(r) = 2\sigma^2 r/G$, where this time $M(r)$ refers mostly to the hypothetical dark matter component, yields

$$\rho(r) = \rho_0 (r_0/r)^2 \tag{9}$$

as the expression corresponding to Equation (7). The case of a trace population around an essentially converged total mass in Newtonian dynamics, e.g., the tenuous stellar halos surrounding the Galactic globular clusters, $\nabla\phi = GM_{\rm tot}/r^2$ yields

$$\rho(r) = \rho_0 e^{(GM_{\rm tot}/\sigma^2 r)}, \tag{10}$$

a density distribution which tends to a constant at large radii. Thus, we see that equilibrium configurations of isothermal tracer populations in the MONDian regime will approximately follow $\rho(r) \propto r^{-3}$ density profiles, while under Newtonian gravity the same populations within the corresponding dark matter halos will show much shallower $\rho(r) \propto r^{-2}$ profiles, which, in the absence of dark matter halos, e.g., tenuous stellar halos about globular clusters, will have density profiles as given by Equation (10).

3. OBSERVATIONAL COMPARISONS

In this section we review the observational situation of tenuous tracer population halos, which now spans a very wide range of systems and astrophysical scales. We begin with a number of recent determinations of the density structure of the stellar halo of our Galaxy. Morrison et al. (2000) implement a careful disk/halo star separation criteria, and obtain $\rho(r) \propto r^{-3}$ for the stellar halo of the MW. Jurić et al. (2008) report a single power law fit $\rho(r) \propto r^{-2.8\pm0.3}$, while Bell et al. (2008) find halo profiles having more structure than simple power laws to yield better fits, but still, $\rho(r) \propto r^{-3}$ for the preferred single power law model. Finally, Sesar et al. (2011) obtain a broken power law as the most accurate description, but again, a best fit single power law of $\rho(r) \propto r^{-2.9}$. There is clearly a broad radial range over which the best fit single power law model yields a slope as expected from Equation (7).

Recent detailed studies of the stellar halo of Andromeda using a variety of techniques and data from the largest modern facilities have reached a consensus for a $\rho \propto r^{-3}$ structure. Ibata et al. (2007) obtain $\Sigma(R) \propto R^{-1.91\pm0.12}$ with data from the Canada–France–Hawaii Telescope, Tanaka et al. (2010) using the Suprime-Cam instrument on the Subaru telescope found $\Sigma(R) \propto R^{-2.17\pm0.15}$, and lastly Gilbert et al. (2012) measure $\Sigma(R) \propto R^{-2.2\pm0.2}$ out to very large distances, 175 kpc, coming to $\Sigma(R) \propto R^{-2.0\pm0.5}$ for 20 kpc $< R <$ 90 kpc once the kinematical substructure is removed. It appears that the stellar halo of M31 is a classic example of the tenuous populations described by Equation (7).

Regarding more external galaxies, tenuous extended stellar halos have been detected over the past few years surrounding numerous systems. Recent detections include Cockcroft et al. (2013), who find evidence for an extended stellar halo about M33 and Bakos & Trujillo (2012), who report finding such structures about a sample of seven late-type spirals from the Sloan Digital Sky Survey (SDSS), in all cases with total masses amounting to only a few percent of the total baryonic mass of the host galaxies. Although the above observations cannot yet yield secure projected density profiles, Jablonka et al. (2010) report a tenuous stellar halo about NGC 3957 with a projected scaling $\Sigma(R) \propto R^{-2.76\pm0.43}$, while Barker et al. (2009) find a faint stellar halo about M81 with a projected scaling $\Sigma(R) \propto R^{-2.0\pm0.2}$, and Bailin et al. (2011) observe a stellar halo about NGC 253 with $\Sigma(R) \propto R^{-2.8\pm0.6}$. In going to larger samples, Zibetti et al. (2004) showed through the stacking of images from 1047 edge-on spiral galaxies from the SDSS that these very generally present extended tenuous stellar halos with volumetric radial density profiles well described by $\rho(r) \propto r^{-3}$.

In going to the spatial distribution of a different tracer population, this time the globular cluster systems of galaxies, it has been well know for many years that the density profile of the GC system of the MW very accurately follows a $\rho(r) \propto r^{-3}$ profile, e.g., Surdin (1994), Racine & Harris (1989). Looking in more detail, more recently Bica et al. (2006) find a $\rho(r) \propto r^{-n}$ profile with $3.2 < n < 3.9$ for all Galactic globular clusters, while the metal-rich population also follows a power law, this time with $\rho(r) \propto r^{-3.2\pm0.2}$ for large radii, and $\rho(r) \propto r^{-3.2\pm0.9}$ if one includes the effects of oblateness in the distribution. The globular cluster system of M31 has a projected power law density profile also in agreement with the expectations of Equation (7), e.g., Racine (1991) determined $\Sigma(R) \propto R^{-2}$. More recently and in more detail, Huxor et al. (2011) obtained a best fit profile composed of three distinct power laws, which, however, if modeled as a single power law for $r > 1$ kpc, can be approximated by the same $\Sigma(R) \propto R^{-2}$ law found earlier by Racine (1991).

Going to more external galaxies, Perelmuter & Racine (1995) found a best fit $\Sigma(R) \propto R^{-2}$ scaling for the globular cluster system of M81. Harris et al. (1984) found the outer projected radial distribution of globular clusters in NGC 4594, the Sombrero galaxy, to be well described by a $\Sigma(R) \propto R^{-2}$ profile. Harris & van den Bergh (1981) also found $\rho(r) \propto r^{-3}$ scalings for the globular cluster systems around seven elliptical galaxies. More recent studies have found a spread in the power law slopes of projected density profiles for globular cluster systems, but taken as a whole, "typical projected power-law indices range from 2 to 2.5 for some low-luminosity Es to 1.5 or a bit lower for the most massive giant ellipticals" Brodie & Strader (2006, p. 211).

Since the studies of Grillmair et al. (1995) and Leon et al. (2000), a number of tenuous stellar halos associated with Galactic globular clusters have been detected. The problem of determining structural parameters is harder than in the cases of the stellar halos surrounding galaxies as the overall numbers of stars are much lower, and the problem of contamination by foreground and background sources, as well as by obscuration, is significant. More modern studies have found a large range of power law slopes in the outskirts of globular clusters, for example, McLaughlin & van der Marel (2005) find projected indexes going from -2 to -6, but report that a population of the most massive clusters shows indexes close to $\Sigma(R) \propto R^{-2}$ and conclude that the extended halos enveloping the clusters they study are suggestive of a generic equilibrium feature, rather than being transient structures. Jordi & Grebel (2010) report projected power law indexes for tenuous stellar halos surrounding 17 Galactic globular clusters; their most reliable results span values from -1 to -4. These authors also note features which are problematic for a standard gravity

interpretation, in the cases of, e.g., NGC 7089 and Pal 1, whose stellar halos are clearly spherical with no sign of any tidal features, in spite of extending in both cases much beyond their Newtonian Jacobi radii. Carballo-Bello et al. (2012) perform a similar study (also including careful CMD modeling to limit contamination) for the extra-tidal halos of 19 Galactic globular clusters. Again, the reported projected power law indexes span a broad range from close to -2 to about -4, excluding clusters showing clear tidal features. Note that for two of the three clusters which overlap with the Jordi & Grebel (2010) sample, NGC 4147 and NGC 5272, Carballo-Bello et al. (2012) report power law indexes of $-2.8^{+0.07}_{-0.05}$ and $-3.18^{+0.08}_{-0.05}$, while Jordi & Grebel (2010) assign to these same clusters values of -1.48 ± 0.24, and of -0.94 ± 0.38, respectively, for a comparable radial range. This simply illustrates that the observational situation is far from converging to definitive answers regarding these systems.

Further, in the case of globular clusters the problem is intrinsically less clear than for the galactic stellar halos, as internal dynamical evolutionary effects might play a part, as well as the gravitational perturbations due to the crossing of the Galactic disk. It is, however, clear that Galactic globular clusters often, if not always, are surrounded by tenuous stellar halos, which, from a Newtonian point of view, must be regarded as "extra tidal" structures. The smooth and round appearances often observed, with all absence of tidal tails, hence become a problem. This problem does not appear under MONDian gravity, where satellite systems are generally expected to be much more robust to tides, e.g., Hernandez & Jiménez (2012). Interestingly, Mackey et al. (2010) find a $\Sigma(R) \propto R^{-n}$ power law structure for the tenuous stellar halo surrounding an extremely isolated globular cluster in M31, which begins as $n \approx 2.5$, and then breaks further outward to $n \approx 3.5$. Also, note that most of the $\Sigma(R) \propto R^{-n}$ indexes in the two recent Jordi & Grebel (2010) and Carballo-Bello et al. (2012) studies cluster about $n = 3$. The presence of as yet undiscovered tidal features among these clusters would tend to artificially steepen their profiles. Note also that Grillmair et al. (1995) cautioned that the difficulties of background subtraction and obscuration corrections will lead to systematics which tend to yield overestimates in n. On the other hand, the large indexes sometimes reported for globular clusters could also be detections of the steepening in the profile expected under MONDian gravity models on approaching the final radius, already mentioned in the discussion following Equation (8).

It thus appears clear that extended tracer population halos, stars, or globular clusters having a small fraction of the light of their host systems, galaxies, or globular clusters are a common feature. Also, such halos are generally never far from the predictions of Equation (7) for equilibrium configurations of isothermal tracer populations in the MONDian regime, to first approximation $\rho(r) \propto r^{-3}$ or $\Sigma(R) \propto R^{-2}$. Within the standard gravity interpretation, explanations of the power law density profiles of galactic stellar halos have been proposed in terms of the accretion and tidal dissolution of substructure falling into the main galaxy, e.g., Bullock et al. (2001), Bullock & Johnston (2005), and Abadi et al. (2006). However, the overall smoothness and uniformity in stellar properties of these systems has been pointed out as problematic for the standard explanation, which naturally implies a degree of randomness in the accreted material, e.g., Ibata et al. (2007), and Bell et al. (2008), who also find from simulations stellar halos not matching observations in terms of the substructure details. Ibata et al. (2007) also show that standard simulations sometimes yield exponents of $\rho(r) \propto r^{-n}$ inconsistent with observations, with $n = 4$ or even $n = 5$. Also, a further explanation must be sought for the observed profiles of the globular cluster systems surrounding galaxies, and yet another for the remarkably smooth "extra-tidal" stellar halos surrounding many of the globular clusters of the MW.

4. DISCUSSION

The relevance of the $\rho(r) \propto r^{-3}$ solution presented here to the observations listed above depends crucially on the validity of three assumptions regarding the tracer population in question, and which enter into the derivation of Equation (7): (1) that it lies within the $a < a_0$ region over which the modified gravity regime is thought to apply; (2) that its velocity dispersion does not depend on radius, i.e., that it is isothermal; and lastly, (3) that there is no orbital anisotropy present in its velocity dispersion, i.e., that it is isotropic. The validity of the first assumption is easy to verify; the radial ranges over which galactic stellar halos and globular cluster populations are observed to comply with the $\rho(r) \propto r^{-3}$ profiles are within the radial ranges where flat rotation curves are seen, and hence, from the accurate rotation curve modeling which MOND affords (e.g., Swaters et al. 2010), also within the $a < a_0$ region. In the case of the tenuous stellar halos surrounding Galactic globular clusters, these appear at radial distances comparable to, but mostly larger than, the regions where the $a < a_0$ threshold is crossed and the velocity dispersion profiles flatten, in the cases where this last have been measured, e.g., Scarpa et al. (2011) and Hernandez et al. (2013).

Regarding the second assumption, in all of the cases listed in the previous section, wherever a radial profile has been measured for the velocity dispersion of the tracer populations in question, these have been shown to be consistent with a constant isothermal solution. Examples of this last point are Battaglia et al. (2006) who, from a sample of 240 halo objects, obtain a velocity dispersion profile for the halo stars in the MW consistent, within errors, with a constant value from 15 kpc to about 70 kpc, and with an inferred anisotropy consistent with an isotropic distribution. Brown et al. (2010) do find a falling trend for the velocity dispersion profile of stars in the MW halo, but only a very mild radial drop, while more recently Samurovic & Lalovic (2011) obtain a velocity dispersion profile for a large sample of 2557 blue horizontal branch stars in the MW from Xue et al. (2008) which is consistent with a constant value out to 70 kpc. Finally, Kafle et al. (2012), using 4664 blue horizontal branch stars from Xue et al. (2011) in the MW halo, observe a radial velocity dispersion which is indistinguishable from flat outward of about 15 kpc, out to their last measured point at close to 60 kpc. Also, in all cases where the velocity dispersion profiles of stars in Galactic globular clusters have been measured out to large radii, these can be seen to be consistent with constant σ values, e.g., Scarpa et al. (2011) and Hernandez et al. (2013). An interesting feature of the two most recent references measuring the velocity dispersion profile of the stellar halo of our Galaxy listed above is that the level for the constant one-dimensional velocity dispersion found is of between 100 and 110 km s^{-1}, which would bring it in accordance with the expectations of the $3\sigma^2 = v^2$ condition we derive in Section 2, since $\sqrt{3} \times 110 = 190$, the observed asymptotic rotation velocity of the MW.

The third assumption is much harder to test empirically, as no reliable measurements of orbital anisotropy exist for any of the astronomical systems treated here. Orbital isotropy is, however,

a natural first order approximation commonly used in the modeling of self-gravitating systems, e.g., Binney & Tremaine (1987), or Drukier et al. (2007), Sollima & Nipoti (2010), and Hernandez & Jiménez (2012), in the modeling of globular clusters under either Newtonian or MONDian approaches. Although an idealization, it provides a convenient reference solution for a variety of dynamical studies of self-gravitating systems; for instance, studies of dynamical friction due to both the hypothetical dark matter and stellar components of dSph galaxies routinely assume isotropic distribution functions for the stars in question, even though this assumption is understood as only a first order approximation (e.g., Sanchez-Salcedo et al. 2006; Goerdt et al. 2006; Cole et al. 2012 to cite a few recent examples). In the absence of any evidence suggesting orbital anisotropy for the systems and radial ranges treated here, e.g., any observed dominant flattening in the light distribution, we chose not to introduce any at this initial point. Further, in the particular case of MOND gravity, it was already shown in Milgrom (1984) that the introduction of a slight degree of anisotropy, which could in principle be present, modifies only slightly the resulting density profiles of self-gravitating systems.

It is of course true that under Newtonian gravity a $\rho(r) \propto r^{-3}$ profile for a tracer population can also be found, but only if one allows for more complex $\sigma(r)$ and radially varying anisotropy parameters. Since the observed density profiles for tenuous halos match the simplest isothermal (as observed in all cases where this function has been measured) and isotropic distribution functions under MONDian gravity, this solution is to be preferred to the fitting of contrived, ad hoc, radial variations in the velocity dispersion and anisotropy parameters of the tracer populations in question under Newtonian gravity, especially as none such variations have been detected.

Clearly, for any astrophysical system where the halo population ceases to be a small perturbation on the total mass, or where the velocity dispersion profile is seen to deviate significantly from the isothermal condition assumed here, our solution will not be relevant. In spite of the approximate nature of the solution (due to the tracer population assumption, the strict isothermal assumption and the forcing of a power law solution), the approximately isothermal profile of various systems where this has been observed, the very low mass contribution of the tracer populations treated, and the good match to a r^{-3} density profile which a wide variety of systems present, give us confidence in that some of the physics has been captured by the modeling.

Finally, it is interesting that some of the systems mentioned in the previous section are not in the deep MOND regime, therefore, from the point of view strictly of MOND as such, no significant modifications to gravity should be apparent. We note that the external field effect of MOND will be substantially modified for different modified gravity theories, of the various types listed in the introduction. Indeed, MOND variants have been discussed where the external field effect is substantially reduced, or even practically disappears, e.g., Milgrom (2011). We note also that our previous results of Hernandez et al. (2012) looking at the observed relative velocities of wide binaries in the solar neighborhood, or of Hernandez et al. (2013) finding MONDian phenomenology in the observed outer dynamics of Galactic globular clusters, both classes of systems not in the deep MOND regime, strongly suggest a modified gravity theory where no external field effect appears.

To summarize, we have shown that under a MONDian gravity force law, the density profiles of isothermal tenuous tracer population halos with isotropic Maxwellian velocities surrounding spherical mass distributions will be well approximated by $\rho \propto r^{-3}$ scalings. We suggest that such equilibrium configurations provide a natural, and certainly general, explanation for the observed close to $\rho \propto r^{-3}$ behavior of: the stellar halos surrounding the MW, M31, and a variety of external galaxies, the density profiles of the globular cluster systems in our Galaxy and Andromeda, and the radial structure of the "extra tidal" stellar halos recently observed surrounding a number of Galactic globular clusters.

The authors thank an anonymous referee for pointing out a number of relevant details which were not sufficiently clear in the original version. Xavier Hernandez acknowledges financial assistance from UNAM DGAPA grant IN103011. Alejandra Jiménez acknowledges financial support from a CONACYT scholarship.

REFERENCES

Abadi, M. G., Navarro, J. F., & Steinmetz, M. 2006, MNRAS, 365, 747
Bailin, J., Bell, E., Chappell, S. N., Radburn-Smith, D. J., & De Jong, R. S. 2011, ApJ, 736, 24
Bakos, J., & Trujillo, I. 2012, arXiv:1204.3082
Barker, M. K., Ferguson, A. M. N., Irwin, M., Arimoto, N., & Jablonka, P. 2009, AJ, 138, 1469
Battaglia, G., Helmi, A., Morrison, H., et al. 2006, MNRAS, 370, 1055
Bekenstein, J. D. 2004, PhRvD, 70, 083509
Bell, E. F., Zucker, D. B., Belokurov, V., et al. 2008, ApJ, 680, 295
Bernal, T., Capozziello, S., Hidalgo, J. C., & Mendoza, S. 2011, EPJC, 71, 1794
Bica, E., Bonatto, C., Barbuy, B., & Ortolani, S. 2006, A&A, 450, 105
Binney, J., & Tremaine, S. 1987, Galactic Dynamics (Princeton, NJ: Princeton Univ. Press)
Brodie, J. P., & Strader, J. 2006, ARA&A, 44, 193
Brown, W. R., Geller, M. J., Kenyon, S. J., & Diaferio, A. 2010, AJ, 139, 59
Bullock, J. S., & Johnston, K. V. 2005, ApJ, 635, 931
Bullock, J. S., Kravtsov, A. V., & Weinberg, D. H. 2001, ApJ, 548, 33
Capozziello, S., & De Laurentis, M. 2011, PhR, 509, 167
Carballo-Bello, J. A., Gieles, M., Sollima, A., et al. 2012, MNRAS, 419, 14
Cockcroft, R., McConnachie, A. W., Harris, W. E., et al. 2013, MNRAS, 428, 1248
Cole, D. R., Dehnen, W., Read, J. I., & Wilkinson, M. I. 2012, MNRAS, 426, 601
Da Costa, G. S. 2012, ApJ, 751, 6
Drukier, G. A., Cohn, H. N., Lugger, P. M., et al. 2007, AJ, 133, 1041
Famaey, B., & McGaugh, S. S. 2012, LRR, 15, 10
Gilbert, K. M., Guhathakurta, P., Beaton, R. L., et al. 2012, ApJ, 760, 76
Goerdt, T., Moore, B., Read, J. I., Stadel, J., & Zemp, M. 2006, MNRAS, 368, 1073
Grillmair, C. J., Freeman, K. C., Irwin, M., & Quinn, P. J. 1995, AJ, 109, 2553
Haghi, H., Baumgardt, H., & Kroupa, P. 2011, A&A, 527, A33
Haghi, H., Baumgardt, H., Kroupa, P., et al. 2009, MNRAS, 395, 1549
Harris, W. E., Harris, H. C., & Harris, G. L. H. 1984, AJ, 89, 216
Harris, W. E., & van den Bergh, S. 1981, AJ, 86, 1627
Hernandez, X., & Jiménez, M. A. 2012, ApJ, 750, 9
Hernandez, X., Jiménez, M. A., & Allen, C. 2012, EPJC, 72, 1884
Hernandez, X., Jiménez, M. A., & Allen, C. 2013, MNRAS, 428, 3196
Hernandez, X., Mendoza, S., Suarez, T., & Bernal, T. 2010, A&A, 514, A101
Huxor, A. P., Ferguson, A. M. N., Tanvir, N. R., et al. 2011, MNRAS, 414, 770
Ibata, R., Martin, N. F., Irwin, M., et al. 2007, ApJ, 671, 1591
Jablonka, P., Tafelmeyer, M., Courbin, F., & Ferguson, A. M. N. 2010, A&A, 513, A78
Jordi, K., & Grebel, E. K. 2010, A&A, 522, A71
Jurić, M., Ivezić, Ž., Brooks, A., et al. 2008, ApJ, 673, 864
Kafle, P. R., Sharma, S., Lewis, G. F., & Bland-Hawthorn, J. 2012, ApJ, 761, 98
Kroupa, P. 2012, PASA, 29, 395
Kroupa, P., Famaey, B., de Boer, K. S., et al. 2010, A&A, 523, 32
Lane, R., Kiss, L. L., Lewis, G. F., et al. 2010, MNRAS, 406, 2732
Lee, J., & Komatsu, E. 2010, ApJ, 718, 60
Leon, S., Meylan, G., & Combes, F. 2000, A&A, 359, 907
Mackey, A. D., Ferguson, A. M. N., Irwin, M. J., et al. 2010, MNRAS, 401, 533
McLaughlin, D. E., & van der Marel, R. P. 2005, ApJS, 161, 304
Mendoza, S., Hernandez, X., Hidalgo, J. C., & Bernal, T. 2011, MNRAS, 411, 226

Milgrom, M. 1983, ApJ, 270, 365
Milgrom, M. 1984, ApJ, 287, 571
Milgrom, M. 1994, ApJ, 429, 540
Milgrom, M. 2011, AcPPB, 42, 2175
Moffat, J. W., & Toth, V. T. 2008, ApJ, 680, 1158
Morrison, H. L., Mateo, M., Olszewski, E. W., et al. 2000, AJ, 119, 2254
Perelmuter, J. M., & Racine, R. 1995, AJ, 109, 1055
Racine, R. 1991, AJ, 101, 865
Racine, R., & Harris, W. E. 1989, AJ, 98, 1609
Samurovic, S., & Lalovic, A. 2011, A&A, 531, A82
Sanchez-Salcedo, F. J., Reyes-Iturbide, J., & Hernandez, X. 2006, MNRAS, 370, 1829
Sanders, R. H., & McGaugh, S. S. 2002, ARA&A, 40, 263
Scarpa, R., Marconi, G., Carraro, G., Falomo, R., & Villanova, S. 2011, A&A, 525, A148
Sesar, B., Jurić, M., & Ivezic, Z. 2011, ApJ, 731, 4
Sollima, A., & Nipoti, C. 2010, MNRAS, 401, 131
Surdin, V. G. 1994, AstL, 20, 398
Swaters, R. A., Sanders, R. H., & McGaugh, S. S. 2010, ApJ, 718, 380
Tanaka, M., Chiba, M., Komiyama, Y., et al. 2010, ApJ, 708, 1168
Thompson, R., & Nagamine, K. 2012, MNRAS, 419, 3560
Xue, X. X., Rix, H. W., Yanni, B., et al. 2011, ApJ, 738, 79
Xue, X. X., Rix, H. W., Zhao, G., et al. 2008, ApJ, 684, 1143
Zhao, H., & Famaey, B. 2010, PhRvD, 81, 087304
Zibetti, S., White, S. D. M., & Brinkmann, J. 2004, MNRAS, 347, 556

Capítulo 6

Fluctuaciones de densidad en gravedad modificada

6.1. Resumen

En este capítulo hacemos una primera aproximación a la formación de estructura en el régimen lineal en gravedad modificada y mostramos que en una aproximación de primer orden es posible formar estructura consistente con la observada hoy en día a partir de las fluctuaciones de materia iniciales, cuyo contraste de densidad es el observado en la radiación cósmica de fondo.

En un contexto de gravedad clásica, se requiere que las fluctuaciones de materia bariónica estén sumergidas en los pozos de potencial ocasionados por fluctuaciones de materia oscura que tienen un contraste de densidad mayor y para así lograr crecer y dar lugar a la estructura que observamos hoy en día.

Además en contraste con el escenario estándar, en gravedad modificada no se tiene una dependencia crucial con las condiciones iniciales debido a que se obtiene una solución que converge independientemente de las condiciones iniciales a una solución atractora $\Delta(M, z)$.

En este trabajo participe en la deducción de las ecuaciones y en su solución numérica, así como en la escritura del mismo junto con mi asesor.

Mon. Not. R. Astron. Soc. **000**, 000–000 (0000) Printed 19 July 2013 (MN LATEX style file v2.2)

A first linear cosmological structure formation scenario under extended gravity

X. Hernandez and M. A. Jiménez
Instituto de Astronomía, Universidad Nacional Autónoma de México, Apartado Postal 70–264 C.P. 04510 México D.F. México.

19 July 2013

ABSTRACT
The inability of primordial baryonic density fluctuations, as observed in the cosmic microwave background (CMB), to grow into the present day astronomical structures is well established, under Newtonian and Einsteinian gravity. It is hence customary to assume the existence of an underlying dark matter component with density fluctuations, $\Delta(M)$, having amplitudes much larger than what CMB observations imply for the baryons. This is in fact one of the recurrent arguments used in support of the dark matter hypothesis. In this letter we prove that the same extended theory of gravity which has been recently shown to accurately reproduce gravitational lensing observations, in absence of any dark matter, and which in the low velocity regime converges to a MONDian force law, implies a sufficiently amplified self-gravity to allow purely baryonic fluctuations with amplitudes in accordance with CMB constraints to naturally grow into the $z = 0$ astrophysical structures detected. The linear structure formation scenario which emerges closely resembles the standard concordance cosmology one, as abundantly calibrated over the last decade to match multiple observational constraints at various redshifts. However, in contrast with what occurs in the concordance cosmology, this follows not from a critical dependence on initial conditions and the fine tuning of model parameters, but from the rapid convergence of highly arbitrary initial conditions onto a well defined $\Delta(M, z)$ attractor solution.

Key words: gravitation — cosmology: theory — (*cosmology:*) dark ages, reionization, first stars — (*cosmology:*) large-scale structure of Universe

1 INTRODUCTION

In Bernal et al. (2011) a relativistic extended gravity model was presented, which working under a FLRW metric was recently shown in Carranza et al. (2013) to be consistent with the observed expansion history of the Universe, including the recent accelerated expansion phase. In Mendoza et al. (2013) we proved that the same relativistic extended gravity scenario, working under an spherically symmetric, static Schwarzschild-like metric, results in a gravitational lensing framework in full accordance with the observed phenomenology, all the above considering exclusively baryonic matter as inferred from observations, without the need of any dark components. The relativistic extended gravity model of Bernal et al. (2011), by construction, converges in the low velocity limit to a MONDian force law, as required to explain galactic rotation curves e.g. Milgrom (1983), Famaey & McGaugh (2012), observed stellar dynamics of dwarf galaxies e.g. McGaugh & Wolf (2010), Hernandez et al. (2010), and the recently measured outer flattening of globular cluster dispersion velocity profiles e.g. Scarpa et al. (2011), Hernandez et al. (2013), in the absence of any dark matter.

Since under the standard gravity scenario, augmented by the introduction of a hypothetical dark matter component, an essentially constant dark matter fraction is required across astrophysical scales, it is reasonable to suspect that a model which replaces the dark matter component by an enhanced self-gravity of the baryons, might naturally also solve the cosmological structure formation puzzle. In this letter, working with the linearised cosmological density contrast evolution equation, we show that indeed, replacing the Newtonian for the MONDian self-gravity expression, yields substantially faster density contrast growth factors. For comparison, in an $a(t) = (3H_0t/2)^{2/3}$ universe, the growth of the density contrast changes from the Newtonian solution of $\Delta \propto (1+z)^{-1}$, to $\Delta \propto (1+z)^{-3}$. Clearly, having 3 orders of magnitude in redshift since recombination, allows for growth factors of 10^9, and hence purely baryonic fluctuations as observed with $\Delta \sim 10^{-5}$ in the CMB can become amply non-linear by substantially high redshifts.

Additionally, we find that the character of the linearised cosmological density contrast evolution equation changes qualitatively from the standard case where solutions are highly sensitive to initial conditions, to an equation hav-

ing a strong attractor solution. This last point replaces the need for delicately crafted initial conditions, to a situation where it is the self-gravity of baryonic perturbations alone what essentially fixes the structure formation scenario.

This resulting structure formation scenario is highly reminiscent of what appears under the standard concordance cosmology, with a bottom up growth of astrophysical structures, but without the need of specifying a detailed primordial fluctuation spectrum, or of calibrating bias, antibias, feedback parameters, etc. The modified baryonic Jeans mass at z_{CMB} is of $4 \times 10^5 M_\odot$, mass-scales which become non-linear by $z \approx 19$, which hence defines the corresponding start of reionization redshifts.

2 EVOLUTION OF SMALL DENSITY PERTURBATIONS IN THE EXPANDING UNIVERSE

We are interested in the growth of gravitational instabilities in the non-relativistic regime within an expanding universe. We shall follow the well known procedure established for the case of standard gravity e.g Longair (2008), and modify only the self-gravity term to use the corresponding MONDian expression. First, we write the fluid dynamical equations including a self-gravity term: the equation of conservation of mass, the Euler equation, and the equation for the self-gravitational potential generated by a density field, $\rho(\mathbf{r})$:

$$\frac{d\rho}{dt} = -\rho \nabla \cdot \mathbf{v} \tag{1}$$

$$\frac{d\mathbf{v}}{dt} = -\frac{1}{\rho}\nabla p - \nabla \phi \tag{2}$$

$$\phi = \phi(\rho, \mathbf{r}) \tag{3}$$

In the Newtonian case, eq.(3) is the standard Poisson equation with an explicit dependence only on ρ. Note that this equations are written in Lagrangian form.

Considering a homogeneous expanding background upon which a small perturbation evolves, $\mathbf{v} = \mathbf{v}_0 + \delta\mathbf{v}$, $\rho = \rho_0 + \delta\rho$, $\phi = \phi_0 + \delta\phi$ and $p = p_0 + \delta p$, we can write equations (1) and (2) keeping only terms to first order in the perturbation to yield:

$$\frac{d}{dt}\frac{\delta\rho}{\rho_0} = \frac{d\Delta}{dt} = -\nabla \cdot \delta\mathbf{v} \tag{4}$$

$$\frac{d(\delta\mathbf{v})}{dt} + (\delta\mathbf{v}\cdot\nabla)\delta\mathbf{v} = \frac{-1}{\rho_0}\nabla\delta p - \nabla\delta\phi \tag{5}$$

where we use the comoving quantities

$$\mathbf{x} = a(t)\mathbf{r}, \tag{6}$$

$$\mathbf{v} = \frac{\delta x}{\delta t} = \frac{da}{dt}\mathbf{r} + a(t)\frac{\mathbf{r}}{dt}, \tag{7}$$

with $\mathbf{v}_0 = da/dt$ identified as the Hubble expansion term and $\delta\mathbf{v}$ the perturbation on the Hubble flow, $a(t)(d\mathbf{r}/dt)$. From equation (7) the perturbed velocity field, $a(t)\mathbf{u}$, now results as:

$$\frac{d\mathbf{u}}{dt} + 2\left(\frac{1}{a}\frac{da}{dt}\right)\mathbf{u} = \frac{-1}{\rho_0 a^2}\nabla\delta p - \frac{1}{a^2}\nabla_c^2(\delta\phi). \tag{8}$$

Considering adiabatic perturbations to replace δp in the above equation for $c_s^2\delta\rho$, and taking the comoving divergence of this same equation, to eliminate $\mathbf{u}$ using the time derivative of equation (4) gives:

$$\frac{d^2\Delta}{dt^2} + 2\left(\frac{1}{a}\frac{da}{dt}\right)\frac{d\Delta}{dt} = \frac{c_s^2}{\rho_0 a^2}\nabla_c^2\delta\rho + \nabla^2\delta\phi, \tag{9}$$

where we have introduced the density contrast as $\Delta = \delta\rho/\rho_0$. In analogy with the standard result, we begin by considering the large scale regime where the pressure term in eq.(9) can be neglected, yielding:

$$\frac{d^2\Delta}{dt^2} + 2\left(\frac{1}{a}\frac{da}{dt}\right)\frac{d\Delta}{dt} = \nabla^2\delta\phi. \tag{10}$$

The quantity $\nabla^2\delta\phi$ depends on the theory of gravity one assumes. In the Newtonian case, $\nabla^2\delta\phi = 4\pi G\delta\rho$, but if the potential is the MONDian one introduced by Mendoza et al. (2011) we should write:

$$\nabla\delta\phi = \frac{\sqrt{a_0 G\delta m}}{r}. \tag{11}$$

Notice that since we are working in the linear regime where the density contrast is small, we can safely assume the accelerations below $a_0 = 1.2 \times 10^{-8} cm/s^2$ limit of the extended gravity force law. For a top hat density fluctuation we can write $\delta m(r) = \frac{4\pi}{3} r^3 \delta\rho$, equation (11) yields for within the fluctuation

$$\nabla\delta\phi = \left(\frac{4\pi}{3} a_0 G r \delta\rho\right)^{1/2}. \tag{12}$$

Now we take the divergence of the gradient of this potential perturbation to obtain the Laplacian of the MONDian potential as,

$$\nabla^2\delta\phi = \nabla\cdot\nabla\delta\phi = \left(\frac{4\pi}{3} a_0 G\delta\rho\right)^{1/2}\frac{1}{r^2}\frac{\partial}{\partial r} r^{5/2}, \tag{13}$$

giving:

$$\nabla^2\delta\phi = \left(\frac{25\pi}{3}\frac{a_0 G\delta\rho}{r}\right)^{1/2}. \tag{14}$$

Evaluating this last expression at the edge of the density fluctuation, we write $r = \left(\frac{3}{4\pi}\delta m/\delta\rho\right)^{1/3}$ where δm is now the total fluctuation mass, to eliminate r from the Laplacian of the MONDian potential, which yields:

$$\nabla^2\delta\phi = \frac{5}{2}\left(\frac{4\pi}{3}\right)^{2/3}\frac{(Ga_0)^{1/2}\rho_0^{2/3}}{(\delta m)^{1/6}}\Delta^{2/3} \tag{15}$$

We can now study the evolution of over-densities in the linear regime in an extended gravity scenario, by substituting the result of equation (15) into (10):

$$\frac{d^2\Delta}{dt^2} + 2\left(\frac{1}{a}\frac{da}{dt}\right)\frac{d\Delta}{dt} = \frac{5}{2}\left(\frac{4\pi}{3}\right)^{2/3}\frac{(Ga_0)^{1/2}\rho_0^{2/3}}{(\delta m)^{1/6}}\Delta^{2/3}, \tag{16}$$

which is the main result of this section. Particular solutions to the above equation and comparisons to the standard Newtonian results appear in the following section.

3 SOLUTIONS FOR PARTICULAR $a(t)$ CASES

We begin by examining the evolution of density fluctuations evolving within a flat universe described by:

$$a(t) = \left(\frac{3H_0}{2}t\right)^{2/3}. \tag{17}$$

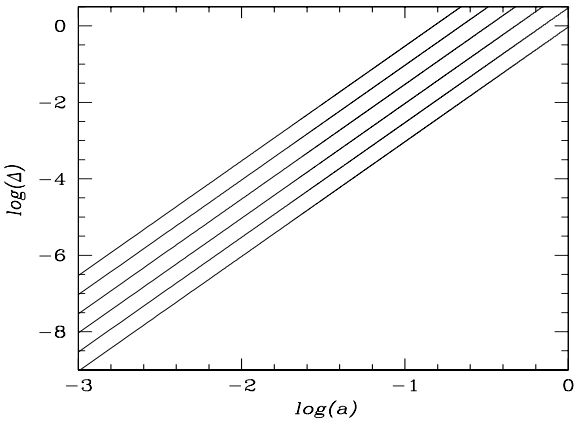

Figure 1. Growth of density contrast in an $a(t) = (3H_0t/2)^{2/3}$ universe for the power law convergent solution of eq.(19). Fluctuation masses of $4 \times (10^5, 10^6, 10^7, 10^8, 10^9$ and $10^{10})M_\odot$ appear in descending order.

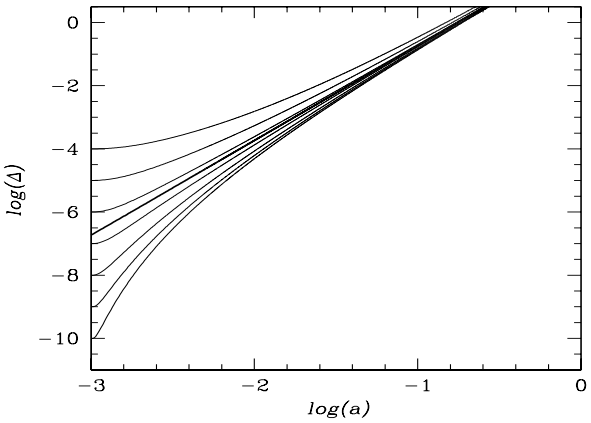

Figure 2. Numerical solutions to eq.(19) for a fluctuation mass of $10^6 M_\odot$, for a range of $\Delta(z_{CMB})$ initial conditions extending over 6 orders of magnitude. Notice the strong convergence to the power law solution of eq.(20), thick curve.

This idealised case will serve merely as a test where solutions are analytical, and comparison to well known standard results can be clearly explored. In the Newtonian case equation (10) becomes:

$$\frac{d^2\Delta}{dt^2} + \left(\frac{4}{3t}\right)\frac{d\Delta}{dt} = \frac{2}{3t^2}\Delta, \tag{18}$$

with a growing mode solution $\Delta \propto t^{2/3} \propto a = (1+z)^{-1}$. Alternatively, when we work in the modified gravity scenario for a Universe that follows $a = (3H_0t/2)^{2/3}$ dynamics, equation (16) describing the evolution of density perturbations becomes:

$$\frac{d^2\Delta}{dt^2} + \left(\frac{4}{3t}\right)\frac{d\Delta}{dt} = 0.124\frac{a_0^{1/2}}{(G\delta m)^{1/6}}\frac{\Delta^{2/3}}{t^{4/3}}. \tag{19}$$

In this last equation we have considered $H_0 = 70km/sMpc^{-1}$ and $\rho_0 = 0.05(3H_0/8\pi G)(1+z)^3$, the contribution of baryonic matter only. It is important to note that in this section, particular $a(t)$ scale factor evolution models are considered merely as convenient parametrisations of the expansion history of the Universe, as calibrated through a large number of empirical observations across a range of redshifts. Thus, we are not assuming a standard GR theory behind any of the $a(t)$ models tested, it has been shown that modified gravity theories of the $f(R)$ type can self-consistently account for the expansion histories obtained under GR models with parameters as calibrated to match cosmological inferences, e.g. Nojiri & Odintsov (2011), Capozziello & De Laurentis (2011), or Carranza et al. (2013) for the particular metric extended gravity theory which converges to the MONDian force law used here.

This time, for equation (19) there exist a unique power law solution, $\Delta = c_1 t^2$ where $c_1 = 1.898 \times 10^{-5}\left(a_0^3/G\delta m\right)^{1/2}$. To write Δ as a function of the scale factor we use $t^2 = 4a^3/9H_0$ to obtain:

$$\Delta = \left(\frac{M_c}{\delta m}\right)^{1/2} a^3 = \left(\frac{M_c}{\delta m}\right)^{1/2} (1+z)^{-3}, \tag{20}$$

where we have introduced

$$M_c = 7.12 \times 10^{-11}\frac{a_0^3}{GH_0^4} = 3.488 \times 10^{10} M_\odot. \tag{21}$$

By comparing eq.(20) to the equivalent solution in the Newtonian case which appears following eq.(18), we see that the $(1+z)^{-1}$ scaling has been replaced by a $(1+z)^{-3}$ one. This shows that growth factors of 9 orders of magnitude, rather than the 3 orders of the Newtonian case, will result for the interval from $z_{CMB} \approx 1000$ to today. Thus, purely baryonic density fluctuations with amplitudes as observed in the CMB, of order $\Delta \approx 10^{-5}$, will have ample time to naturally grow under their own self-gravity alone into the non-linear regime, by substantially high redshifts. Therefore, the requirement under the Newtonian approach of a hypothetical underlying undetected dark component with density fluctuations many orders of magnitude larger than what the observed density component shows, is removed. Results for the evolution of the growth factor from eq.(20) are shown in figure (1), for fluctuation masses of $4\times(10^5, 10^6, 10^7, 10^8, 10^9$ and $10^{10})M_\odot$, appearing in descending order. The lower fluctuation mass limit of $4 \times 10^5 M_\odot$ was chosen as the baryonic MONDian Jeans mass at recombination of σ^4/Ga_0 with σ the sound speed of 3000 K hydrogen gas, e.g. Mendoza et al. (2011).

Notice also that in this case, the power law solution has a unique normalisation, as happens e.g. when one solves for a power law solution to the hydrostatic equilibrium of a Newtonian isothermal self-gravitating gas, the singular isothermal solution which results furnishes not only a definitive power law behaviour, but also a unique amplitude fully determined by the physical parameters of the problem. Here, G, a_0 and H_0 fully define the amplitude and evolution of the density contrast at all redshifts, once a fluctuation mass is chosen. This last point is related to the strongly attractive character which the power law solution eq.(20) has.

From the $\Delta = \Delta_{CMB}(1+z_{CMB})/(1+z)$ solutions of the Newtonian case, we see that taking different Δ_{CMB}

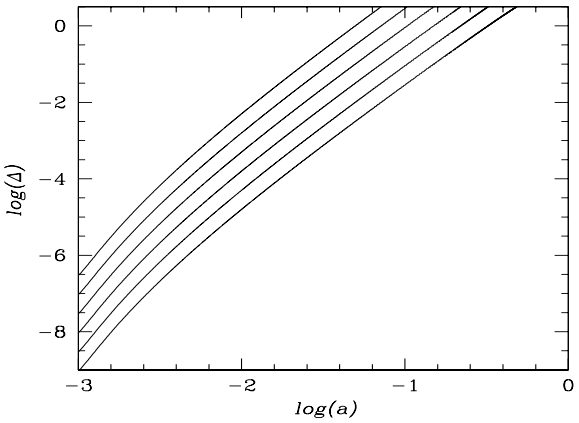

Figure 3. Growth of density contrast in a universe having an $a(t)$ evolution as the concordance case, for the attractor solution to eq.(23). Fluctuation masses of $4 \times (10^5, 10^6, 10^7, 10^8, 10^9$ and $10^{10}) M_\odot$ appear in descending order.

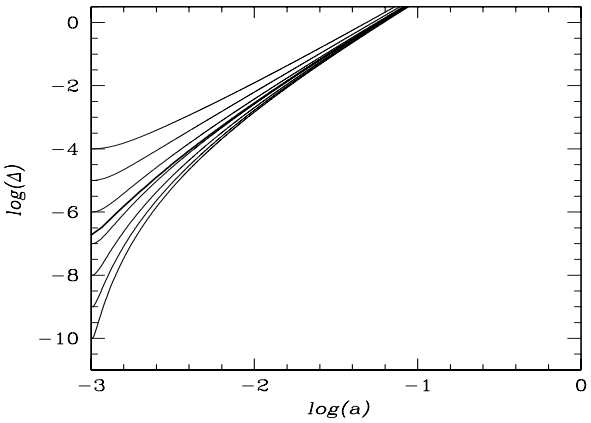

Figure 4. Numerical solutions to eq.(23) for a fluctuation mass of $10^6 M_\odot$, for a range of $\Delta(z_{CMB})$ initial conditions extending over 6 orders of magnitude. Notice the strong convergence to the attractor solution of eq.(23), thick curve.

initial conditions results in evolutionary tracks in (Δ, z) space which remain parallel throughout. Thus, initial conditions $\Delta_{CMB}(M)$ are preserved during the linear evolutionary phase. The consequence of this feature is the delicate dependence of the standard structure formation scenario upon the initial conditions, the details of which hence become crucial to determining the ensuing structure formation scenario.

The situation emerging from the modified MONDian force law in eq.(16) is thoroughly different; Δ in the source term in the right hand side appears to a power smaller than 1, and hence if we take an enhanced solution having a slightly larger amplitude at a given reference redshift than a given reference solution, the source term will be proportionally smaller than the increase in Δ itself, so that now, the reference solution will catch up with the enhanced variant. It is clear that the power law solution to eq.(16) of eq.(20) will thus be a strongly attractive solution. This is shown explicitly in figure (2), where a number of numerical solutions to eq.(19) are shown for a constant fluctuation mass of $10^6 M_\odot$, for a range of initial conditions at $a = 10^{-3}$, covering 6 orders of magnitude, all with $d\Delta/dt = 0$ at $a = 10^{-3}$. The solid line shows the convergent solution for the same mass, of eq.(20), which is clearly a very strongly attractive solution. We thus see that the resulting structure formation scenario will be highly independent of the initial conditions, and also, that initial density contrast values at z_{CMB} in the galactic region, much smaller than the $\Delta \sim 10^{-5}$ values observed for the extragalactic scales now measured, will be amply sufficient to yield non-linear structures by high redshifts.

At this point we examine the evolution of the density contrast, but under a realistic $a(t)$ model. The evolution of the expansion factor for a flat universe for the concordance cosmology case, as abundantly calibrated to yield accordance with a large number of observations across a redshift range extending out to z_{CMB} is:

$$a(t) = \left(\frac{\Omega_m}{\Omega_\Lambda}\right)^{2/3} \left[sinh\left(\frac{3}{2}\sqrt{\Omega_\Lambda} H_0 t\right)\right]^{2/3}. \quad (22)$$

As already mentioned, the above equation is taken as merely a convenient fit to the actual $a(t)$ evolution of the Universe, which is accurately reproduced by choosing the numerical parameter values $\Omega_m = 0.3$ and $\Omega_\Lambda = 0.7$. Introducing this expression in equation (16) we have:

$$\frac{d^2\Delta}{dt^2} + A(t)\frac{d\Delta}{dt} = B(t)\frac{\Delta^{2/3}}{dm^{1/6}} \quad (23)$$

where:

$$A(t) = \frac{2H_0\Omega_\Lambda}{tanh\left(\frac{3}{2}\sqrt{\Omega_\Lambda} H_0 t\right)}, \quad (24)$$

$$B(t) = \frac{c_2}{\left[sinh\left(\frac{3}{2}\sqrt{\Omega_\Lambda} H_0 t\right)\right]^{4/3}}, \quad (25)$$

and c_2 is given by

$$c_2 = \frac{5}{2}\left(\frac{4\pi\Omega_m}{3\Omega_\Lambda}\right)^{2/3} (a_0 G)^{1/2} \rho_0^{2/3}. \quad (26)$$

By solving eq.(23) numerically, we find again a strongly attractive solution given by taking initial conditions at z_{CMB} from the power law solution of eq.(20), which are shown in figure (3) for the same fluctuation masses appearing in figure (1). The strongly attractive character of the solutions shown in figure (3) can again be traced to the structure of eq.(16), and is shown explicitly in figure (4), which is analogous to figure (2). We note that for $log(a) \geqslant -2$ the growth factor evolution shown in figure (3) can be accurately fitted by:

$$\Delta = \left(\frac{M_{cr}}{\delta m}\right)^{1/2} a^{3.16} = \left(\frac{M_{cr}}{\delta m}\right)^{1/2} (1+z)^{-3.16}, \quad (27)$$

where this time $M_{cr} = 6.5 \times 10^{13} M_\odot$. By comparing figure (3) to the $a = (3H_0 t/2)^{2/3}$ case of figure (1), we see that for the more realistic case having an $a(t)$ evolution as that of the

concordance cosmological model, the enhanced amount of time implied by a given redshift interval now allows for substantially more growth for the density fluctuations treated. In fact, from eq.(27), we see that the smallest primordial structures, those having the MONDian baryonic Jeans mass at z_{CMB} of $4\times10^5 M_\odot$, will become non-linear by a redshift of 19. This last point provides a good qualitative agreement with re-ionisation constraints e.g. $z = 11.1 \pm 1.1$ for the redshift at which the Universe is half re-ionised of the recent Plank results, Planck Collaboration (2013).

Notice that our result of eq.(16) will also apply to other modified relativistic theories of gravity which in the $v << c$ limit tend to a MONDian force law e.g. Bekenstein (2004) or Zhao & Famaey (2010). We end by commenting that by merely changing the Newtonian for the MONDian self-gravity term in the density contrast evolution equation, not only does the enhanced self-gravity results in a sufficiently amplified growth factor evolution no longer requiring any dark matter, but also, strongly convergent solutions appear which eliminate the need for carefully tuned initial conditions.

4 CONCLUSIONS

We have shown that if the Newtonian self-gravity term in the cosmological linear evolution fluctuation density contrast equation is substituted for the equivalent MONDian one, purely baryonic density perturbations with amplitudes compatible with CMB restrictions at z_{CMB} and masses ranging from $4\times10^5 - 4\times10^{10} M_\odot$ will enter the non-linear regime by redshifts of between 19 and 2.2 respectively. The resulting structure formation scenario is hence highly reminiscent of the one appearing under the standard concordance cosmology, with a bottom up growth of cosmological structures. The modified baryonic Jeans mass at z_{CMB} is of $4\times10^5 M_\odot$ and hence the corresponding start of reionization redshifts will be of ≈ 19.

This eliminates the necessity of invoking a hypothetical underlying dark matter component at z_{CMB} having density fluctuations with amplitudes several orders of magnitude above what is observed for the empirically measured baryonic component.

A strongly convergent growth factor solution results, which also eliminates the need for an additional primordial fluctuation generating mechanism.

ACKNOWLEDGEMENTS

Xavier Hernandez acknowledges financial assistance from UNAM DGAPA grant IN103011-3. Alejandra Jimenez acknowledges financial support from a CONACYT scholarship.

REFERENCES

Bekenstein , J. D. 2004, Phys. Rev. D 70, 083509
Bernal, T., Capozziello, S., Hidalgo, J. C., & Mendoza, S. 2011, Eur. Phys. J. C, 71, 1794
Capozziello, S., & De Laurentis, M., 2011, PhR 509, 167
Carranza, D.A., Mendoza, S., & Torres, L.A., 2013, Eur. Phys. J. C. 73, 2282
Famaey, B., McGaugh, S. S., 2012, LRR 15, 10
Hernandez, X., Mendoza, S., Suarez, T., & Bernal, T. 2010, A&A, 514, A101
Hernandez, X., Jimnez, M. A., & Allen, C., 2013, MNRAS 428, 3196
Longair, M., 2008, Galaxy Formation (Springer, Berlin Heidelberg New York)
McGaugh, S. S., & Wolf, J. 2010, ApJ 722, 248
Mendoza, S., Hernandez, X., Hidalgo, J. C., & Bernal, T. 2011, MNRAS, 411, 226
Mendoza, S., Bernal, T., Hernandez, X., Hidalgo, J. C., & Torres, L. A. 2013, MNRAS, Advance Access, doi:10.1093/mnras/stt752
Milgrom, M. 1983, ApJ, 270, 365
Nojiri, S., & Odintsov, S. D., 2011, PhR 505, 59
Planck Collaboration 2013, arXiv:1303.5076
Scarpa, R., Marconi, G., Carraro, G., Falomo, R., & Villanova, S., 2011, A&A 525, 148
Zhao, H., & Famaey, B. 2010, Phys. Rev. D, 81, 087304

6. FLUCTUACIONES DE DENSIDAD EN GRAVEDAD MODIFICADA

Capítulo 7

Conclusiones y trabajo futuro

7.1. Conclusiones

El objetivo de esta tesis fue poner a prueba las dos predicciones principales de los esquemas de gravedad modificada cuyos límites son tipo MOND; para ello usamos las observaciones disponibles de los movimientos propios de estrellas binarias abiertas de $1M_{\odot}$ y separaciones mayores a $7000UA$ ya que es en estos sistemas donde la aceleración es del orden de a_0 y los esquemas de gravedad modificada predicen un límite superior plano para la distribución de velocidades relativas, mientras que en gravedad newtoniana esta distribución tendría que tener una envolvente que decae con la raíz cuadrada de la separación del sistema binario.

Para dos muestras independientes de estrellas binarias encontramos que la distribución de velocidades relativa esta en acuerdo con la predicción de los esquemas de gravedad modificada y en contradicción con la tercera ley de Kepler.

También consideramos las observaciones disponibles de la dispersión de velocidades como función del radio de dieciséis CGs en los cuales se observa que el perfil de dispersión de velocidades proyectado se aplana en la periferia del cúmulo, dentro de la gravedad estándar este comportamiento es inesperado ya que en estos objetos la materia oscura no juega un papel relevante para la dinámica del cúmulo y deberían observarse perfiles que decaen con la raíz cuadrada del radio.

Con la ley de fuerza propuesta por Mendoza et al. (2012) cuyos límites son tipo MOND modelamos cada CG como un sistema autogravitante de estrellas con simetría esférica y logramos reproducir todas las restricciones observacionales y encontramos que la masa total del cúmulo y la dispersión de velocidades asintótica siguen una relación Tully-Fisher.

El modelo desarrollado para CGs fue aplicado a la galaxia elíptica gigante NGC 4649 y nuevamente logramos reproducir todas las restricciones observacio-

nales para esta galaxia incluyendo su perfil de brillo y el perfil de dispersión de velocidades asintóticamente plano, corroborando así la consistencia de nuestro modelo.

Encontramos que en la mayoría de los cúmulos el radio al cuál el perfil se vuelve plano coincide en promedio con el radio al cual la aceleración es del orden de a_0 como lo esperan las teorías de gravedad modificada. El radio de marea newtoniano en general resulta ser mucho más grande que el radio al cual el perfil de dispersión de velocidades se aplana, descartando así a las fuerzas de marea newtonianas como las responsables del aplanamiento del perfil en el contexto de la física newtoniana.

También encontramos que las observaciones de la distribución de CGs en nuestra galaxia y en Andrómeda, así como la distribución de densidad del halo de estrellas en la Vía Láctea y en M31 y las estrellas alrededor de los cúmulos globulares, corresponde a la distribución esperada por los modelos de gravedad modificada para cualquier halo isotérmico de partículas de prueba alrededor de una distribución esférica de masa.

Por último, hacemos una primera aproximación a la formación de estructura en un contexto de gravedad modificada, encontrando que es posible formar estructuras compatibles a las observadas hoy en día a partir de fluctuaciones de densidad como las observadas en la radiación cósmica de fondo sin la necesidad de materia oscura, este hecho es un buen indicio de que es posible construir una cosmología en gravedad modificada compatible con las observaciones.

En esta tesis mostramos que una de las predicciones fundamentales de las teorías de gravedad modificada tipo MOND es correcta, además vimos como dentro de este esquema la fenomenología observada en cúmulos globulares se explica de manera natural y realizamos un primer acercamiento a la formación de estructura encontrando resultados consistentes con las observaciones.

Así que podemos concluir que si bien la teoría final de cómo se debe modificar la gravedad es aún discutida, nuestros resultados apuntan a que en efecto es necesario modificar la ley de gravedad para poder explicar las observaciones astrónomicas a todas las escalas.

7.2. Trabajo futuro

Con el trabajo desarrollado en esta tesis nos hemos convencido de la necesidad de modificar la gravedad para poder explicar y entender una gran variedad de observaciones astronómicas, es necesario continuar explorando la cosmología resultante de estos esquemas, en mi trabajo futuro pretendo seguir explorando la formación de estructura en este contexto, calcular las oscilaciones bariónicas

acústicas y trabajar en la construcción de un escenario de formación de estructura sin la necesidad de incluir materia oscura si es esto posible.

Bibliografía

Santillan, A. & Santillan, A. 1991, Revista Mexicana de Astronomia y Astrofisica, 22, 255

Bekenstein, J. D. 2004, Phys. Rev. D, 70, 083509

Mendoza, S., Mendoza, S., Mendoza, S., & Mendoza, S. 2011, Eur. Phys. J. C, 71, 1794

Bosma, A. 1981, AJ, 86, 1825

Bochanski, J. J., Bochanski, J. J., Bochanski, J. J., & Bochanski, J. J. 2010, AJ, 139, 2566

McGaugh, S. S. & McGaugh, S. S. 2012, Living Reviews in Relativity, 15, 10

Felten, J. 1984, ApJ, 286, 3

Jiménez, M. A. & Jiménez, M. A. 2012, ApJ, 750, 9

Allen, C., Allen, C., & Allen, C. 2012, European Physical Journal C, 72, 1884

Allen, C., Allen, C., & Allen, C. 2013a, MNRAS, 428, 3196

Allen, C., Allen, C., & Allen, C. 2013b, ApJ, 770, 83

Squires, G., Squires, G., Squires, G., & Squires, G. 1998, ApJ, 504, 636

Tremaine, S. & Tremaine, S. 2010, MNRAS, 401, 977

Nasser, L., Nasser, L., Nasser, L., & Nasser, L. 2013, ApJ, 768, 142

Kroupa, P. 2012, PASA, 29, 395

McGaugh, S. S. 2011, Physical Review Letters, 106, 121303

Torres, L. A., Torres, L. A., Torres, L. A., Torres, L. A., & Torres, L. A. 2012, ArXiv e-prints

Bernal, T., Bernal, T., Bernal, T., & Bernal, T. 2011, MNRAS, 411, 226

Milgrom, M. 1983a, ApJ, 270, 371

Milgrom, M. 1983b, ApJ, 270, 384

Milgrom, M. 1983c, ApJ, 270, 365

Toth, V. T. & Toth, V. T. 2010, ArXiv e-prints

Oort, J. H. 1932, BAIN, 6, 249

Burstein, D., Burstein, D., Burstein, D., & Burstein, D. 1982, ApJ, 261, 439

McGaugh, S. S. & McGaugh, S. S. 2002, ARA&A, 40, 263

Falomo, R. & Falomo, R. 2010, A&A, 523, A43

Villanova, S., Villanova, S., Villanova, S., Villanova, S., & Villanova, S. 2011, A&A, 525, A148

Carraro, G., Carraro, G., Carraro, G., & Carraro, G. 2007, A&A, 462, L9

Olling, R. P. & Olling, R. P. 2011, ApJS, 192, 2

Zwicky, F. 1933, Helvetica Physica Acta, 6, 110